University of New Mexico

UNM Digital Repository

Civil Engineering ETDs

Engineering ETDs

Summer 8-1-2023

DEVELOPMENT OF THE NAVIGATOR: A LAGRANGIAN SMART SENSING SYSTEM TO CHARACTERIZE AQUATIC ECOSYSTEMS.

Aashish Sanjay Khandelwal

Follow this and additional works at: https://digitalrepository.unm.edu/ce_etds



Part of the Civil and Environmental Engineering Commons

Recommended Citation

Khandelwal, Aashish Sanjay. "DEVELOPMENT OF THE NAVIGATOR: A LAGRANGIAN SMART SENSING SYSTEM TO CHARACTERIZE AQUATIC ECOSYSTEMS.." (2023). https://digitalrepository.unm.edu/ ce_etds/309

This Dissertation is brought to you for free and open access by the Engineering ETDs at UNM Digital Repository. It has been accepted for inclusion in Civil Engineering ETDs by an authorized administrator of UNM Digital Repository. For more information, please contact disc@unm.edu.

Aashish S Khandelwal
Candidate
Civil, Construction & Environmental Engineering
Department
This dissertation is approved, and it is acceptable in quality and form for publication:
Approved by the Dissertation Committee:
Dr. Ricardo González-Pinzón, Chairperson
Dr. David Van Horn
Dr. Mark Stone
Dr. Stefan Krause

DEVELOPMENT OF THE NAVIGATOR: A LAGRANGIAN SMART SENSING SYSTEM TO CHARACTERIZE AQUATIC ECOSYSTEMS.

By

AASHISH S KHANDELWAL

B.E., Civil Engineering, Mumbai University, 2015M.S., Civil Engineering, The University of New Mexico, 2020M.Arch., Architecture, The University of New Mexico, 2020

DISSERTATION

Submitted in Partial Fulfillment of the

Requirement for the Degree of

Doctor of Philosophy

Engineering

The University of New Mexico

Albuquerque, New Mexico

August 2023

Acknowledgements

I would like to express my deepest gratitude to my advisor, Dr. Ricardo Gonzalez-Pinzon, for his unwavering support, leadership, guidance, and encouragement throughout my doctoral journey. His expertise, dedication, and insightful feedback have been invaluable in shaping the direction of my research.

I am also immensely grateful to the members of my dissertation committee, Dr. Dave Van Horn, Dr Mark Stone, and Dr Stefan Krause, for their time, expertise, and support. I would like to thank Eco-Hydro lab members for their help and support. I would like to acknowledge the support and encouragement of my friends and fellow graduate students, who have provided me with a network of support and company. I extend my heartfelt thanks to the faculty and staff of the Center for Water and Environment for providing a stimulating academic environment and access to valuable resources.

I'm grateful to my family, particularly my mother Prabha, aunt Nandini, and Marie for their unwavering love, understanding, and constant belief in my abilities. Their unfaltering support and encouragement have fueled my accomplishments.

Lastly, I would like to express my gratitude to all the collaborators who generously volunteered their time and expertise for my research. This research was supported by the National Science Foundation (NSF) and the New Mexico Water Resources Research Institute (NMWRRI). I am grateful for their financial support, which allowed me to conduct my research effectively.

DEVELOPMENT OF THE NAVIGATOR: A LAGRANGIAN SMART SENSING SYSTEM TO CHARACTERIZE AQUATIC ECOSY STEMS.

BY

AASHISH S KHANDELWAL

B.E., Civil Engineering, Mumbai University, 2015

M.S., Civil Engineering, The University of New Mexico, 2020

M.Arch., Architecture, The University of New Mexico, 2020

Ph.D., Engineering, The University of New Mexico, 2023

ABSTRACT

Most freshwater aquatic studies rely on Eulerian monitoring, i.e., water quality and quantity are monitored using grab samples or semi-continuous sensors deployed at fixed cross-sections. While Eulerian monitoring is practical, it provides a limited understanding of spatial and temporal heterogeneity and their effects on environmental processes. This dissertation summarizes the design and application of The Navigator, an alternative Lagrangian monitoring system that offers cost-effective solutions for in-situ, real-time data collection in lotic and lentic freshwater ecosystems such as streams, rivers, ponds, and reservoirs. The Navigator features a suite of methods – an autonomous surface vehicle (ASV) with GPS and LTE connectivity, water quality sensors, depth sonar, computer vision camera, cloud computing, and a webpage dashboard to visualize data in real-time. With these technologies, The Navigator provides insight into where, how, and why water quality and quantity change in time and space as it moves through the current or flows following user-specified pathways.

First, we tested our prototype of The Navigator in the monitoring of water quality parameters at high spatial-temporal resolution along the Rio Grande and a retention pond in

Albuquerque, NM. Then, we deployed the Navigator to quantify experimental mixing lengths downstream of the outfall of a wastewater treatment plant in the Rio Grande near Albuquerque, NM, under various flow regimes. Lastly, we deployed The Navigator to examine the role of Santa Rosa Lake in attenuating the propagation of wildfire disturbances generated 170 km upstream during and after the Hermit's Peak-Calf Canyon wildfire. We quantified changes in water density, turbidity, and other water quality parameters along the river-lake section using Lagrangian monitoring.

Table of Contents

List of Figures	_viii
List of Tables	xi
Chapter 1	1
1. General Introduction	1
1.1 Context	1
1.2 Objectives	3
1.3 Dissertation Layout	4
1.4 Chapter references	4
Chapter 2	7
2. Development of The Navigator: A Lagrangian smart sensing system to characteriz	e
aquatic ecosystems	7
2.1 Introduction	7
2.2 Methods	11
2.3 Validation and field testing	19
2.4 The Navigator comparison with existing technology	32
2.5 Conclusions_	30
2.6 Chapter references	32
Chapter 3	_ 35
3. Comparison of experimental and empirical mixing lengths downstream of a	
wastewater treatment plant discharging into an arid river	_ 35
3.1 Introduction	35
3.2 Methods	38
3.3 Results and Discussion	45
3.4 Conclusions_	53
3.5 Chapter references	55
Chapter 4	_ 59
4. The Role of Santa Rosa Lake in the propagation of disturbances from the Hermit's	,
Peak-Calf Canyon wildfire.	_ 59
4.1 Introduction	59

	4.2 Methods	6
	4.3 Results	6
	4.4 Discussion	7:
	4.5 Conclusions	7′
	4.6 Chapter references	78
	4.7 Supplemental Information	8
Chapter 5		85
	5.1 Summary	8:
	5.2 Patent	80
	5.3 Commercialization plan	89
	5.4 Chapter refrences	90
Appendix	A: Participation in peer-reviewed manuscripts	91

List of Figures

Figure 1.1. Measurement approaches in Limnology
Figure 2.1. Figure 1: The Navigator: parts, design and exploded diagram. The dimensions and 3D printed models in CAD can be accessed here: The Navigator CAD model. Part descriptions are available in Table 1
Figure 2.2. The Navigator hardware (left) and software schematic (right)
Figure 2.3. A Map of New Mexico, USA, with red boxes enclosing the study sites. A) 7th-order study reach along the Rio Grande where The Navigator was used in drifting mode on day 1 (May 19th, 2022) and day 2 (May 20th, 2022). B) Hermit's Peak-Calf Canyon Fire perimeter in red and boundaries of the impacted watershed draining to Santa Rosa Lake. The Navigator was deployed in autonomous mode to follow a waypoint path across the lake on August 19th, 2022. C) Recreational fishing pond in the City of Albuquerque, where The Navigator was deployed in autonomous mode following a grid pattern on November 11th, 2022.
Figure 2.4. Longitudinal heatmap profile of water quality parameters collected by The Navigator along the Rio Grande River near Albuquerque, NM. The blue dots indicate USGS flow gages, green shade indicates low values and red indicates high values. Clock time is indicated in hh: mm.
Figure 2.5. The Navigator is monitoring Santa Rosa Lake, NM, to understand the water quality impact of monsoon runoff on the reservoir from the Hermit peaks/ Calf Canyon wildfire. The blue dot indicates USGS flow gages for Pecos River below the dam; green indicates low values, and red indicates a high value for water quality parameters. Clock time is in hh: mm.
Figure 2.6. a) The Navigator monitoring the Bob Gerding catch and release pond, Albuquerque, NM. b1-b5) Images captured by The Navigator while monitoring. c) Heatmap of the water quality parameters and depth data collected by The Navigator
Figure 2.7. Comparison spider map of three autonomous surface vehicle platforms and The Navigator
Figure 3.1. (A and B) Study reach location and (C) satellite photo of the area near the outfall of the City of Albuquerque's wastewater treatment plant
Figure 3.2. Rio Grande discharge (blue) for the USGS08330000 at Central Bridge (Q_{up}) , Southside Water Reclamation Plant outfall flow $(Q_{wtp}; grey)$, and daily mean Q_{wwtp} values (black). Red dotted lines indicate fieldwork days, and the red rectangle represents the period when the river ran dry, and the WWTP provided all the river flow downstream of the WWTP.
Figure 3.3. Drone-based infrared imaging showing the higher temperature plume from the WWTP effluent (light grey, ~20-25 °C) hanging on the left bank of the Rio Grande (black ~15 °C)

downstream of the Albuquerq different flow conditions (Q_{up} bank data. Dash lines indicate	issolved oxygen and temperature observed upstream and ue wastewater treatment plant (WWTP) effluent during $: Q_{wwtp}$). Left bank (outfall side) data are on top of right the experimental mixing lengths (L_m), where left and right rence downstream of the WWTP
downstream of the Albuquerq different flow conditions (Q_{up} bank data. Dash lines indicate	H and specific conductivity observed upstream and ue wastewater treatment plant (WWTP) effluent during $: Q_{wwtp}$). Left bank (outfall side) data are on top of right the experimental mixing lengths (L_m) , where left and right rence downstream of the WWTP
	mpirical (L) mixing lengths as a function of the dilution equations 1-6 are described in Table 1
_	tream of the Albuquerque WWTP outfall. The bank history te images from Google Earth
red line represents the burn pe the Gallinas Creek watershed. km downstream from the head Montezuma; GL _{56 km} , Gallinas	monitoring of the Hermit's Peak-Calf Canyon wildfire. The reimeter. The red area represents the burn scar boundary of GFT _{22 km} , Gallinas Creek near La Placita fire station, 22 dwaters of Gallinas Creek; GMZ _{29 km} , Gallinas Creek near Creek near Lourdes; PSR _{170 km} , Pecos River upstream of Pecos River downstream of Santa Rosa Lake
PBS _{190 km} , Pecos River downs	PSR _{170 km} Pecos River upstream of Santa Rosa Lake and tream of Santa Rosa Lake. Lake levels for Santa Rosa Lake 2
upstream of Santa Rosa Lake,	the variations in water quality at PSR _{170 km} , Pecos River and PBS _{190 km} , Pecos River downstream of Santa Rosa iod
temperature collected with Th (green, blue, and red) and post	ved oxygen, specific conductivity, turbidity, pH, and water e Navigator. Data were collected during the monsoon t-monsoon (orange) periods. The red zone indicates the ifted as the lake level rose from 1432.5 m to 1435.8 m 72
	the variations in water quality from the incoming Pecos Lake and along Santa Rosa Lake
	rpycnal delta dynamics, we examined the seasonal regimes y parameter R
	paring monsoon and post-monsoon hyperpycnal flows based a
Figure 4.S1. Sonde time series of QA	QC data from monitoring sites
	ng water quality in Santa Rosa Lake (left), and the kayak e monitoring the Pecos River (right)83

Figure 4.S3. Simple linear regression analysis turbidity and suspended-sediment concentration	
data for U.S. Geological Survey stream samples on Gallinas River near Montezuma, NM	1
June 2022- Oct 2022	,∠
Figure 4.S4. Anoxic zone on Pecos river-Santa Rosa Lake delta on Aug 19, 2022	<u>;</u> ∠

List of Tables

Table 2.1. The Navigator component description and costs in USD, as of December 2022	13
Table 3.1. Empirical formulas used to compare mixing lengths.	44
Table 3.2. Hydrologic characteristics of the Rio Grande near Albuquerque, NM	45
Table 4.1. Lake conditions during the Lagrangian monitoring with The Navigator. Discharge values are contextualized with records.	65
Table 4.2. Average turbidity, temperature, total suspended sediments (TSS), and density of rive water and lake water for different Lagrangian monitoring days and the corresponding non-dimensional density parameter R	

Chapter 1

General Introduction

1.1 CONTEXT

The study of freshwater ecosystems is undergoing a transformative phase, shifting from the challenge of collecting sufficient data to measure processes to dealing with an abundance of signals and deciphering their meanings (Pellerin et al 2016; Arabi et al. 2020; Rode et al. 2016). Advances in technology, such as miniaturized sensors, real-time measurements, and autonomous platforms, have led to a growing quantity, frequency, and resolution of data (Horsburgh et al. 2015; McCabe et al. 2017; Krajewski et al. 2006; Griffiths et al. 2022). This has raised the possibility of a future where limnologists can simultaneously measure the rates of multiple processes at various scales and in near real-time (Glasgow et al. 2004), which would greatly benefit managers and scientists. However, the influx of data presents a challenge in distinguishing the desired signal from the noise of overlapping spatiotemporal scales (Blöschl et al. 2019; Kraus 2017).

In ecohydrology, determining the variables that can or need to be monitored is an initial step, as it provides the foundation for designing successful studies. From this, a selection of the type of pattern that will be used to explain observed processes follows, i.e., spatial, temporal, or a combination of both (Doyle and Ensign 2009). Temporal patterns, achieved through repeated observations at a fixed location over time (e.g., water quality data from a sonde at a fixed location), referred to as Eulerian monitoring, have yielded important insights to ecohydrologists (Romero et al. 2016; Burns et al. 2019). Another approach, which involves capturing purely spatial patterns at a specific moment in time, and is referred to as synoptic monitoring, has

gained popularity through advancement in satellite imagery (Casper et al. 2012; Krajewski et al. 2006). A third approach, which entails generating a single pattern that combines both temporal and spatial information by collecting data along a flow path, and is referred to as Lagrangian monitoring (e.g., water temperature data obtained from a drifting buoy) has been vastly underutilized in freshwater ecosystems, despite being standard practice in atmospheric and marine sciences (Gruberts et al. 2012, Bertani et al. 2016, Hensley et al. 2020). Within this context, the introduction and rapid adoption of Lagrangian monitoring techniques can be a means to link and integrate Eulerian and synoptic data, and increase our understanding of where, how, and why water quality and quantity change in time and space (Post et al. 2007; Ball et al. 2021; Kraus 2017) (Figure 1.1).

Lagrangian monitoring can enhance our understanding of freshwater ecosystems and contribute to effective and timely management of freshwater resources (Griffiths et al. 2022; Bertani et al. 2016; Brown, Battaglin, and Zuellig 2009). However, upfront and day-to-day costs remain prohibitively expensive in freshwater applications (Hensley et al. 2020). To date, the HYCAT by Xylem is the only complete solution that is commercially available, but its \$110,000-170,000 price tag is prohibitively expensive for most users.

This dissertation focuses on the development of The Navigator, an affordable (~\$5,100) and novel smart sensing Lagrangian monitoring technology that can collect water quality parameters and transmit data in real-time that are currently uncommon, i.e., at the sub-minute scale and following natural flow currents, resulting in better understanding of spatiotemporal patterns and improved predictions of water quality and quantity dynamics.

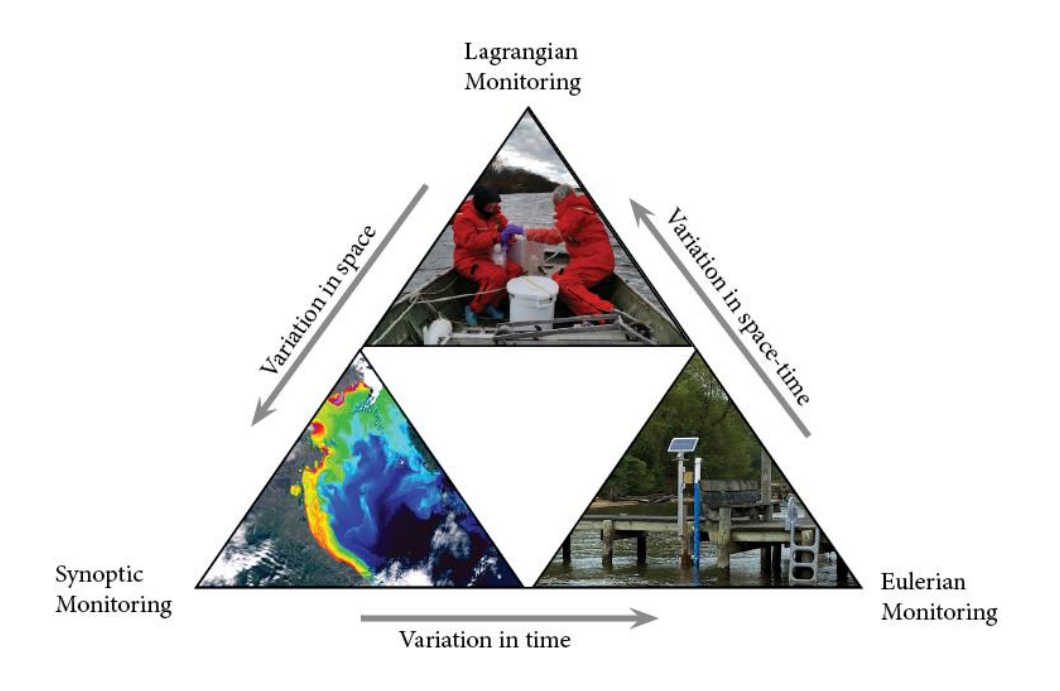


Figure 1.1. Monitoring approaches typically used in Ecohydrology.

1.2 OBJECTIVES

The specific objectives of my dissertation are:

- Design, deploy, and test The Navigator, an autonomous surface vehicle (ASV) for Lagrangian monitoring of freshwater ecosystems.
- Quantify experimental mixing lengths downstream of a wastewater treatment plant under various flow regimes and examine the predictive ability of long-standing empirical equations routinely used for predicting mixing lengths.
- 3. Investigate the role of a flood-control reservoir in controlling the propagation of wildfire disturbances generated from the Hermit's Peak-Calf Canyon through a combination of Eulerian and Lagrangian monitoring techniques.

1.3 DISSERTATION LAYOUT

Chapter 2 focuses on the design, development, and validation of The Navigator, a smart Lagrangian monitoring system. In Chapter 3 we quantified mixing lengths downstream of a wastewater treatment plant under various flow regimes using The Navigator. In Chapter 4 we used The Navigator to investigate the wildfire disturbance propagation from the Hermit's Peak-Calf Canyon wildfire. Lastly, Chapter 5 presents a comprehensive summary of the overall findings and conclusions derived from the research conducted throughout the dissertation.

1.4 CHAPTER REFERENCES

- Arabi, Behnaz, Mhd. Suhyb Salama, Jaime Pitarch, and Wouter Verhoef. 2020. "Integration of In-Situ and Multi-Sensor Satellite Observations for Long-Term Water Quality Monitoring in Coastal Areas." Remote Sensing of Environment 239 (March): 111632. https://doi.org/10.1016/j.rse.2020.111632.
- Ball, Grady, Peter Regier, Ricardo González-Pinzón, Justin Reale, and David Van Horn. 2021. "Wildfires Increasingly Impact Western US Fluvial Networks." *Nature Communications* 12 (1): 2484. https://doi.org/10.1038/s41467-021-22747-3.
- Bertani, I., M. Del Longo, S. Pecora, and G. Rossetti. 2016. "Longitudinal Variability in Hydrochemistry and Zooplankton Community of a Large River: A Lagrangian-Based Approach." *River Research and Applications* 32 (8): 1740–54. https://doi.org/10.1002/rra.3028.
- Blöschl, Günter, Marc F.P. Bierkens, Antonio Chambel, Christophe Cudennec, Georgia Destouni, Aldo Fiori, James W. Kirchner, et al. 2019. "Twenty-Three Unsolved Problems in Hydrology (UPH) a Community Perspective." *Hydrological Sciences Journal* 64 (10): 1141–58. https://doi.org/10.1080/02626667.2019.1620507.
- Brown, Juliane B., William A. Battaglin, and Robert E. Zuellig. 2009. "Lagrangian Sampling for Emerging Contaminants Through an Urban Stream Corridor in Colorado1." *JAWRA Journal of the American Water Resources Association* 45 (1): 68–82. https://doi.org/10.1111/j.1752-1688.2008.00290.x.
- Burns, Douglas A., Brian A. Pellerin, Matthew P. Miller, Paul D. Capel, Anthony J. Tesoriero, and Jonathan M. Duncan. 2019. "Monitoring the Riverine Pulse: Applying High-Frequency Nitrate Data to Advance Integrative Understanding of Biogeochemical and Hydrological Processes." WIRES Water 6 (4): e1348. https://doi.org/10.1002/wat2.1348.
- Casper, Andrew F., Barnali Dixon, Eric T. Steimle, Mike L. Hall, and Robyn N. Conmy. 2012. "Scales of Heterogeneity of Water Quality in Rivers: Insights from High Resolution Maps Based on Integrated Geospatial, Sensor and ROV Technologies." *Applied Geography* 32 (2): 455–64. https://doi.org/10.1016/j.apgeog.2011.01.023.
- Doyle, Martin W., and Scott H. Ensign. 2009. "Alternative Reference Frames in River System Science." *BioScience* 59 (6): 499–510. https://doi.org/10.1525/bio.2009.59.6.8.
- Glasgow, Howard B, JoAnn M Burkholder, Robert E Reed, Alan J Lewitus, and Joseph E Kleinman. 2004. "Real-Time Remote Monitoring of Water Quality: A Review of Current Applications, and Advancements in Sensor, Telemetry, and Computing Technologies." *Journal of Experimental*

- Marine Biology and Ecology, VOLUME 300 Special Issue, 300 (1): 409–48. https://doi.org/10.1016/j.jembe.2004.02.022.
- Griffiths, Natalie A., Peter S. Levi, Jeffery S. Riggs, Christopher R. DeRolph, Allison M. Fortner, and Jason K. Richards. 2022. "Sensor-Equipped Unmanned Surface Vehicle for High-Resolution Mapping of Water Quality in Low- to Mid-Order Streams." ACS ES&T Water 2 (3): 425–35. https://doi.org/10.1021/acsestwater.1c00342.
- Gruberts, Dāvis, Jana Paidere, Artūrs Škute, and Ivars Druvietis. 2012. "Lagrangian Drift Experiment on a Large Lowland River during a Spring Flood." *Fundamental and Applied Limnology*, January, 235–49. https://doi.org/10.1127/1863-9135/2012/0154.
- Hensley, Robert T., Margaret J. Spangler, Lauren F. DeVito, Paul H. Decker, Matthew J. Cohen, and Michael N. Gooseff. 2020. "Evaluating Spatiotemporal Variation in Water Chemistry of the Upper Colorado River Using Longitudinal Profiling." *Hydrological Processes* 34 (8): 1782–93. https://doi.org/10.1002/hyp.13690.
- Horsburgh, Jeffery S., Stephanie L. Reeder, Amber Spackman Jones, and Jacob Meline. 2015. "Open Source Software for Visualization and Quality Control of Continuous Hydrologic and Water Quality Sensor Data." *Environmental Modelling & Software* 70 (August): 32–44. https://doi.org/10.1016/j.envsoft.2015.04.002.
- Krajewski, Witold F., Martha C. Anderson, William E. Eichinger, Dara Entekhabi, Brian K. Hornbuckle, Paul R. Houser, Gabriel G. Katul, et al. 2006. "A Remote Sensing Observatory for Hydrologic Sciences: A Genesis for Scaling to Continental Hydrology." Water Resources Research 42 (7). https://doi.org/10.1029/2005WR004435.
- Kraus. 2017. "Ecohydrological Interfaces as Hot Spots of Ecosystem Processes Krause 2017 Water Resources Research Wiley Online Library." 2017. https://agupubs.onlinelibrary.wiley.com/doi/10.1002/2016WR019516.
- McCabe, Matthew F., Matthew Rodell, Douglas E. Alsdorf, Diego G. Miralles, Remko Uijlenhoet, Wolfgang Wagner, Arko Lucieer, et al. 2017. "The Future of Earth Observation in Hydrology." Hydrology and Earth System Sciences 21 (7): 3879–3914. https://doi.org/10.5194/hess-21-3879-2017.
- Pellerin et al. 2016. "Emerging Tools for Continuous Nutrient Monitoring Networks: Sensors Advancing Science and Water Resources Protection Pellerin 2019 JAWRA Journal of the American Water Resources Association Wiley Online Library." 2016. https://onlinelibrary.wiley.com/doi/abs/10.1111/1752-1688.12386%4010.1111/%28ISSN%291752-1688.open-water-data-initiative.
- Post, David M., Martin W. Doyle, John L. Sabo, and Jacques C. Finlay. 2007. "The Problem of Boundaries in Defining Ecosystems: A Potential Landmine for Uniting Geomorphology and Ecology." *Geomorphology*, 36th Binghamton Geomorphology Symposium, 89 (1): 111–26. https://doi.org/10.1016/j.geomorph.2006.07.014.
- Rode, Michael, Andrew J. Wade, Matthew J. Cohen, Robert T. Hensley, Michael J. Bowes, James W. Kirchner, George B. Arhonditsis, et al. 2016. "Sensors in the Stream: The High-Frequency Wave of the Present." *Environmental Science & Technology* 50 (19): 10297–307. https://doi.org/10.1021/acs.est.6b02155.
- Romero, Estela, Romain Le Gendre, Josette Garnier, Gilles Billen, Cédric Fisson, Marie Silvestre, and Philippe Riou. 2016. "Long-Term Water Quality in the Lower Seine: Lessons Learned over 4 Decades of Monitoring." *Environmental Science & Policy* 58 (April): 141–54. https://doi.org/10.1016/j.envsci.2016.01.016.
- Sushant C. 2018. "Water Quality Monitoring Systems Market by Component (PH Sensors, DO Sensors, Temperature Sensors, Turbidity Sensors, and Others) and Application (Utilities, Industrial,

Commercial, and Residential): Global Opportunity Analysis and Industry Forecast, 2018 - 2025." Market Overview.

UNM Rainforest Innovations Portfolio. 2022. "2023-005 - The Navigator: A Lagrangian Smart Sensing System to Characterize Aquatic Ecosystems." November 2022. https://innovations.unm.edu/technologies/technology-portfolio/.

Chapter 2

Development of The Navigator: A Lagrangian sensing system to characterize surface freshwater ecosystems.

Aashish Khandelwal¹, Tzion Castillo^{1,2}, Ricardo González-Pinzón¹

¹Civil, Construction and Environmental Engineering, University of New Mexico, Albuquerque, NM USA

²Electrical Engineering, University of New Mexico, Albuquerque, NM USA

This manuscript is currently in publication in the journal Water Research

2.1 INTRODUCTION

Recent advances in high-resolution sensors, real-time telemetry, analytical equipment, and computer technology, among others, have sparked the 'renaissance of hydrology' (Gabrielle, 2019). In the context of surface water quality dynamics, this technological revolution has enabled the monitoring of multiple solutes across the periodic table (Abbott et al., 2018; Burns et al., 2019; Kirchner and Neal, 2013; Rode et al., 2016), in some cases at sub-hour resolutions (Jarvie et al., 2018; Lloyd et al., 2016; Nichols et al., 2022), and over multiple decades (Dupas et al., 2018; Huang et al., 2022; Li et al., 2020; Matson et al., 2021). However, due to affordability issues, those advances have contributed to an improved understanding and management of surface water resources only in a small number of watersheds across the globe (Arsenault et al., 2023; Devaraj et al., 2022). To date, thus, we still lack reliable, continuous, and consistent information on the extent and dynamics of surface water quantity and quality at local, regional, and global scales (United Nations Environment Programme, 2021). To tackle this shortcoming,

the UN's sustainable development goal 6 (SDG6) aims to increase data availability for evidence-based management, regulations, and policymaking to "ensure access to water and sanitation for all".

While satellite observations can help monitor regional-to-continental scale processes (e.g., evapotranspiration, intercontinental water and dust fluxes) and help identify relevant large-scale features (e.g., anoxic zones, flooding, and hurricanes) (Arabi et al., 2020; Li et al., 2022; Román et al., 2019; Wieland and Martinis, 2019), the temporal and spatial resolution of their information is typically inadequate to support local-to-regional scale decision-making associated with the management of surface water resources (Manfreda et al., 2018; Tapley et al., 2019). These limitations have kept Eulerian monitoring, i.e., the tracking of water quantity and quality at a site and over time, as the current standard technique applied in consulting, research, and enforcement of regulations associated with freshwater resources (Doyle and Ensign, 2009).

Eulerian monitoring of surface freshwaters can be done through grab sampling followed by laboratory analyses or semi-continuous sensors in situ (e.g., optical and wet-chemistry sensors) and has been used to quantify water quantity and quality dynamics at sub-hour to monthly frequencies. Eulerian monitoring is spatially limited due to the sparseness of instrumented sites, and this is particularly inconvenient for analyses featuring highly heterogeneous and rapidly changing environments (Krause et al., 2015). Also, since Eulerian monitoring fundamentally integrates the spatial heterogeneity, dynamics, and watershed modifications upstream of the monitoring site (González-Pinzón et al., 2019), this technique falls short when linking causation and correlation. Some of the most common examples of these challenges are differentiating between point and distributed sources of contamination in water quality assessments and separating rainfall, snowmelt, and groundwater contributions from

stream flow measurements. An alternative to overcoming some of the challenges of Eulerian monitoring is the use of Lagrangian monitoring, where water parcels are tracked as they move through aquatic systems.

Lagrangian monitoring of surface waters can be done with crews sampling or monitoring from a moving vehicle (e.g., boat or kayak) or using instrumented autonomous surface vehicles (ASVs; also known as uncrewed surface vehicles USVs). Due to the intractability and remoteness associated with Lagrangian monitoring, and high personnel costs, there is a strong demand for ASVs. While Lagrangian monitoring has been widely used in oceanography using drifters (Subbaraya et al. 2016) and in atmospheric studies using balloons (Businger et al., 1996), its upfront, maintenance, and operational costs remain prohibitively expensive for the monitoring of surface freshwater ecosystems. Currently, most commercially available ASVs for freshwater ecosystems are adaptations of ASVs used in oceanography, which has resulted in large-size and costly vehicles for example, the Teledyne Z-Boat 1800RP.

The advantages brought by Lagrangian monitoring can be better explained by comparing Eulerian and Lagrangian monitoring of a marathon race and the propagation of a disturbance in a river corridor. After the start of the events, Eulerian monitoring helps quantify what happens over time at fixed cross-sections, such as the finish line or a bridge. Therefore, Eulerian-based statistical analyses are limited to piece-wise rankings, histograms (or probability density functions), percentile analyses, and averages. On the other hand, Lagrangian monitoring would let us link spatiotemporal variations of relevant quantities such as stride length, cadence, heart rate, vertical oscillation, ground contact time, and speed for a runner, or temperature, dissolved oxygen, turbidity, and other water quality parameters changing as the disturbance moves downstream. The only requisite is that runners and rivers 'wear' sensors. From those individual

quantities and the relationships among them, e.g., change of heart rate as a function of change in elevation and change in dissolved oxygen levels as a function of turbidity, more robust spatiotemporal analyses can be performed to characterize a runner's performance during a marathon or a river's response to a disturbance.

Since most of the progress made to date in the study and management of freshwater ecosystems is based on the use of Eulerian monitoring, any productive discussion about ways to improve the monitoring of freshwater ecosystems should consider strengthening the capabilities of existing infrastructure. For example, there are over 10,000 USGS streamflow stations around the US, and some are also instrumented with water quality sensors ("USGS WaterWatch -- Streamflow conditions," n.d.). However, to our knowledge, there is no active program pursuing Lagrangian-based monitoring between sites located along river corridors. Integrating more traditional Eulerian monitoring sites with Lagrangian capabilities, thus, can help researchers, consultants, and stakeholders better understand *where*, *how*, and *why* water quality and quantity change in time and space.

In this chapter, we present the development of an ASV, *The Navigator*, with sensing technology to collect and transmit water quality data in real-time over spatial and temporal scales that are currently uncommon, i.e., at the sub-minute scale and following flow currents or GPS waypoints. We describe the components and architecture of The Navigator and demonstrate its applicability in the Lagrangian monitoring of surface water bodies in New Mexico (USA) to: 1) identify water quality changes associated with land use changes along a 7th-order reach in the Rio Grande, 2) identify the fate of wildfire disturbances ~175 km downstream of a burned watershed affected by the largest wildfire ever recorded in the state, 3) monitor the water quality of a recreational fishing pond in the City of Albuquerque.

2.2 METHODS

2.2.1 The Navigator: Overview

The Navigator features a GPS tracker to monitor spacetime variations and to allow the recovery of the vehicle, a thruster and rudder system that can be automated using an autopilot, a data logger that can be coupled to water quality sensors (i.e., optical, wet chemistry, fluorometers), and real-time data transmission capabilities through LTE cellular service. The Navigator is ideal for Lagrangian monitoring applications in river systems without major obstructions, irrigation and drainage channels, and lentic systems (e.g., lakes, reservoirs, estuaries). The Navigator can monitor water quality parameters over longer durations than other ASVs commercially available, is lighter than other alternatives (2.5-5x lighter), and can be coupled to different sensor heads, offering high versatility. Figure 1 and Table 1 present all parts included in The Navigator and their assemblage to make the system work. Supplementary Information A1 provides access to a 3D-CAD view of The Navigator.

2.2.2 Structure and Hardware Design

We used a catamaran (i.e., twin hulls) framework to create a small-size vehicle with minimum flow resistance, better stability, and higher payload (Ferri et al., 2015). Each hull (C1 in Table 1) is made of expanded polystyrene (XPS) foam and has three layers of fiberglass outside. The two hulls are connected by a carbon fiber rod structure using 3D-printed brackets attached to the hulls (C2 in Table 1). A Pelican box (C3) houses electronics and batteries and is fastened to the front two carbon rods (C1). The thruster (C4) and servo (C5) with rudder are mounted on the back rods (C1). Since the vehicle's weight is distributed over two hulls, The

Navigator has a shallow draft of 125 mm.

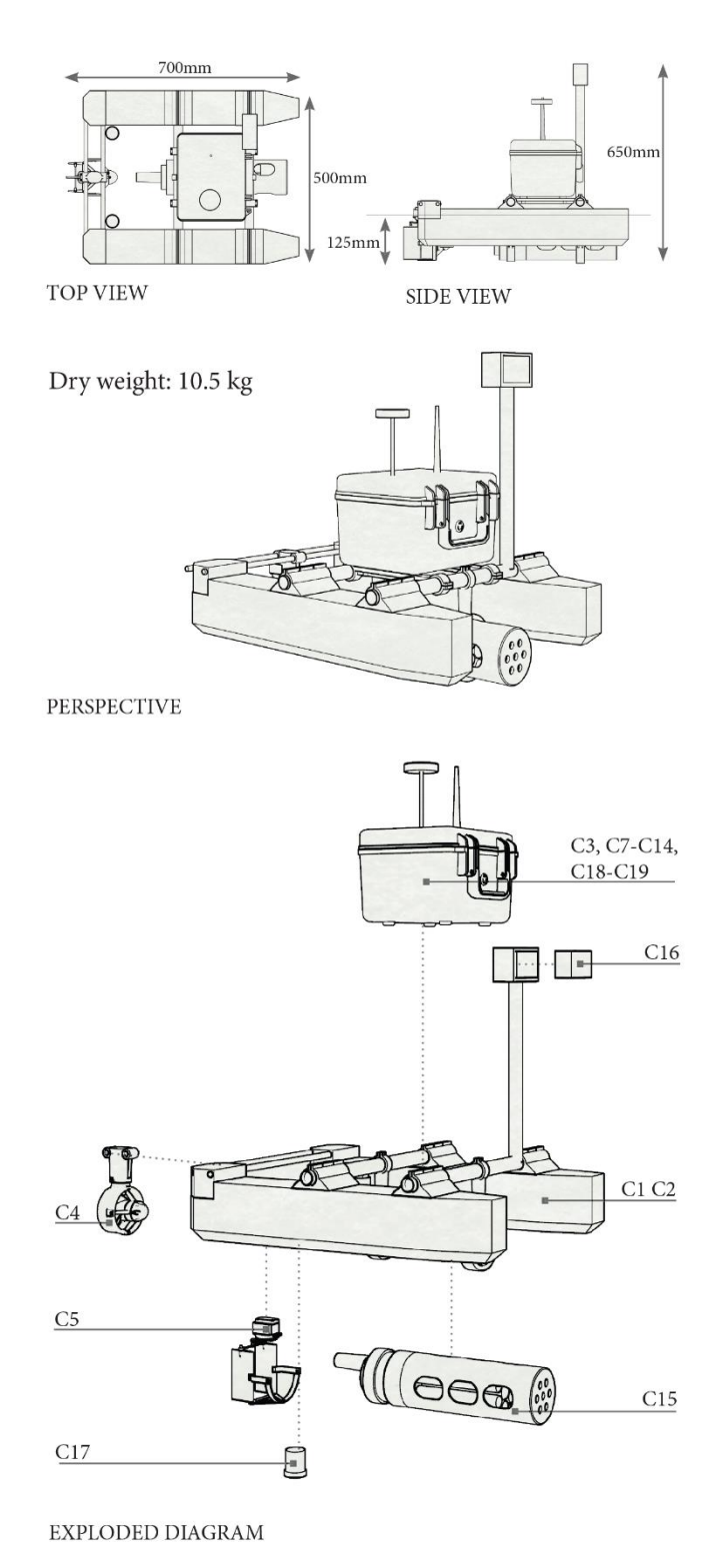


Figure 2.1. Figure 1: The Navigator: parts, design and exploded diagram. The dimensions and 3D printed models in CAD can be accessed here: <u>The Navigator CAD model</u>. Part descriptions are available in Table 1.

Table 2.1: The Navigator component description and costs in USD, as of December 2022.

1	Table 2.1: The Navigator component description and costs in USD, as of December 2022.			
Part	Name	Image	Description	Cost (YY 2022 USD)
C1	Hull: Fiberglass with Foam and carbon fiber rods		An insulation foam sheet with a thickness of 5.1 cm is used for the hull's shape. Three layers of fiberglass cloth (50 m²) were coated outside using epoxy resin and hardener (250 ml). Carbon rods are used as beams.	\$110
C2	3D printed components		Approximately 1 kg of acrylonitrile butadiene styrene (ABS) filament was used for 3D printing the rudder and carbon rod connections to provide durability and UV resistance to The Navigator.	\$22
C3	Protector case: Pelican		This rugged case features an automatic purge valve that equalizes air pressure and a watertight silicone O-ring lid. This case protects all the hardware in The Navigator from impacts and water splashes.	\$80
C4	Thruster: Blue Robotics T200		The T200 thruster is a popular underwater thruster used for The Navigator. Its flooded motor design makes it powerful, efficient, compact, and affordable.	\$236
C5	Digital Servo: Annimos 20KG with 5V power converter	20% a state of the	This Annimos 20KG digital servo with high torque and full metal gear is waterproof and helps control the steering of The Navigator with a control angle of 270°.	\$16
C6	Radio Transmitter: Emax E8		A 2.4GHz dual band antenna radio transmitter features an 8 channel RF module.	\$59
C7	Wing Receiver: RadioMaster R88		2.4GHz radio receiver for remote control, with a range of ~1 km.	\$20
C8	Autopilot: Cube purple with mini carrier		This autopilot is designed to control boats, cars, or rovers. It provides hardware and an embedded software ecosystem to automate autonomous maneuvering in The Navigator.	\$340

Part	Name	Image	Description	Cost (YY 2022 USD)
C9	GPS: Here 3	The Course of th	This GPS is a high-precision global navigation satellite system (GNSS) that supports real time kinematic (RTK) positioning and is built with controller area network (CAN) protocol. It is also designed to be dust-proof and splash-proof, which is ideal for The Navigator.	\$125
C10	Telemetry Radio Transmitter and Receiver: 3DR		915MHz transmitter and receiver, responsible for relaying images between the ASV and ground station computer with a range of 3-5km.	\$88
C11	Lithium polymer battery: Ovonic	Sand Sand	Set of 4 Lithium polymer batteries, Voltage: 11.1V, Cell: 3S, Capacity: 5500mAh, Discharge: 50C. These batteries power every component of The Navigator.	\$55
C12	Solar panel: Eco Worthy 25W 12V		Waterproof solar panel 41.9 cm x 32 cm capable of providing 25W. This panel helps extend battery life.	\$36
C13	Solar Charge Controller: GV-5	DENSAL CHARMS NAME OF THE PROPERTY OF THE PRO	This controller acts as an interface between the solar panel and the batteries, preventing them from overcharging.	\$99
C14	Microcontroller: Raspberry Pi 4		The Raspberry Pi 4 is a powerful, user- programmable microprocessor board that can be easily programmed with several popular IDE software programs like Linux. It includes LTE and Bluetooth communications for The Navigator.	\$100
C15	Multiparameter sonde: Yosemitech Y4000	40000	The Yosemitech Y4000 multiparameter sonde is one of the most comprehensive and affordable water quality monitoring products available to monitor dissolved oxygen, conductivity, turbidity, pH, chlorophyll, blue-green algae, and temperature.	\$3,100
C16	Spatial AI stereo camera: OAK-D Lite	0 0	The OAK—D Lite is a spatial AI powerhouse, capable of simultaneously running advanced neural networks while providing depth from two stereo cameras.	\$149
C17	Ping Sonar: Blue Robotics		The Ping Sonar is a single-beam echosounder that measures distances of up to 50 meters underwater. A 30° beam width and an open-source software interface make it a powerful tool for The Navigator.	\$360

Part	Name	Image	Description	Cost (YY 2022 USD)
C18	LTE modem dongle: ZTE MF833V		4G LTE USB modem dongle provides a mobile internet connection to the Raspberry Pi and real-time data transfer.	\$50
C19	Penetrator: Blue Robotics WetLink		This item is used to seal electrical cables as they pass into a component or through a pelican case. Each set includes a bulkhead, seal, plug, O-ring, and nut.	\$56
Total cost (YY 2022 USD)			\$5,101	

The thruster (C4) can provide a thrust force of ~3 kg providing a cruise velocity of ~0.8m/s. The digital servo (C5) controls the steering, using a dual rudder design capable of providing sharp turns (0.75m turning radius). The servo's maximum torque is up to 21.5 kg/cm @6.8V. The dual rudder system (C2) connected to the servo was designed and manufactured by us and is 3D printable. The thruster is fixed, while the rudder is mounted directly behind the thruster.

The Navigator has two maneuvering modes: 1) drift mode, controlled by the operator, and 2) autonomous mode, following GPS waypoints. For drift mode, the operator controls a radio transmitter (C6). The commands sent by the operator are received by the radio control receiver (C7).

During autonomous mode, the autopilot (C8) gets continuous geolocation, roll, pitch, and heading data from GPS data (C9). This allows it to hold the course and follow GPS waypoints. The user can change between autonomous and drift modes using a switch on the controller (C6). The geolocation, depth, roll, and pitch information are transferred continuously to the user using a telemetry transmitter with a range of ~5km (C10) on The Navigator and a matching receiver (C10) attached to a field laptop can be affected by terrain factors. Power is supplied to The Navigator through four packs of lithium polymer batteries (C11). In our tests, this power provided a range of ~30 km in autonomous mode. A small solar panel (C12) and a controller

(C13) were added to extend the battery's capacity. Lithium batteries (C11) were selected because they provide a better weight-energy density ratio, high performance, and longevity. A 12V power converter is used to supply the sonde, and a 5V power converter is used to power the servo (C5) and the microcontroller board Raspberry Pi (C14).

The Navigator includes a multiparameter water quality sonde Yosemitech - Model Y4000 (C15). We chose this sonde due to its compact size, low cost, and ease of integration. The Y4000 monitors dissolved oxygen, conductivity, turbidity, pH, chlorophyll, and temperature. An integrated wiper system can prevent biofouling, air bubbles, and debris, thus reducing erroneous data. The multiparameter sonde is controlled using the Raspberry Pi board (C14) to define temporal resolution, deploy the sensor heads, and save data files. The sonde can be calibrated using the multi-sensor PC tool by Yosemite Technologies.

The Navigator features an OAK-D Lite 13MP depth camera (C16) to collect field photographs and a 30-degree single-beam echosounder ping sonar (C17) to measure depth. The camera is connected to the Raspberry Pi board (C14) and the sonar is connected to the autopilot (C8). The Navigator has an LTE modem with a cellular SIM card (C18) connected to the Raspberry Pi (C14) to transfer real-time data that can be shared worldwide. Finally, penetrators (C18) are used to have watertight seal electrical cables as they pass into the pelican case (C3).

2.2.3 Software Design

The Navigator software provides easy-to-replicate and customized monitoring solutions to a broad range of users, and all our code is publicly hosted on GitHub (see Supplementary Information A2). The Navigator uses an Ubuntu Desktop 22.04.1 LTS Linux operating system running on the Raspberry Pi 4 4GB (C14). The software is designed as a set of Robot Operating System 2 (ROS2) nodes. To understand the architecture of our software, it is necessary to

understand the ROS2 ecosystem it is built on. When using ROS2, the code is organized into packages containing nodes based on their function, and those nodes communicate with each other through messages. The nodes create and observe such messages by publishing and subscribing to specific topics. This provides flexibility, as users can integrate additional ROS2 packages to fit their needs without modifying already integrated nodes. Within the code developed for The Navigator, we have several nodes responsible for a task onboard the vehicle. Figure 2 presents the architecture of our software, with representative titles for the roles of the nodes and connections showing the topics that the nodes communicate through publishing and subscription.

The Autopilot system uses ArduPilot's ArduRover version 3.5.2 firmware. The Autopilot requires setup and calibration tasks, which are well-documented on the ArduPilot website. The operator needs to install a ground station on their field laptop to communicate with the Cube autopilot (C8) through the telemetry radio (C10). The data transmitted include GPS waypoints, battery health, the autopilot's sensor health, etc. We used ArduPilot's Mission Planner software because it is the most popular and has an extensive database with community support and documentation. Other options include APM Planner and QGroundControl, among others. No modification of The Navigator source code is required to switch between ground stations software.

The ground station, which may be housed at an onshore building, a mobile unit, or a boat, is crucial for deploying The Navigator. The ground control station's primary equipment is a laptop with ground control software installed. Additional components are a USB telemetry transmitter (C10) connected to the computer and an RC transmitter (C6). Wireless communication methods via telemetry transmitters are generally used to assign missions to The

Navigator. The ground station keeps track of the status of The Navigator and its onboard hardware and sends control instructions to remotely operated missions.

We used Ubidots to create a website to communicate with The Navigator and visualize and download data. Ubidots provides a free tier for educational use and is easy to set up. We created a simple interface for viewing previous data over a wide time range, visualizing real-time updates when data are received, and restricted viewing access as specified by the user. Any website using HTTP could be used to communicate with The Navigator, but some slight modification of The Navigator source code would be necessary. The data sent to the website includes sonde readings, camera status, and GPS locations. Data are displayed as time-series plots with colored ranges and a map with pinpoints. The data are sent through the onboard USB LTE modem (C18).

We used the Luxonis Depth AI platform to save images taken from the Oak D lite camera (C16) in The Navigator. This platform combines artificial intelligence, computer vision, depth perception (Stereo, ToF), and segmentation. We programmed Luxonis Depth AI to save images for our initial field tests.

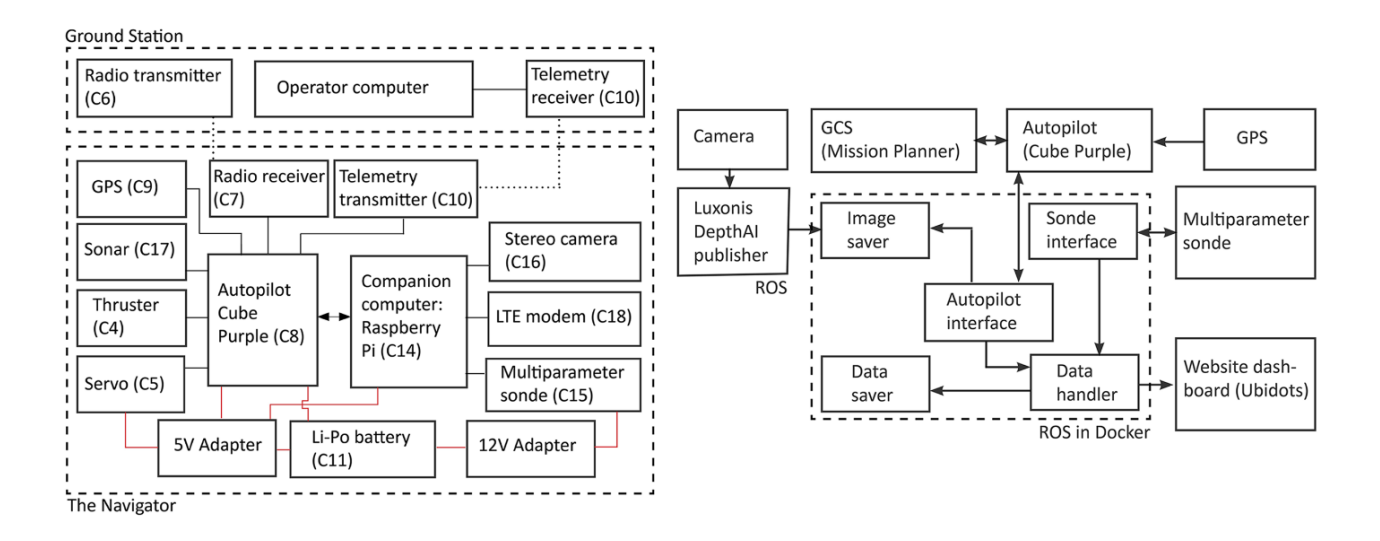


Figure 2.2: The Navigator hardware (left) and software schematic (right).

2.3 VALIDATION AND FIELD TESTING

We tested The Navigator in three applications. First, the Lagrangian monitoring of a 7th-order river reach in the Rio Grande using the drifting mode to understand where, how, and why water quality changes. Second, we monitored Santa Rosa Lake following GPS waypoints to characterize post-fire disturbances from the largest recorded wildfire in New Mexico, i.e., the Hermits Peak-Calf Canyon wildfire that occurred in the spring of 2022. Third, we monitored a small urban detention pond in the City of Albuquerque using the autonomous mode to collect high spatial resolution water quality data and depth along a grid path.

Before each field day, we calibrated each sensor following the manufacturer's recommendations. With the field information collected from water quality sensors and GPS data, we generated heatmaps using R's spacetime and trajectories package (Pebesma, 2016). These heatmaps (KMZ graphic format) were later imported into Google Earth to create layered water quality maps to display water quality data in a longitudinal framework.

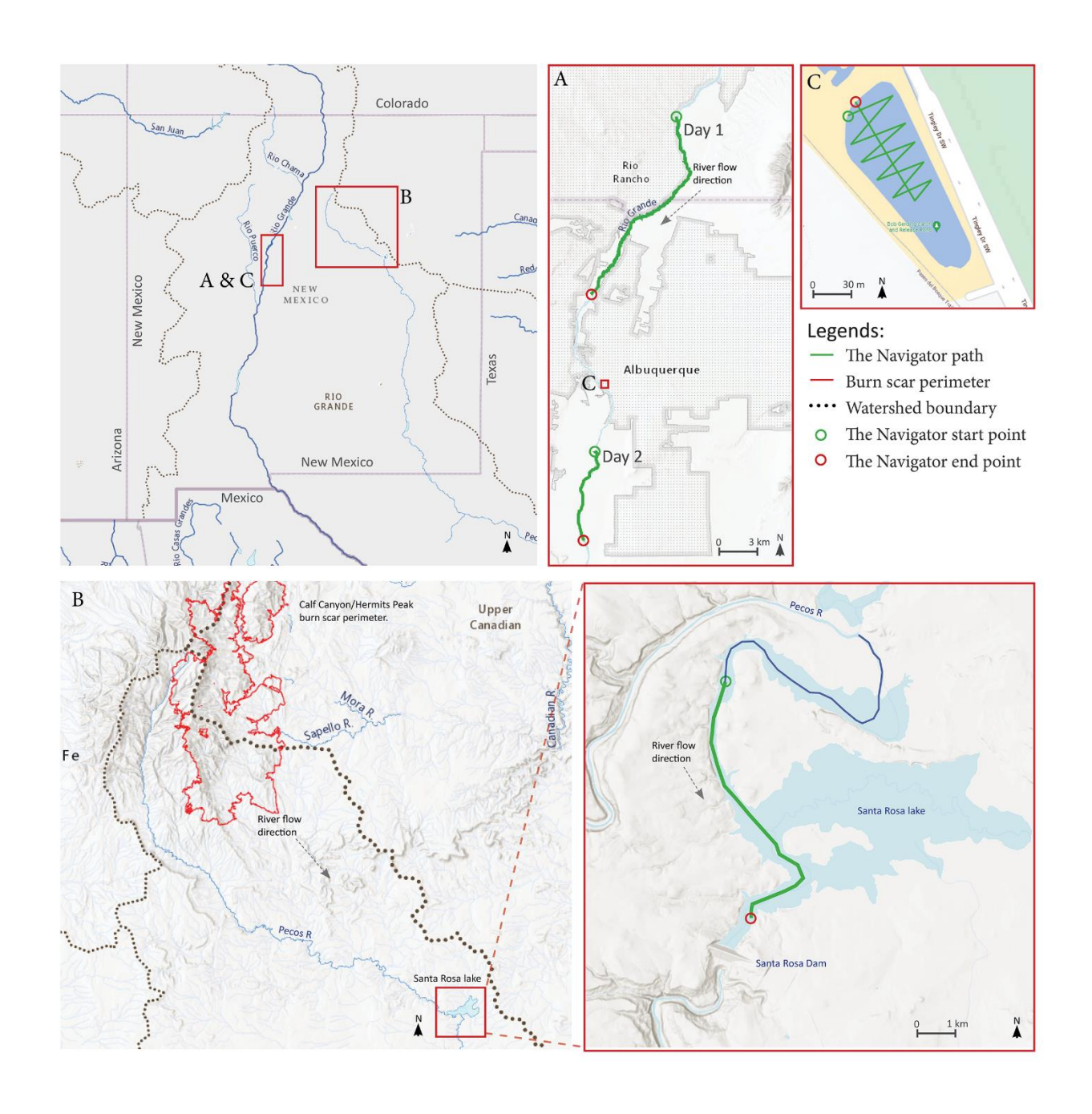


Figure 2.3: A Map of New Mexico, USA, with red boxes enclosing the study sites. A) 7th-order study reach along the Rio Grande where The Navigator was used in drifting mode on day 1 (May 19th, 2022) and day 2 (May 20th, 2022). B) Hermit's Peak-Calf Canyon Fire perimeter in red and boundaries of the impacted watershed draining to Santa Rosa Lake. The Navigator was deployed in autonomous mode to follow a waypoint path across the lake on August 19th, 2022. C) Recreational fishing pond in the City of Albuquerque, where The Navigator was deployed in autonomous mode following a grid pattern on November 11th, 2022.

2.3.1 The Navigator: Drifting Mode Operation

On May 19 (day 1) and May 20, 2022 (day 2), we monitored 28.43 km of the Rio Grande near the City of Albuquerque in drifting mode, i.e., moving with the river's current. The watershed draining area is ~37,221 km² and features ~55% shrub and grassland, 36% forest, and ~2.8% developed land ("Model My Watershed," n.d.). The study reach starts ~58 km downstream of Cochiti Lake, a flood and flow control reservoir that removes sediment from the river (Massong et al., 2010). This section of the river features the City of Rio Rancho's wastewater treatment plant (WWTP) return effluent, the City of Albuquerque's water intake for drinking supply, storm and agricultural return flow channels, and the City of Albuquerque's WWTP return effluent. Due to low flow conditions, i.e., 21.8 m³/s compared to a 30-year median of 70 m³/s (USGS gage 08330000), we were not able to collect data along a 15.3 km reach between Montaño Bridge and Rio Bravo Bridge (Figure 3A) because the flow was too shallow and unsuitable for The Navigator. The United States Geological Survey (USGS) operates several stream gages in this reach, i.e., USGS 08329918 at Alameda Bridge, USGS 08329928 near Paseo Del Norte Bridge, and USGS 08330830 at Valle de Oro, which we used to report flow data.

We collected data every 2-min for 5 h and 48 min on day 1 and for 4h and 52 min on day 2. This corresponded to an average of one sampling event every 114 m on day 1 and every 80 m on day 2. The Navigator collected GPS, turbidity, pH, temperature, dissolved oxygen (DO), and specific conductivity (SC) data (Figure 4 and Figure S1). We activated the remote steering controller only when the vehicle was drifting near thick riparian vegetation and near the diversion dam used by the water treatment plant's intake facility. We followed The Navigator

using a kayak through the study reaches and verified the functioning of real-time data telemetry with the Ubidots website dashboard.

The data collected by The Navigator revealed spatial and temporal changes in water quality parameters (Figure 4). On day 1, we observed an increase in water temperature from 17.0 to 22.6 °C (Figure 4), which may be due in part to daily changes in air temperature over the monitoring period. We also observed a longitudinal increase in specific conductivity from 273.3 to 291.7 μS/cm, with abrupt changes near releases from the WWTP of the City of Rio Rancho (i.e., 273.8 to 299.6 μS/cm) and runoff outlets from unlined channels or arroyos (i.e., 281.3 to 290.4 μS/cm). These changes were local as lateral discharges were orders of magnitude smaller than that from the Rio Grande, e.g., ~0.3 m³/s in the Rio Rancho WWTP and 23.4 m³/s in the river. During our monitoring, the inflatable diversion dam controlling the water intake from the Rio Grande into the water treatment plant of the City of Albuquerque was raised and created water stagnation upstream and high turbulence downstream. To avoid the dam, we directed The Navigator to the fish bypass channel and detected changes in turbidity from 33-37 FNU upstream to 40-49 FNU downstream.

On day 2, The Navigator registered drastic water quality changes as it passed through the Albuquerque WWTP outfall, which has a maximum capacity of 76 MGD (i.e., $3.3 \text{ m}^3/\text{s}$), making it the largest in New Mexico. That day, the Rio Grande's average flow was $18.9 \text{ m}^3/\text{s}$, and the ABQ WWTP effluent discharge was $2.3 \text{ m}^3/\text{s}$. We recorded specific conductivity values increasing from $276.1 \text{ to } 689.8 \text{ }\mu\text{S/cm}$ and temperatures rising from $18.7 \text{ to } 22.9 ^{\circ}\text{C}$ (Figure 4). The temperature and conductivity values gradually decreased downstream of the WWTP point source for $\sim 4 \text{ km}$ and then rose gradually as a part of a diel cycle. Similarly, The Navigator registered changes in DO from 6.5 to 5.3 mg/L, turbidity from 53.1 to 8.8 FNU, and pH from $8.1 ^{\circ}$

to 7.1. These values also gradually rose to those upstream of the Albuquerque WWTP. This study shows how The Navigator can monitor water quality parameters at higher spatial and temporal resolutions, supporting identifying sources and assessing their impacts at spatial scales unattainable by Eulerian monitoring or grab sampling.

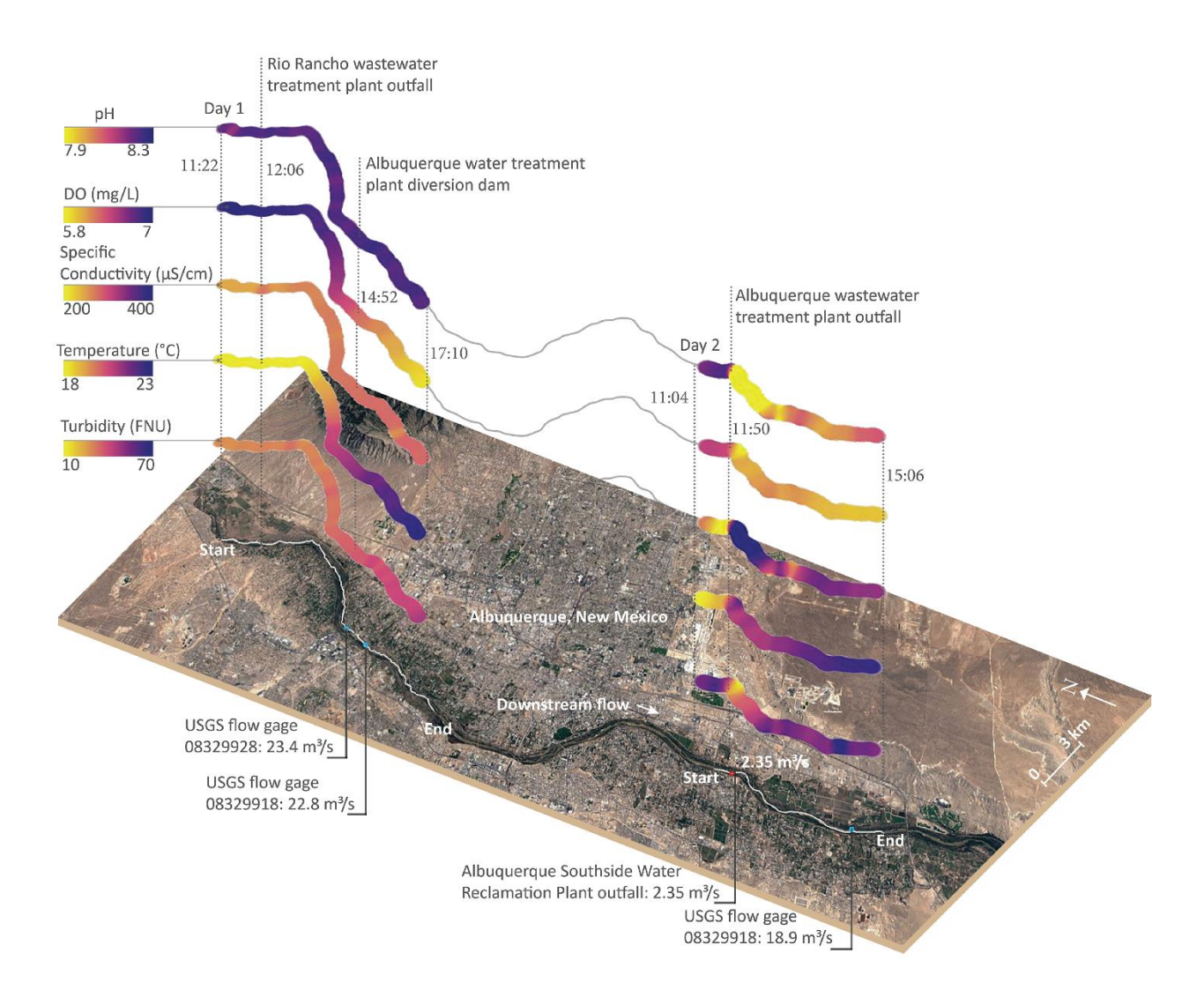


Figure 2.4: Longitudinal heatmap profile of water quality parameters collected by The Navigator along the Rio Grande River near Albuquerque, NM. The blue dots indicate USGS flow gages, green shade indicates low values and red indicates high values. Clock time is indicated in hh: mm.

2.3.2 The Navigator: Autonomous Mode Operation Following GPS waypoints

The Navigator is equipped with an autopilot system capable of following GPS waypoints to track water quality changes autonomously. With support for site access from the US Army Corps of Engineers (USACE) Albuquerque District, we conducted a high-resolution Lagrangian monitoring of water quality changes associated with the mobilization of wildfire disturbances after the Hermit's Peak-Calf Canyon Fire (Figure 2.3 B). To contextualize, as of early 2023, this wildfire is the largest ever recorded in New Mexico and burned 138,188 hectares between April and June 2022. The fires began from out-of-control prescribed burns ("Hermit Peaks Fire," 2022) and expanded aggressively due to sustained high-wind and dry conditions that are part of a climate change-induced megadrought gripping vast areas of the western United States (Freedman and Fears, 2020). Postfire, after the storms from the monsoon season started to mobilize burned materials from the burned area into Gallinas Creek and into the Pecos River, we monitored water quality from Santa Rosa Lake and its upstream delta, which are located ~175 km downstream from the burn scar perimeter.

Since our goal was to determine how the discontinuity of a river system brought by a flow-regulating dam impacts the propagation of wildfire disturbances in a fluvial network, we monitored the Pecos River Delta-Santa Rosa Lake transition for ~8 km at a fine sampling spatial scale of about one sample every 64 m. The study was conducted on August 19, 2022, after a precipitation event of 9.4 mm fell over the burn scar on August 17-18, 2022 (USGS Atmosphere gage 354150105275301) and mobilized debris and sediments. The longitudinal monitoring followed the direction of the flow, which was 13.1 m³/s, exceeding the median of 1.0 m³/s between 1977-2022 (USGS gage 08382650) ("USGS WaterWatch -- Streamflow conditions,".).

The Navigator's data revealed drastic changes in the spatial patterns of water quality parameters (Figure 5). DO transitioned from ~ 6 mg/L in the Pecos River upstream of the delta, to anoxic conditions (~0 mg/L) near the delta, and then rose as the water reached the dam. The DO sag and recovery patterns were inversely proportional to the turbidity values, suggesting that microbial respiration or chemical oxygen demands (DO sink) and photosynthesis (DO source) were largely controlled by sediment fluxes from the wildfire (Ball et al. 2021; Smith et al. 2011; Reale et al. 2015). pH values were lower in zones with low DO, suggesting increased aerobic microbial metabolism and CO₂ releases associated with the high influx of sediment from wildfire material (Chapra, 2008). Specific conductivity and temperature increased along the flow path following the DO trend. During the monitoring activity, high sediment loads come from Gallinas Creek and the Pecos River sinking along the delta due to the reduced flow velocity. We also saw floating debris and bubbles from wildfire disturbances remaining near the surface of the lake.

Our monitoring with The Navigator indicated drastic changes in water quality parameters over short distances along the lake in response to post-wildfire rainfall-runoff events occurring hundreds of kilometers upstream. This allowed us to identify hotspots and plausible sources and sinks of physicochemical parameters. Since the monitoring lasted <2h, our data from the lake are not as affected by diel cycles as those from the Rio Grande. This study with The Navigator helped us understand how lakes affect the longitudinal propagation of wildfire disturbances along fluvial networks, acting as sinks and resetting the mobilization of wildfire material that becomes part of the lakebed. Our results bring into focus the importance of longitudinal monitoring and highlight the importance of selecting adequate sampling locations and spatial coverages.

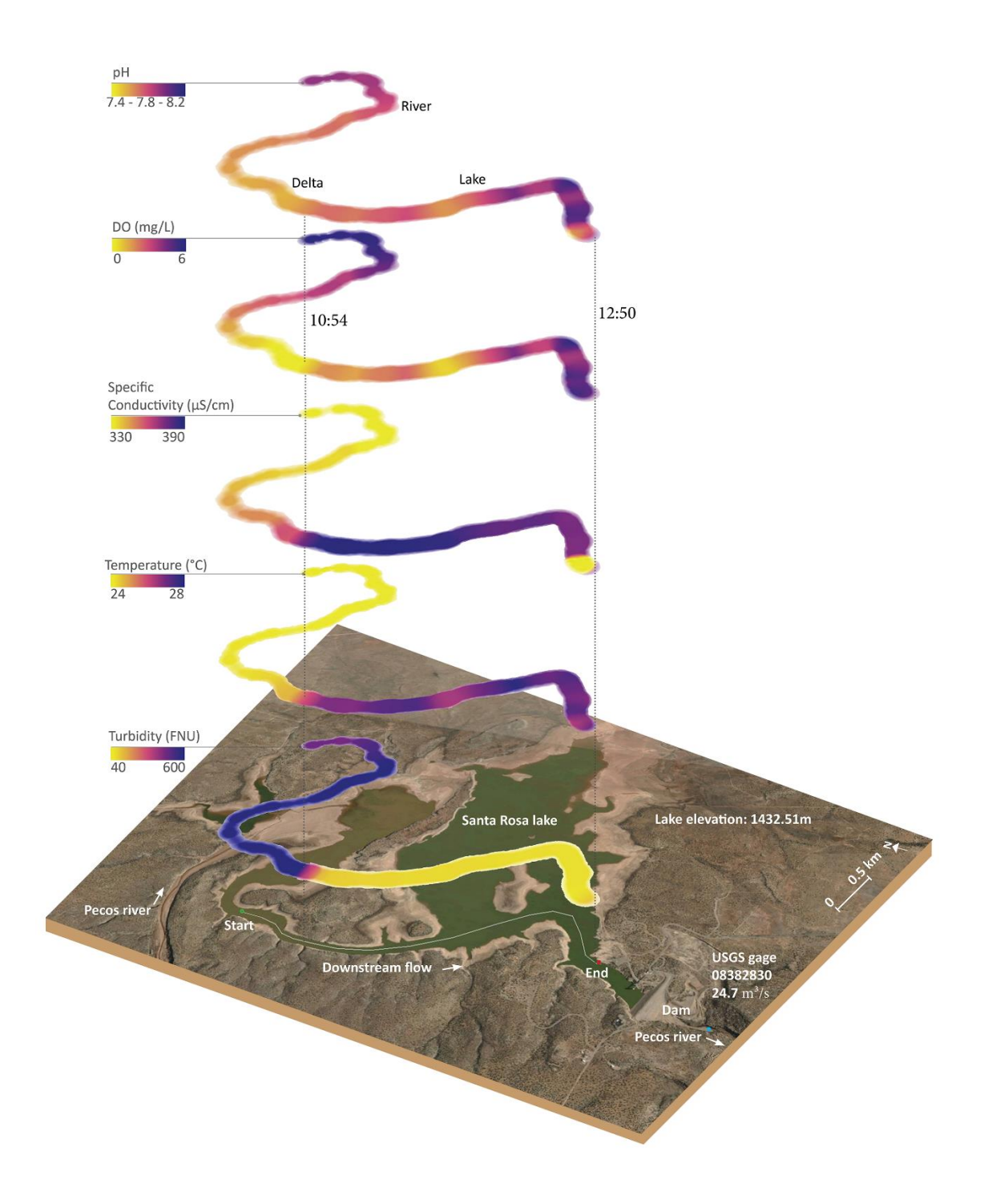


Figure 2.5: The Navigator is monitoring Santa Rosa Lake, NM, to understand the water quality impact of monsoon runoff on the reservoir from the Hermit peaks/ Calf Canyon wildfire. The blue dot indicates USGS flow gages for Pecos River below the dam; green indicates low values, and red indicates a high value for water quality parameters. Clock time is in hh: mm.

Following a grid path.

On November 11, 2022, we deployed The Navigator in a recreational fishing pond in the City of Albuquerque (Figure S3). We used a GPS grid path mission of 400 m to monitor the north side of the pond using Mission Planner. This monitoring activity lasted 25 min, was completed at an average speed of 0.27 m/s, and used a sampling frequency of one sample per minute, amounting to about one sample every 16 m. The Navigator monitored turbidity, pH, temperature, DO, conductivity, oxygen reduction potential (ORP), and chlorophyll-A. We also added the depth sonar and an Oak D-lite camera. We chose a zig-zag grid path to gather high spatial resolution of water quality parameters and test the vehicle's maneuverability.

As expected, we observed minimum changes in surface water quality parameters due to the small size of the pond and the short duration of our test (Figure 6). Even though the pond is relatively deep with respect to its surface area, the sensors in The Navigator cannot reach deeper layers to detect vertical heterogeneities. The values observed in this short study fall within expectations for low sediment, small ponds. Logistically, this test is analogous to monitoring a point source or the confluence of two streams. Thus, the autonomy of The Navigator would allow researchers and practitioners to monitor wide water bodies from a single location while collecting high spatial resolution data on water quality parameters and depth.

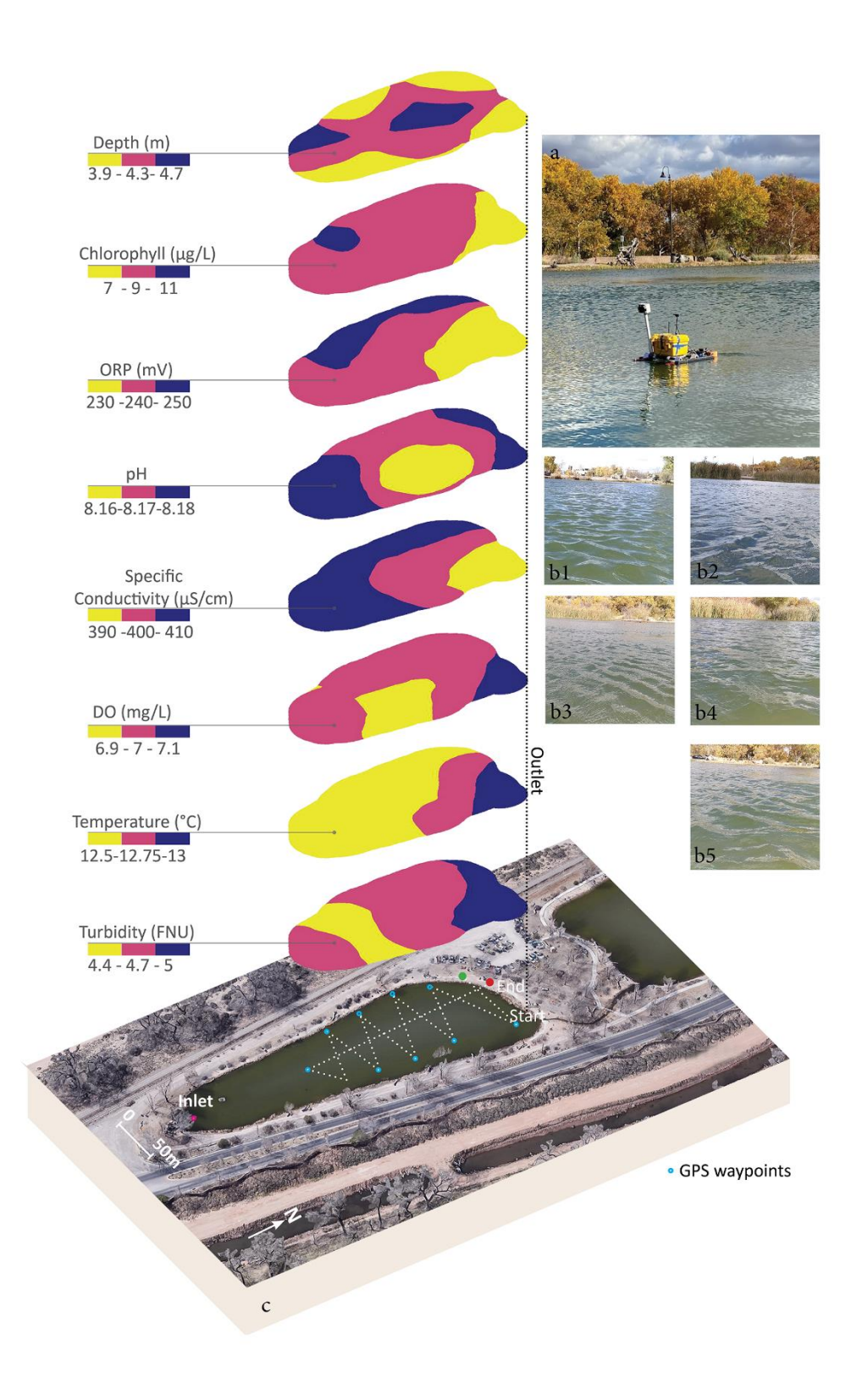


Figure 2.6: a) The Navigator monitoring the Bob Gerding catch and release pond, Albuquerque, NM. b1-b5) Images captured by The Navigator while monitoring. c) Heatmap of the water quality parameters and depth data collected by The Navigator.

2.4 THE NAVIGATOR: COMPARISON WITH EXISTING TECHNOLOGY

While numerous ASVs have been developed, most have focused on oceanography and only a few on freshwater applications. We compared the performance of The Navigator with three other monitoring platforms that were designed for longitudinal monitoring of freshwater systems: 1) the Xylem HYCAT, 2) the Teledyne Z-Boat 1800RP, and 3) the Oak Ridge National Laboratory (ORNL) AquaBOT (Griffiths et al., 2022). The spider map in Figure 7 represents a qualitative comparison because a quantitative comparison would disregard the fact that they were built for different applications and can be custom-made. For example, the AquaBOT is designed specifically for the water quality monitoring of low-mid order streams and is ~2.5x times larger than The Navigator. The Teledyne Z-Boat 1800 is designed for hydrographic surveys that require higher payloads and is ~4-7x heavier (38-78 kg) and ~5x larger than The Navigator. The Xylems HYCAT can monitor bathymetry and water quality and is ~5x (53kg) heavier than The Navigator.

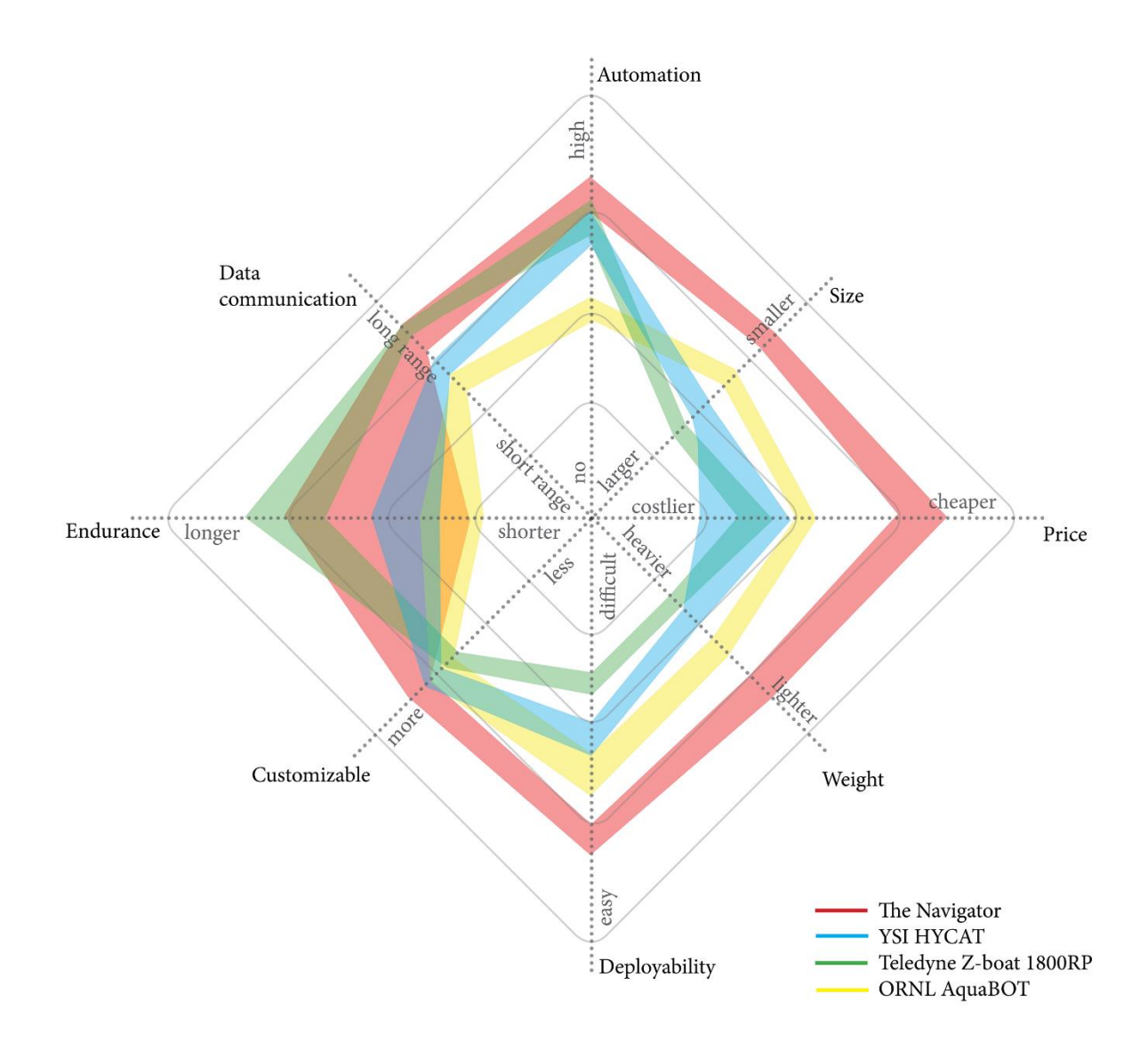


Figure 2.7: Comparison spider map of three autonomous surface vehicle platforms and The Navigator.

2.5 CONCLUSIONS

The Navigator is a do-it-yourself (DIY), innovative, cost-effective (USD 5,101 in 2022), easily adaptable solution for Lagrangian monitoring of surface waters that can support progress in hydrologic sciences, watershed management, health, and wellbeing efforts worldwide. The Navigator can generate and share high spatial- and temporal-resolution water quality parameters,

site photos, and depth surveys using off-shelf technologies that are affordable, open source, and easy to integrate with other sensor platforms. The off-shelf emerging technologies used are cutting-edge, making The Navigator smarter, cheaper, smaller, lighter, and more reliable than other ASV systems. The Navigator can generate and share data in real-time to help make informed decisions leading to improved environmental and human health outcomes, supporting the development of more sustainable and resilient societies.

Our field test data prove that The Navigator can help researchers, consultants, and stakeholders better understand the coupling of aquatic and human systems. This system provides tools to assist in planning, restoration, mitigation, enforcement, and disaster response efforts. The emphasis of this technology on understanding local-to-watershed scale spatial variations of natural and anthropogenic stressors can better inform holistic approaches for freshwater resource management. The Navigator allows for sampling spatial heterogeneities in water quality parameters at sub-hour to multi-day resolutions, providing data-rich solutions with minimum upfront (Table 1), maintenance, and operational costs.

The Navigator facilitates the linkage between Eulerian datasets collected at a site (e.g., USGS stream flows and water quality data) and Lagrangian-based monitoring to provide a better understanding of where, how, and why spatiotemporal variation in water chemistry and biogeochemical processing occurs. This technology has numerous critical applications, primarily in the water technology and energy and food sectors (i.e., across the food-energy-water FEW nexus). The technologies like the Navigator can help develop holistic strategies to manage FEW resources as it provides high spatiotemporal resolution capturing the impacts of land use changes, point and diffuse sources, and climate variability on freshwater systems. It can help identify risks relevant to the water supply for drinking, industrial, and agricultural activities and

address concerns from the associated return flows (e.g., combined sewer overflows, thermal pollution, excess nutrients, etc.). This system can inform agencies about water quality issues related to excess loads, dilution requirements, unwanted leakages to aquatic ecosystems, and gaining and losing conditions in rivers and lakes. The spatiotemporal water quality data generated by this development can support the development of regulation and enforcement of environmental flows, thermal pollution, and mitigation and restoration efforts post-disturbance (e.g., wildfires, spills, land use changes, etc.). Overall, The Navigator can help address questions involving mass and energy balances in surface water ecosystems and support evidence-based decision-making.

2.6 CHAPTER REFERENCES

- Abbott, B.W., Gruau, G., Zarnetske, J.P., Moatar, F., Barbe, L., Thomas, Z., Fovet, O., Kolbe, T., Gu, S., Pierson-Wickmann, A.-C., Davy, P., Pinay, G., 2018. Unexpected spatial stability of water chemistry in headwater stream networks. Ecol. Lett. 21, 296–308. https://doi.org/10.1111/ele.12897
- Arabi, B., Salama, Mhd.S., Pitarch, J., Verhoef, W., 2020. Integration of in-situ and multi-sensor satellite observations for long-term water quality monitoring in coastal areas. Remote Sens. Environ. 239, 111632. https://doi.org/10.1016/j.rse.2020.111632
- Arsenault, R., Martel, J.-L., Brunet, F., Brissette, F., Mai, J., 2023. Continuous streamflow prediction in ungauged basins: long short-term memory neural networks clearly outperform traditional hydrological models. Hydrol. Earth Syst. Sci. 27, 139–157. https://doi.org/10.5194/hess-27-139-2023
- Burns, D.A., Pellerin, B.A., Miller, M.P., Capel, P.D., Tesoriero, A.J., Duncan, J.M., 2019. Monitoring the riverine pulse: Applying high-frequency nitrate data to advance integrative understanding of biogeochemical and hydrological processes. WIREs Water 6, e1348. https://doi.org/10.1002/wat2.1348
- Businger, S., Chiswell, S.R., Ulmer, W.C., Johnson, R., 1996. Balloons as a Lagrangian measurement platform for atmospheric research. J. Geophys. Res. Atmospheres 101, 4363–4376. https://doi.org/10.1029/95JD00559
- Chapra, S.C., 2008. Surface Water-Quality Modeling. Waveland Pr Inc, Long Grove, Ill.
- Devaraj, S., Jenifa Latha, C., Geetha Priya, M., Jesudhas, C.J., Yarrakula, K., 2022. Hydrological Modelling for Ungauged Basins: An Overview of the Past, Present, and Future Directions, in: Panneerselvam, B., Pande, C.B., Muniraj, K., Balasubramanian, A., Ravichandran, N. (Eds.), Climate Change Impact on Groundwater Resources: Human Health Risk Assessment in Arid and Semi-Arid Regions. Springer International Publishing, Cham, pp. 313–327. https://doi.org/10.1007/978-3-031-04707-7_17
- Doyle, M.W., Ensign, S.H., 2009. Alternative Reference Frames in River System Science. BioScience 59, 499–510. https://doi.org/10.1525/bio.2009.59.6.8

- Dupas, R., Minaudo, C., Gruau, G., Ruiz, L., Gascuel-Odoux, C., 2018. Multidecadal Trajectory of Riverine Nitrogen and Phosphorus Dynamics in Rural Catchments. Water Resour. Res. 54, 5327–5340. https://doi.org/10.1029/2018WR022905
- Ferri, G., Manzi, A., Fornai, F., Ciuchi, F., Laschi, C., 2015. The HydroNet ASV, a Small-Sized Autonomous Catamaran for Real-Time Monitoring of Water Quality: From Design to Missions at Sea. IEEE J. Ocean. Eng. 40, 710–726. https://doi.org/10.1109/JOE.2014.2359361
- Freedman, A., Fears, D., 2020. The western U.S. is locked in the grips of the first human-caused megadrought, study finds. Wash. Post.
- Gabrielle, V., 2019. The Renaissance of Hydrology Eos [WWW Document]. URL https://eos.org/features/the-renaissance-of-hydrology (accessed 9.26.19).
- González-Pinzón, R., Dorley, J., Regier, P., Fluke, J., Bicknell, K., Nichols, J., Khandelwal, A., Wolf, E., Caruana, S.N., Horn, D.J.V., 2019. Introducing "The Integrator": A novel technique to monitor environmental flow systems. Limnol. Oceanogr. Methods 17, 415–427. https://doi.org/10.1002/lom3.10322
- Griffiths, N.A., Levi, P.S., Riggs, J.S., DeRolph, C.R., Fortner, A.M., Richards, J.K., 2022. Sensor-Equipped Unmanned Surface Vehicle for High-Resolution Mapping of Water Quality in Low-to Mid-Order Streams. ACS EST Water 2, 425–435. https://doi.org/10.1021/acsestwater.1c00342
- Hermit Peaks Fire [WWW Document], 2022. URL https://inciweb.nwcg.gov/incident-information/nmsnf-hermits-peak-fire (accessed 2.5.23).
- Huang, J., Borchardt, D., Rode, M., 2022. How do inorganic nitrogen processing pathways change quantitatively at daily, seasonal, and multiannual scales in a large agricultural stream? Hydrol. Earth Syst. Sci. 26, 5817–5833. https://doi.org/10.5194/hess-26-5817-2022
- Jarvie, H.P., Sharpley, A.N., Kresse, T., Hays, P.D., Williams, R.J., King, S.M., Berry, L.G., 2018. Coupling High-Frequency Stream Metabolism and Nutrient Monitoring to Explore Biogeochemical Controls on Downstream Nitrate Delivery. Environ. Sci. Technol. 52, 13708–13717. https://doi.org/10.1021/acs.est.8b03074
- Kirchner, J.W., Neal, C., 2013. Universal fractal scaling in stream chemistry and its implications for solute transport and water quality trend detection. Proc. Natl. Acad. Sci. 110, 12213–12218. https://doi.org/10.1073/pnas.1304328110
- Krause, S., , Jörg Lewandowski, , Clifford N. Dahm, , Klement Tockner, 2015. Frontiers in real-time ecohydrology a paradigm shift in understanding complex environmental systems Krause 2015 Ecohydrology Wiley Online Library [WWW Document]. URL https://onlinelibrary.wiley.com/doi/full/10.1002/eco.1646 (accessed 9.26.19).
- Li, B., Yang, G., Wan, R., 2020. Multidecadal water quality deterioration in the largest freshwater lake in China (Poyang Lake): Implications on eutrophication management. Environ. Pollut. 260, 114033. https://doi.org/10.1016/j.envpol.2020.114033
- Li, Wei, Xie, X., Li, Wanqiu, van der Meijde, M., Yan, H., Huang, Y., Li, X., Wang, Q., 2022.

 Monitoring of Hydrological Resources in Surface Water Change by Satellite Altimetry. Remote Sens. 14, 4904. https://doi.org/10.3390/rs14194904
- Lloyd, C.E.M., Freer, J.E., Johnes, P.J., Collins, A.L., 2016. Using hysteresis analysis of high-resolution water quality monitoring data, including uncertainty, to infer controls on nutrient and sediment transfer in catchments. Sci. Total Environ. 543, 388–404. https://doi.org/10.1016/j.scitotenv.2015.11.028
- Manfreda, S., McCabe, M.F., Miller, P.E., Lucas, R., Pajuelo Madrigal, V., Mallinis, G., Ben Dor, E., Helman, D., Estes, L., Ciraolo, G., Müllerová, J., Tauro, F., De Lima, M.I., De Lima, J.L.M.P., Maltese, A., Frances, F., Caylor, K., Kohv, M., Perks, M., Ruiz-Pérez, G., Su, Z., Vico, G., Toth, B., 2018. On the Use of Unmanned Aerial Systems for Environmental Monitoring. Remote Sens. 10, 641. https://doi.org/10.3390/rs10040641
- Massong, T., Makar, P., Bauer, T., 2010. RECENT CHANNEL INCISION AND FLOODPLAIN EVOLUTION WITHIN THE MIDDLE RIO GRANDE, NM.

- Matson, P.G., Stevenson, L.M., Griffiths, N.A., DeRolph, C.R., Jett, R.T., Fortner, A.M., Jones, M.W., Jones, N.J., Mathews, T.J., 2021. Multidecadal biological monitoring and abatement program assessing human impacts on aquatic ecosystems within the Oak Ridge Reservation in eastern Tennessee, USA. Hydrol. Process. 35, e14340. https://doi.org/10.1002/hyp.14340
- Model My Watershed [WWW Document], n.d. URL https://modelmywatershed.org/analyze (accessed 2.3.23).
- Nichols, J., Khandelwal, A.S., Regier, P., Summers, B., Van Horn, D.J., González-Pinzón, R., 2022. The understudied winter: Evidence of how precipitation differences affect stream metabolism in a headwater. Front. Water 4.
- Pebesma, E., 2016. Handling and Analyzing Spatial, Spatiotemporal and Movement Data [WWW Document]. URL https://edzer.github.io/UseR2016/#spatiotemporal-data-movement-data (accessed 1.18.23).
- Rode, M., Wade, A.J., Cohen, M.J., Hensley, R.T., Bowes, M.J., Kirchner, J.W., Arhonditsis, G.B., Jordan, P., Kronvang, B., Halliday, S.J., Skeffington, R.A., Rozemeijer, J.C., Aubert, A.H., Rinke, K., Jomaa, S., 2016. Sensors in the Stream: The High-Frequency Wave of the Present. Environ. Sci. Technol. 50, 10297–10307. https://doi.org/10.1021/acs.est.6b02155
- Román, M.O., Stokes, E.C., Shrestha, R., Wang, Z., Schultz, L., Carlo, E.A.S., Sun, Q., Bell, J., Molthan, A., Kalb, V., Ji, C., Seto, K.C., McClain, S.N., Enenkel, M., 2019. Satellite-based assessment of electricity restoration efforts in Puerto Rico after Hurricane Maria. PLOS ONE 14, e0218883. https://doi.org/10.1371/journal.pone.0218883
- Tapley, B.D., Watkins, M.M., Flechtner, F., Reigber, C., Bettadpur, S., Rodell, M., Sasgen, I., Famiglietti, J.S., Landerer, F.W., Chambers, D.P., Reager, J.T., Gardner, A.S., Save, H., Ivins, E.R., Swenson, S.C., Boening, C., Dahle, C., Wiese, D.N., Dobslaw, H., Tamisiea, M.E., Velicogna, I., 2019. Contributions of GRACE to understanding climate change. Nat. Clim. Change 9, 358–369. https://doi.org/10.1038/s41558-019-0456-2
- United Nations Environment Programme, 2021. Progress on Ambient Water Quality 2021 Update. USGS WaterWatch -- Streamflow conditions [WWW Document], n.d. URL https://waterwatch.usgs.gov/new/index.php (accessed 1.9.23).
- Wieland, M., Martinis, S., 2019. A Modular Processing Chain for Automated Flood Monitoring from Multi-Spectral Satellite Data. Remote Sens. 11, 2330. https://doi.org/10.3390/rs11192330

Chapter 3

Comparison of experimental and empirical mixing lengths downstream of a wastewater treatment plant discharging into an arid river.

Aashish Khandelwal¹, Tzion Castillo^{1,2}, Ricardo González-Pinzón¹

¹Civil, Construction and Environmental Engineering, University of New Mexico, Albuquerque, NM USA

²Electrical Engineering, University of New Mexico, Albuquerque, NM USA

3.1 INTRODUCTION

Globally, large volumes of untreated and treated wastewater generated by domestic, industrial, and commercial sources are discharged into rivers, lakes, and marine systems, typically as point sources (Rice, Wutich, and Westerhoff 2013; UNESCO 2020). According to the United Nations, the global volume of treated wastewater generated in 2018 was approximately 340 billion cubic meters, and it is projected to increase by 51% to 574 billion cubic meters by the year 2050 (United Nations Environment Programme 2021). While technological advances have played a significant role in increasing the capacity to treat wastewater and improve its quality (Angelakis and Snyder 2015), multiple contaminants of concern, such as microplastics, pharmaceuticals, and per- and polyfluoroalkyl substances (PFAS) remain largely untreated (Aymerich et al. 2017; Podder et al. 2021; Tiwari et al. 2017; Meng, Kelly, and Wright 2020). Given the urgent need to increase water supply through water reuse of partially and fully treated wastewaters for landscaping (Baawain et al. 2020), irrigation (Mortensen et al. 2016), and human consumption (Mizyed 2013), the interest in understanding

environmental mixing, dilution, and overall wastewater management in fluvial systems is reemerging (Antweiler, Writer, and Murphy 2014; Aymerich et al. 2017; Kraus et al. 2017).

There are best practice guidelines for establishing mixing zones, i.e., areas where active mixing and dilution of effluents occur (EPA 305(b) report 2009). In these mixing zones, pollutant concentrations can temporarily exceed water quality standards until contaminants are mixed and diluted by receiving water bodies. Near wastewater treatment plant (WWTP) outfalls, mixing zones are primarily influenced by the orientation of the outfall, its size, and the differences in flow and densities between the river and the effluent. Farther downstream, mixing is more influenced by the river's geomorphology (i.e., width, depth, sinuosity) and dilution capacity (G. H. Jirka, Doneker, and Hinton 1996; Campos, Morrisey, and Barter 2022). In practice, mixing zones (a 2D problem) are estimated through mixing lengths (1D solutions), i.e., the distance downstream from a point source over which the concentration of solutes in a receiving river are heterogenous vertically or laterally (Rutherford 1994). Mixing lengths are typically computed using empirical formulas derived from one-dimensional solute transport models and consider physical and hydraulic parameters describing the river's potential for dispersion and mixing through turbulence (Table 1) (Chapra 1997; Fischer 1979; Ward 1973; G. Jirka and Weitbrecht 2005; Rup 2006; Cleasby and Dodge 1999). However, most of those equations have not been tested in the field with high-resolution techniques and under various flow conditions but remain in use as standard practice.

Conceptually, 1D mixing length equations assume that water is mixed vertically and laterally relatively quickly (Ward 1973; Fischer 1979). Most of those equations do not explicitly account for water temperature and density differences between the river and the effluent, even though temperature-related stratification affects mixing in lentic (e.g., lakes) and lotic systems

(e.g., streams). Understandably, the technology and resources available to derive empirical mixing length equations in the 1970s did not allow for multi-flow verification or realistic tests under different conditions imposed by the dynamics of the river (i.e., sediment, temperature, and solute concentrations along the hydrograph) and its interaction with a much more constant effluent. However, these unaccounted-for considerations are highly relevant in arid and semi-arid regions, where WWTP effluents can be dominant sources of water in rivers during dry periods (Mortensen et al. 2016; Hur et al. 2007), and where the continuously dwindling rivers flows are the primary source of water for multiple users and uses (Cooke, Rutherford, and Milne 2010). There, WWTP effluents may cause sustained water quality deterioration under drought conditions (Murphy et al. 2018; Hur et al. 2007; Kamjunke et al. 2022), and the correct estimation of mixing lengths becomes more imperative to protect communities (Campos, Morrisey, and Barter 2022).

Recent technological advances offer alternatives to refining the estimation of mixing lengths and zones. Through high-resolution in-situ monitoring, water quality parameters such as temperature, dissolved oxygen, pH, and turbidity can be tracked to detect where they become homogenous across transects downstream of point sources (Cleasby and Dodge 1999). Also, remote sensing using satellite imagery can provide spatially distributed information on some water quality parameters, such as temperature, chlorophyll-a, and turbidity (Gholizadeh, Melesse, and Reddi 2016). However, their information's temporal and spatial resolution are typically inadequate to support local-scale and dynamic decision-making for managing surface water resources. Drone-based infrared and photogrammetric surveys have also gained popularity as they can provide better spatial resolution. Still, short battery lives, low payload capacity, high costs, and overwhelming regulatory restrictions severely limit the area they can cover. An

alternative to overcoming these challenges is using Lagrangian monitoring (i.e., as the flow goes), where water parcels are tracked, and mixing lengths are quickly established where and when the homogeneity of water quality parameters is detected.

In this study, we quantified experimental mixing lengths downstream of a WWTP discharge in the Rio Grande near Albuquerque, NM, and compared our results against six commonly used empirical equations. Our experimental fieldwork was done under six different river flow conditions, generating river to WWTP discharges ranging from 1 to 33. Therefore, our study site provided unique opportunities to investigate how mixing lengths vary as a function of flow dynamics in shallow, wide river reaches. We quantified experimental mixing lengths monitoring the two banks of the river using Lagrangian sampling with The Navigator (Khandelwal et al., in review) and an instrumented kayak, and also used Eulerian monitoring across river transects when navigating the river was impossible due to low flows. From our results, we discuss the challenges associated with erroneous estimates of mixing lengths and opportunities to develop improved estimates.

3.2 METHODS

Study area

We studied a ~9 km reach of the Rio Grande near Albuquerque under six flow conditions ranging from 3.7 m³/s to 50.9 m³/s, with a mean discharge of 16.7 m³/s. This reach is located ~55 km downstream from Cochiti Lake, a large flood control reservoir maintained by the U.S. Army Corps of Engineers, which receives most of the flow from snowmelt and removes most of the sediments from the river. The reach is also located near the City of Albuquerque, where the treated effluent of the Southside Water Reclamation Plant is discharged. This wastewater treatment plant (WWTP) serves over 600,000 people and has an average daily effluent discharge

of 2.6-3.2 m³/s (Brown and Caldwell 2011). The WWTP outfall features a rock-lined channel merging into the left bank of the river at an angle of 45°. Our study reach starts 1.2 km upstream of the outfall of the wastewater treatment plant of the City of Albuquerque and ends 7.8 km downstream of the point source.

The United States Geological Survey (USGS) operates gage USGS08330000 at Central Bridge, \sim 8.0 km upstream of the start of the reach, and gage USGS08330830 at Valle De Oro, \sim 4.7 km downstream of the outfall. We obtained discharge values from these gages upstream (Q_{up}) and downstream of the WWTP (Q_{down}). The Albuquerque Bernalillo County Water Utility Authority monitors the effluent coming from the WWTP, providing discharge (Q_{wwtp}) and water quality data at an hourly resolution (Figure 1). The effluent from the WWTP is relatively constant with respect to the Rio Grande, and in some dry periods, it may make up most of the flow in the river (Figure 2). In 2022 more than 40% of the Rio Grande watershed experienced exceptional drought in early summer (Pratt 2022) and, in consequence, the Rio Grande ran dry near Albuquerque for the first time in 40 years, and the WWTP effluent supplied all the discharge in the river. Since Q_{up} : Q_{wwtp} ranges between 1-33.3, our study site provides unique opportunities to investigate how mixing lengths vary as a function of flow in shallow, wide river reaches.

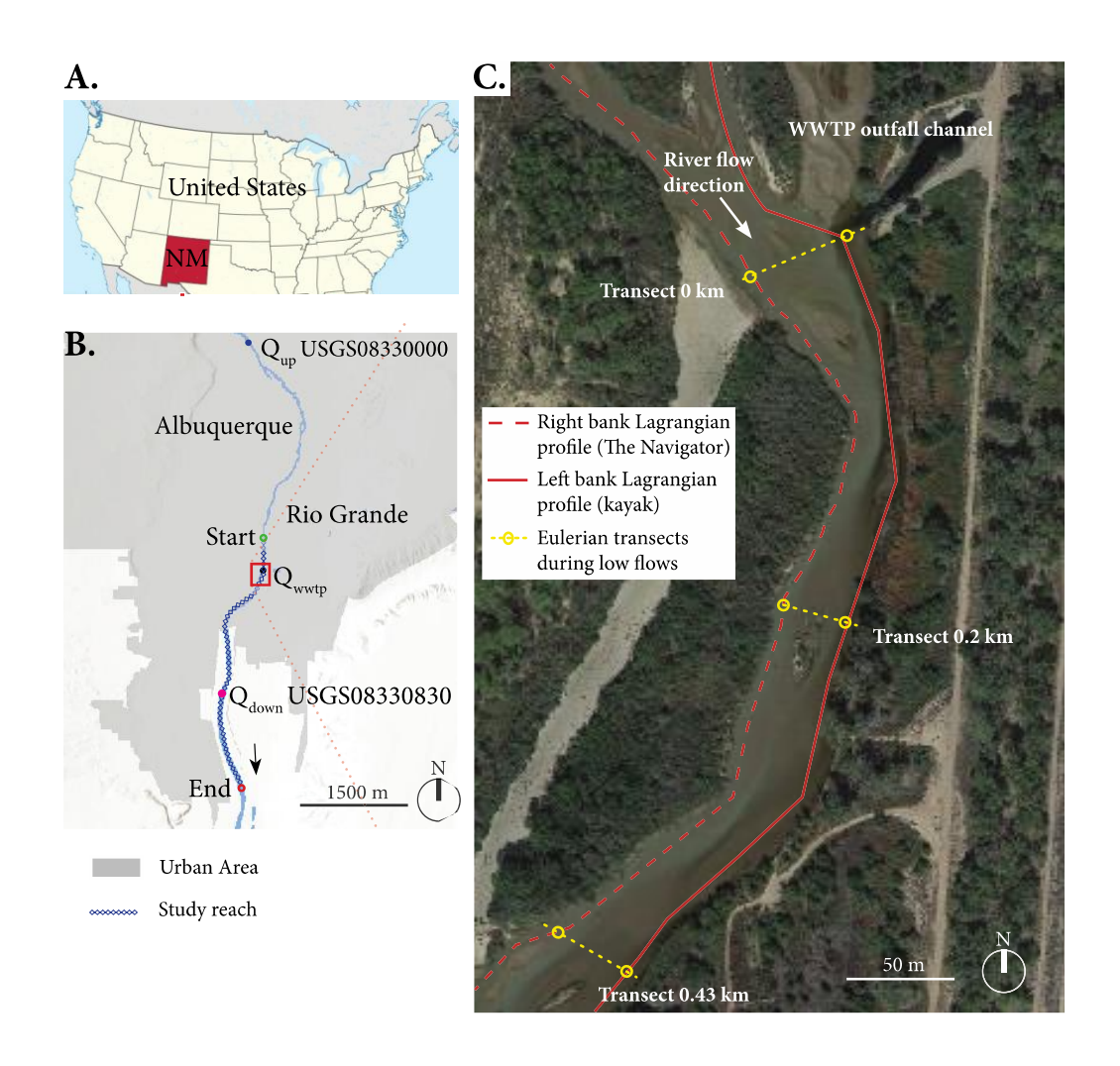


Figure 3.1: (A and B) Study reach location and (C) satellite photo of the area near the outfall of the City of Albuquerque's wastewater treatment plant.

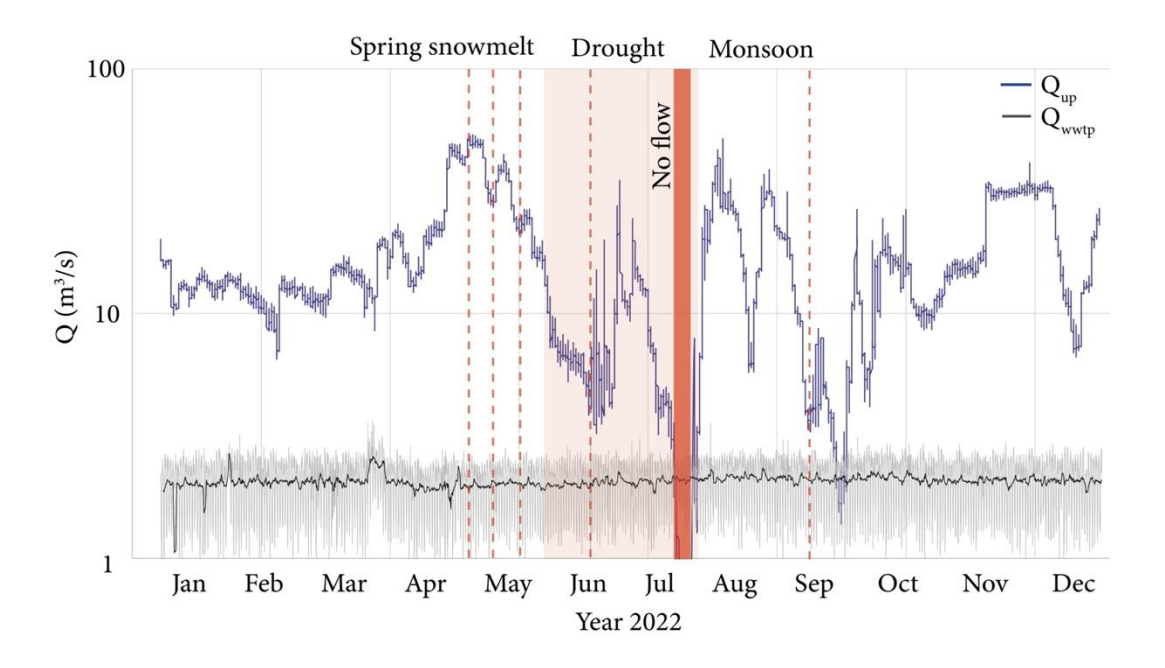


Figure 3.2: Rio Grande discharge (blue) for the USGS08330000 at Central Bridge (Q_{up}) , Southside Water Reclamation Plant outfall flow $(Q_{wtp}; grey)$, and daily mean Q_{wwtp} values (black). Red dotted lines indicate fieldwork days, and the red rectangle represents the period when the river ran dry, and the WWTP provided all the river flow downstream of the WWTP.

Field Measurements

Infrared imagery: We used a drone equipped with a thermal imaging infrared camera (FLIR Vue Pro R 640) and an RGB camera (20 MP 1" CMOS) to visualize the mixing of WWTP effluent and river water with surface water temperature profiles. This fieldwork was completed on Nov 11, 2021, when Q_{up} : Q_{wwtp} = 6.21 (Figure 3). Although the collected imagery was ideal for visualizing mixing patterns near the WWTP-river confluence, the technology only monitors temperature, is costly, and drone flying restrictions near the Albuquerque International Airport restricted its use in our area of interest. Thus, we only used the information collected from thermal imagery to design our Lagrangian and Eulerian monitoring.

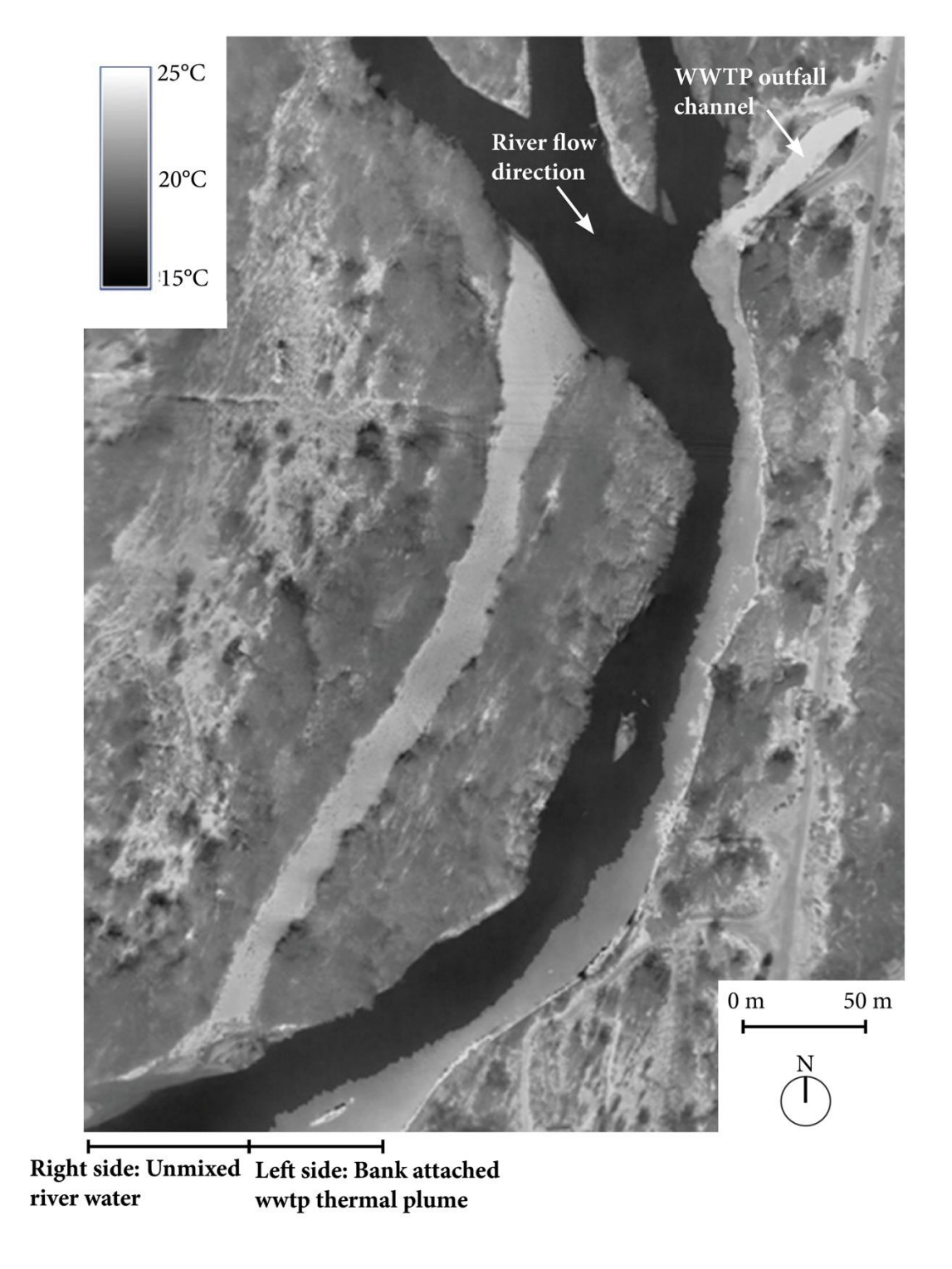


Figure 3.3: Drone-based infrared imaging showing the higher temperature plume from the WWTP effluent (light grey, ~20-25 °C) hanging on the left bank of the Rio Grande (black, ~15 °C).

High-resolution Lagrangian monitoring: We monitored the spatiotemporal variability of multiple water quality parameters along our study's left and right banks reach to characterize

mixing lengths. These data were collected on the left bank using The Navigator, an autonomous surface vehicle (ASV) instrumented with a GPS tracker and multiparameter sondes that monitor temperature, dissolved oxygen, pH, and specific conductivity at a depth of 0.2 m (Khandelwal, González-Pinzón, and Castillo 2023 under review). On the right bank, we used a kayak carrying a multiparameter YSI EXO2 sonde and a handheld GPS tracker to monitor the same parameters. The monitoring was completed under four different flow conditions, i.e., Q_{up} : Q_{wwtp} of 5.5, 7.3, 12.5, and 22.1. On average, the data were collected at a spatial resolution of 72-102 m, over 2hr 16min - 3hr 48min of navigation.

Eulerian monitoring: In low flows with Q_{up} : Q_{wwtp} of 3.6 and 2.4, we could not navigate the study reach and used Eulerian monitoring. We used the same multiparameter YSI EXO2 sondes along 11 transects spaced 200 m-2 km apart, depending on site access to the river. Before each Lagrangian or Eulerian monitoring field day, we calibrated each sensor following the manufacturer's recommendations.

Estimation of mixing lengths and comparison with existing models

We generated heatmaps for water quality parameters using the spacetime and trajectories package from R (Pebesma 2016) and the sondes and GPS data. We estimated experimental mixing lengths (L_m) for each parameter as the distance required for left and right bank values to become $\pm 5\%$ equal or uniform downstream of the WWTP outfall (Fisher, 1979). Using this criterion, we confirmed that water quality parameter values upstream of the WWTP outfall were uniform.

The heatmaps (KMZ files) were arranged next to one other and imported into Google

Earth to create layered water quality maps to display water quality data under different dilution
ratios. The resolution of the Eulerian monitoring was increased using linear interpolation
between transects to generate a higher resolution heatmap.

Existing mixing length models

We compare our experimental estimates of mixing lengths (L_m) with multiple empirical equations (L; Table 1). The reach characteristics required to populate those equations include average velocity, depth, width, channel irregularity, and longitudinal slope values. The hydraulic parameters velocity, depth, and width were obtained from USGS data from the upstream station. Onsite observations of channel meandering and inspection of satellite imagery were used to determine a qualitative measure of channel irregularity (sinuosity) and longitudinal slopes.

Table 3.1: Empirical formulas used to compare mixing lengths.

Source	Equation		
Mixing length zone	$L = \frac{kb^2U}{} \tag{1}$		
(Fischer 1979)	$L = \frac{Ru_*}{Ru_*} \tag{1}$		
Length of the longitudinal mixing zone (Rutherford 1994)	$L = 0.536 \frac{U s^2}{D_y} \tag{2}$		
Mixing length equation (G. Jirka and Weitbrecht 2005; Skorbiłowicz et al. 2017)	$L = 0.4 \frac{U s^2}{D_y} \tag{3}$		
Mixing length equation (Rup 2006; Skorbiłowicz et al. 2017)	$L = 0.29 \frac{U s^2}{D_y} \tag{4}$		
One half width mixing equation. (Cleasby and Dodge 1999)	$L = \frac{0.4(b/2)^2 U}{D_y} \tag{5}$		
European Union rule of thumb for river mixing zone. (Environmental Quality Standards 2008)	$L = 10 b \tag{6}$		

In Table 1, L is the empirical mixing length, b is the channel width, U is the mean velocity, R is the hydraulic radius, u_* is the shear velocity, s is the linear transverse scale, D_y is

the transverse dispersion coefficient ($D_y \sim 0.3 \text{ m}^2/\text{s}$ for the Rio Grande), and k is a channel type constant ($k \sim 10$ for the Rio Grande).

3.3 RESULTS AND DISCUSSION

Flow conditions and historical drought

The Rio Grande is a highly managed arid river system, providing water for 6 million people and irrigating 2 million acres of land. Drought years strain water operations, making flow management complex. Nearly 75% of the river's water is used for agriculture, and managing low flows represent an environmental concern for endangered species native to the Rio Grande, particularly the Rio Grande Silvery Minnow (Pratt 2022). In 2022, 40% of the Rio Grande watershed experienced exceptional drought, resulting in record-low flows during the summer and fall. In 2022, near Albuquerque, New Mexico, the river faced ~19.5% lower flows than the average flow since 1970. During the fieldwork days of this study, the river flow at Q_{up} ranged from 50.9 m³/s to 3.74 m³/s, and the wastewater flow at Q_{wwtp} ranged from 3.01 m³/s to 1.56 m³/s. These flow values generated dilution ratios between 22.1 and 2.4. Also, river depths ranged from 0.2- 0.9 m (Table 2).

Table 3.2: Hydrologic characteristics of the Rio Grande near Albuquerque, NM.

$rac{Q_{up}}{Q_{wwtp}}$	Q_{up} (m 3 /s)	Q _{wwtp} (m³/s)	Q _{down} (m ³ /s)	Depth (m)	Width, b (m)	Area (m²)	Hydraulic radius, <i>R</i> (m)	Mean velocity, U (m/s)	Linear transverse scale, s (m)
2.4	3.74	1.6	5.4	0.2	18	4	0.2	0.9	12.6
3.6	7.0	2.0	8.5	0.3	27	8	0.3	0.9	18.9
5.5	15.0	2.7	15.6	0.5	38	17	0.4	0.9	26.6
7.3	22.1	3.0	19.0	0.6	44	25	0.6	0.9	30.8
12.5	33.4	2.7	32.0	0.7	53	37	0.7	0.9	37.1
22.1	50.9	2.3	50.7	0.9	65	59	0.9	0.9	45.5

Experimental mixing lengths

The experimental mixing lengths observed from our datasets follow a bell-shaped pattern with river flows and dilution ratios Q_{up} : Q_{wwtp} , i.e., low and high flows have smaller mixing lengths and intermediate flows have greater magnitudes (Figures 4-6). Multiple mixing lengths were obtained from each water quality parameter tracked for a specific river flow or dilution ratio, even though they all followed the same bell-shaped patterns (Figures 4-6). This suggests that contrasting phenomena at low and high flows may affect mixing length patterns similarly. Noticeably, all the empirical equations used to compare our experimental observations (Table 1) predicted a monotonically increasing mixing length with discharge and misrepresented our data (Figure 6).

As river flows decrease, the outfall effluent has a higher depth and momentum, supporting a relatively fast and expansive mixing driven by kinetic energy in a process analogous to jet diffusion (Gomolka, Twarog, and Zeslawska 2022). The reduced river depth limits vertical spreading, causing the negatively buoyant effluent to rise rapidly, contributing to horizontal mixing (Pouchoulin et al. 2020). Additionally, the shallow depth of the river increases the relevance of shear stresses on stirring and mixing, enhancing the dispersion of the effluent and, thus, reducing mixing lengths (Chen et al. 2013).

We observed increased mixing lengths at intermediate river flows. Experimental observations with air and water have shown that fluids tend to remain attached to surfaces at increased flow velocities, a phenomenon known as the Coanda effect (Lalli et al. 2010). This attachment is due to pressure differences caused by differential flow velocities and contributes to "bank-hugging" of effluent plumes. Also, as river flows increase, river temperatures decrease, and the difference in water densities between the river and the WWTP increase, creating water

stratification, which results in reduced mixing (Elçi 2008; Buxton et al. 2022). The EPA regulations under Clean Water Act recommend avoiding bank-hugging plumes or dominance of the Coanda effect in receiving water bodies that are used for irrigation, that host migrating and endangered fish, or where recreational activities can be impacted by non-mixing plumes (Clean Water Act Section 316(a) 2007).

At higher flows, mixing lengths consistently decreased due to increased turbulent mixing, which overcame the dominance of Coanda and water stratification effects (Campos, Morrisey, and Barter 2022). Since the wastewater temperature was consistently higher than that of the river, effluent plumes rose, contributing to faster vertical mixing. Combined with increased turbulent and vertical mixing, the higher dilution potential under high flows shortened mixing lengths (Lewis et al. 2020).

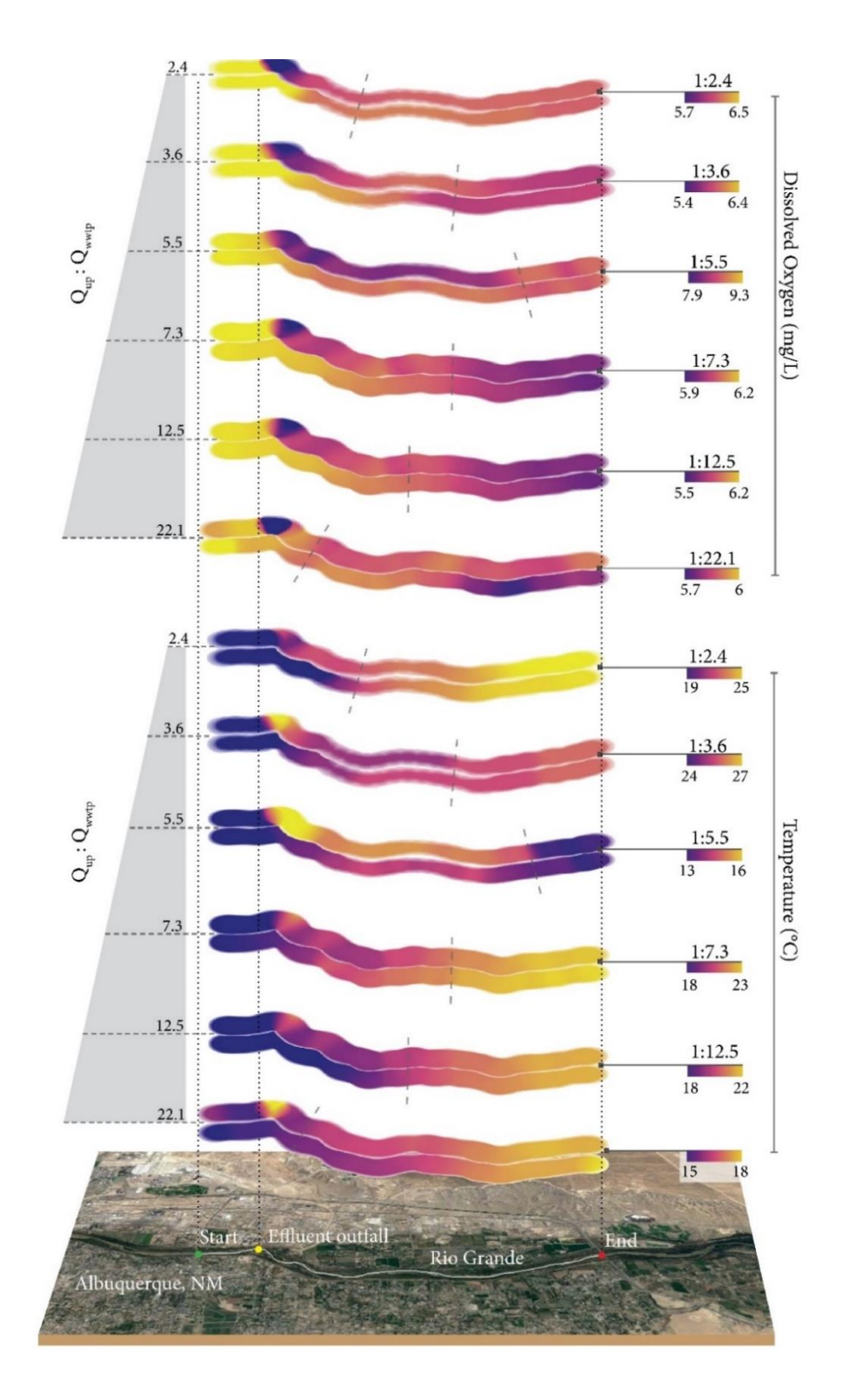


Figure 3.4: Longitudinal profiles of dissolved oxygen and temperature observed upstream and downstream of the Albuquerque wastewater treatment plant (WWTP) effluent during different flow conditions (Q_{up} : Q_{wwtp}). Left bank (outfall side) data are on top of right bank data. Dash lines indicate the experimental mixing lengths (L_m), where left and right bank data are within 5% difference downstream of the WWTP.

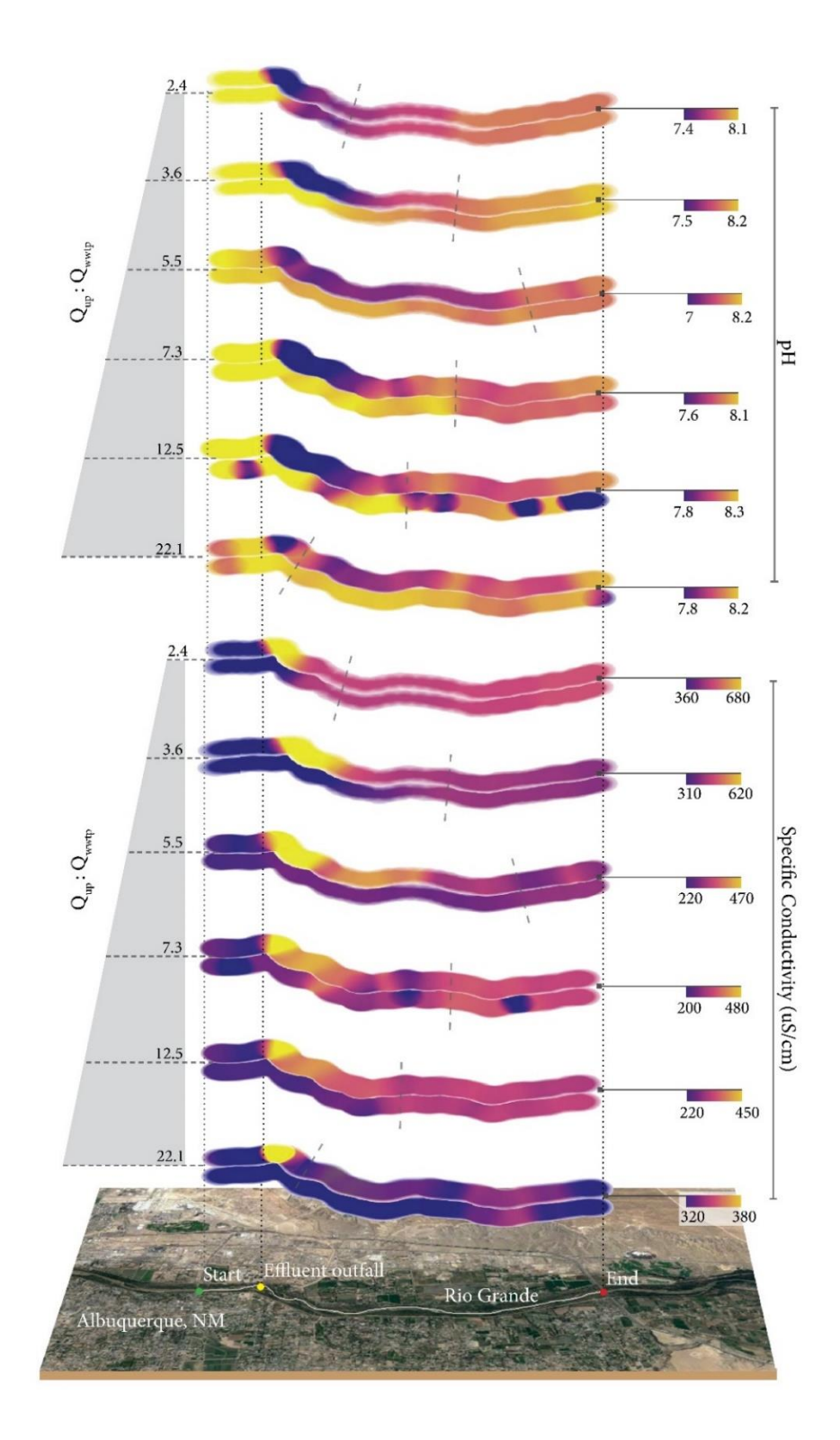


Figure 3.5: Longitudinal profiles of pH and specific conductivity observed upstream and downstream of the Albuquerque wastewater treatment plant (WWTP) effluent during different flow conditions (Q_{up} : Q_{wwtp}). Left bank (outfall side) data are on top of right bank data. Dash lines indicate the experimental mixing lengths (L_m), where left and right bank data are within 5% difference downstream of the WWTP.

Experimental mixing lengths vs. empirical mixing lengths

We compared our experimental mixing lengths with the one-dimensional empirical equations from Table 1 (Figure 5). Notably, none of the empirical equations can reproduce the bell-shaped mixing length pattern observed for all water quality parameters using Lagrangian monitoring. Those empirical equations are monotonically increasing and vary from simple to intermediately complex considerations derived from one-dimensional transport models. Generally, the shortest mixing length prediction was obtained with Equation 6, which only uses width to predict mixing (Environmental Quality Standards 2008), and the longest prediction was obtained with Equation 1 (Fischer 1979) which, unlike the others tested, accounts for shear stresses. Also, generally, the discrepancy between the predictions with empirical equations grew with river discharge, as all are proportional to flow velocity. In low flows with $2.4 < Q_{up}$: $Q_{wwtp} < 3.6$, our experimental mixing lengths were 1.5x to 7.5x longer than the predictions with empirical equations. In the intermediate flow region where the Coanda effect dominated, experimental mixing lengths were 2.5x-13x greater. In the highest Q_{up} : $Q_{wwtp} = 22.1$, experimental mixing lengths were 3x-7.5x smaller.

While empirical equations have found widespread use in engineering practice for analyzing mixing phenomena, their derivation disregarded complexities that may be relevant in real-world practice. For example, most equations assume straight channel geometries, uniform cross-sections, and steady flow conditions. However, streams and rivers undergo highly dynamic flow and sediment transport processes, making vertical, lateral, and longitudinal mixing highly dynamic. In this context, our field observations based on Lagrangian monitoring have revealed shifting mechanisms dominating mixing, i.e., jet diffusion, Coanda effect, and turbulent mixing (Figure 6).

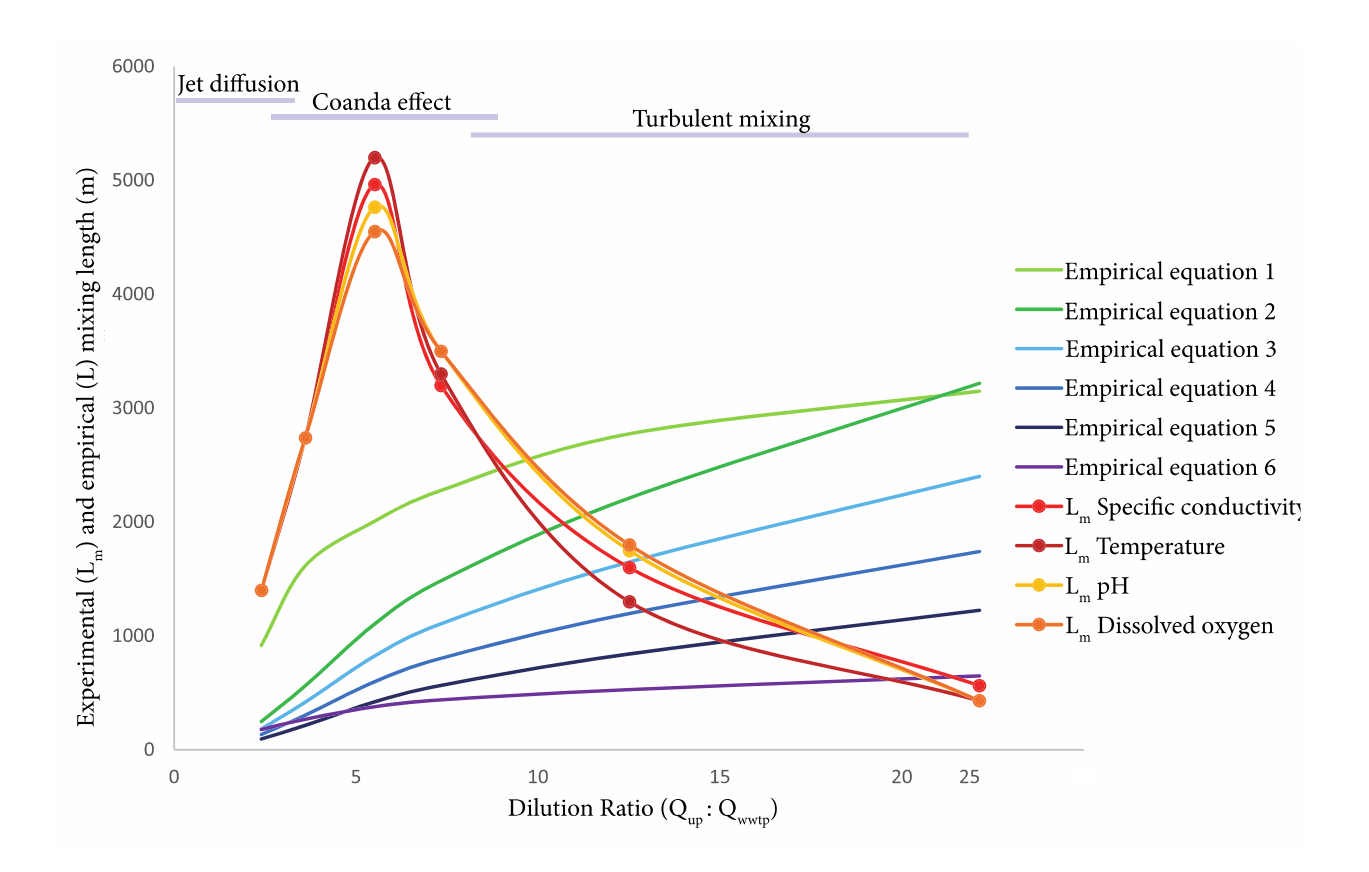


Figure 3.6: Experimental (L_m) and empirical (L) mixing lengths as a function of the dilution ratio $(Q_{up}:Q_{wwtp})$. Empirical equations 1-6 are described in Table 1.

Impacts of mixing lengths on ecosystem services

Mixing lengths are relevant in water quality assessments and studies of ecosystem dynamics in streams and rivers. In water resource management, mixing lengths help assess risk and mitigation strategies that communities downstream of point and distributed sources should have to reduce pollution exposure when streams or rivers are used for irrigation, fishing, ceremonial uses, groundwater recharge, and drinking water purposes. Regions located between a contaminant source and the mixing length are prone to undergo pollution issues as water properties (e.g., temperature, solutes, and sediments) are not homogenized and could overwhelm ecosystems (Campos, Morrisey, and Barter 2022; Skorbiłowicz et al. 2017).

In most cases, the effluent discharged from a WWTP contains higher levels of contaminants than the receiving stream or river, which can negatively impact ecosystem health and functioning (Martí, Riera, and Sabater 2009; Pascual-Benito et al. 2020; Castelar et al. 2022). For example, the slow mixing of warmer plumes from WWTP can lead to reduced oxygen levels, impacting fish communities (Caissie 2006; Isaak et al. 2010; Perkins et al. 2012). Also, concentrated pharmaceutical and personal care products can be toxic to fish, amphibians, and invertebrates, disrupting hormone systems, impairing reproductive functions, and causing behavioral changes in these organisms (Wang et al. 2021; Issac and Kandasubramanian 2021; Ding et al. 2022; Adegoke et al. 2023; Hernando et al. 2006).

While longer mixing length predictions generate more conservative and cautious estimates to help protect downstream water users, our results indicate that commonly used empirical equations may consistently underpredict mixing lengths in intermediate flow regimes, where the Coanda effect controls mixing. This underprediction could result in higher pollution risks for human populations capturing water from the same bank of upstream effluent discharges.

Besides water quality issues, relatively high-velocity effluents discharging from WWTPs may cause erosion problems which, over time, can destabilize riverbanks and changes the river's geomorphology (Duró et al. 2020). Between 1996-2023, the erosion occurring near the Albuquerque WWTP outfall resulted in a ~9400 m² area lost on the left bank side (Figure 7), affecting vegetation recruitment, which promotes even more erosion. To tackle these long-standing problems, the City of Albuquerque initiated a \$4.7 million restoration project in 2022 to realign the outfall, facilitate mixing with river water during low flow conditions, and restore crucial habitats for endangered fish and birds (Davis 2022). For that, the restoration project used root wads, which are clusters consisting of logs, roots, and boulders strategically placed along

the riverbank to create suitable fish habitats and mitigate streambed erosion. It is worth noting that the bank upstream of the outfall has exhibited consistent vegetation cover over the same period.

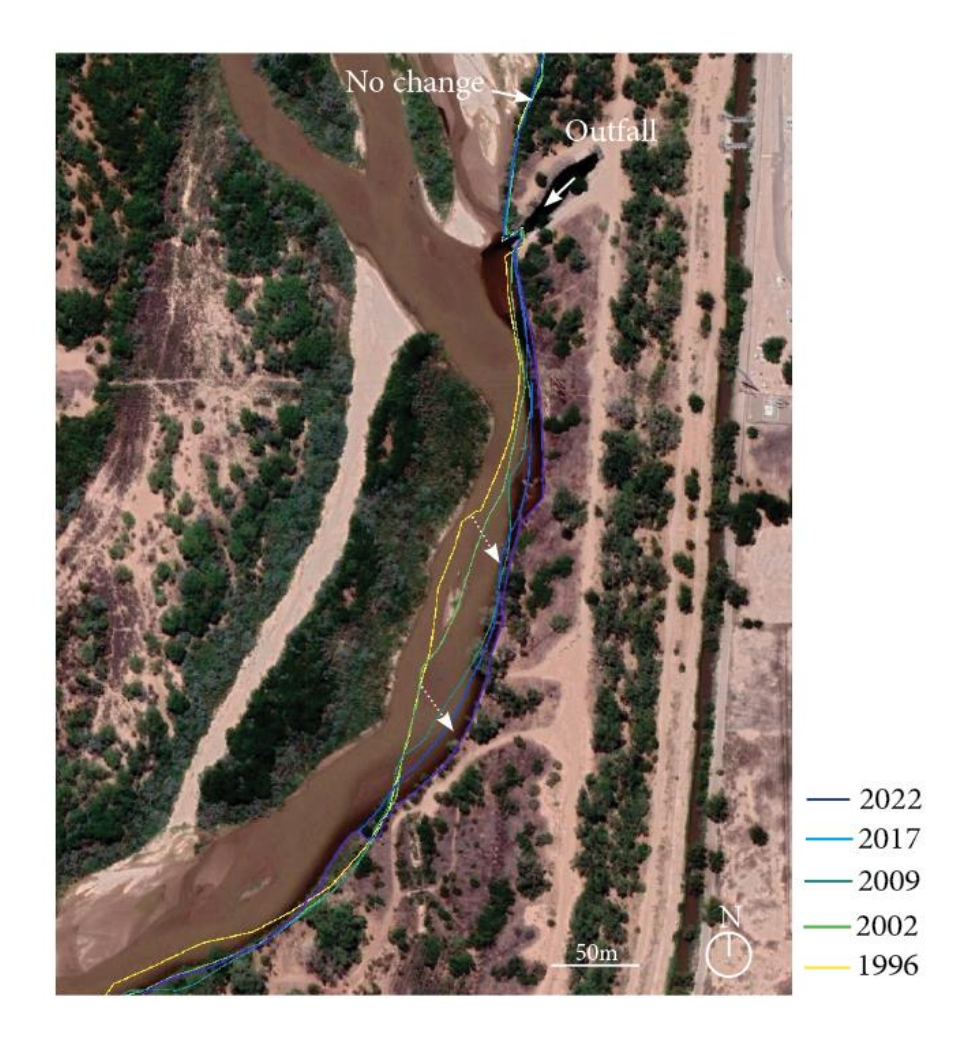


Figure 3.7: Bankline evolution downstream of the Albuquerque WWTP outfall. The bank history has been obtained with satellite images from Google Earth.

3.4 CONCLUSIONS

Using high-resolution Lagrangian and Eulerian monitoring, our study assessed the impact of flow dynamics on mixing lengths downstream of a WWTP effluent discharge in the Rio Grande near Albuquerque, NM. The Lagrangian reference frame was critical to visualizing mixing lengths from the perspective of four different water quality parameters (i.e., dissolved

oxygen, temperature, pH, and specific conductivity). The Eulerian reference frame allowed us to continue our experimental work under the extremely low flow conditions that halted our use of Lagrangian equipment flowing down the river. Both Lagrangian and Eulerian monitoring designs were initially informed by infrared imagery. Our results show that the empirical equations traditionally used to estimate mixing lengths did not describe our experimental dataset correctly. While our experimental data revealed "bell-shaped" mixing lengths as a function of river: WWTP discharges, all empirical equations predicted monotonically increasing mixing lengths. Those mismatches between experimental and empirical mixing lengths are likely due to the existence of threshold processes defining mixing at different flow regimes, i.e., jet diffusion at low flows, the Coanda effect at intermediate flows, and turbulent mixing at higher flows, which are unaccounted for by the one-dimensional empirical formulas.

The successful use of The Navigator and an instrumented kayak (since we had one prototype of The Navigator available) to monitor both banks of the Rio Grande and test empirical equations commonly used in a problem long-thought to be well understood calls for increased use of Lagrangian monitoring to better understand environmental dynamics. With the advent of real-time telemetry and high-resolution sensors, Lagrangian monitoring can rapidly and cost-effectively generate datasets that can more accurately describe flow and transport dynamics. Our findings also highlight the importance of combining Eulerian and Lagrangian efforts to provide a more robust understanding of the dynamics of mass and energy fluxes and how they affect coupled human-environment systems.

3.5 REFERENCES:

- Adegoke, Kayode Adesina, Folasade Abimbola Adu, Abel Kolawole Oyebamiji, Abayomi Bamisaye, Rasheed Adewale Adigun, Samuel Olaniyi Olasoji, and Oluwasayo Esther Ogunjinmi. 2023. "Microplastics Toxicity, Detection, and Removal from Water/Wastewater." *Marine Pollution Bulletin* 187 (February): 114546. https://doi.org/10.1016/j.marpolbul.2022.114546.
- Angelakis, Andreas N., and Shane A. Snyder. 2015. "Wastewater Treatment and Reuse: Past, Present, and Future." *Water* 7 (9): 4887–95. https://doi.org/10.3390/w7094887.
- Antweiler, Ronald C., Jeffrey H. Writer, and Sheila F. Murphy. 2014. "Evaluation of Wastewater Contaminant Transport in Surface Waters Using Verified Lagrangian Sampling." *Science of The Total Environment* 470–471 (February): 551–58. https://doi.org/10.1016/j.scitotenv.2013.09.079.
- Aymerich, I., V. Acuña, C. Ort, I. Rodríguez-Roda, and Ll. Corominas. 2017. "Fate of Organic Microcontaminants in Wastewater Treatment and River Systems: An Uncertainty Assessment in View of Sampling Strategy, and Compound Consumption Rate and Degradability." *Water Research* 125 (November): 152–61. https://doi.org/10.1016/j.watres.2017.08.011.
- Baawain, Mahad S., Abdullah Al-Mamun, Hamid Omidvarborna, Amal Al-Sabti, and B. S. Choudri. 2020. "Public Perceptions of Reusing Treated Wastewater for Urban and Industrial Applications: Challenges and Opportunities." *Environment, Development and Sustainability* 22 (3): 1859–71. https://doi.org/10.1007/s10668-018-0266-0.
- Brown and Caldwell. 2011. "Southside Water Reclamation Plant Rehabilitation and Asset Management Plan." Open-File Report. Open-File Report. https://www.abcwua.org/wp-content/uploads/Sewer_system/201005_SWRP_RRAMP_Brown_and_Caldwell_1.pdf.
- Buxton, Todd H., Yong G. Lai, Nicholas A. Som, Eric Peterson, and Ben Abban. 2022. "The Mechanics of Diurnal Thermal Stratification in River Pools: Implications for Water Management and Species Conservation." *Hydrological Processes* 36 (11): e14749. https://doi.org/10.1002/hyp.14749.
- Caissie, D. 2006. "The Thermal Regime of Rivers: A Review." *Freshwater Biology* 51 (8): 1389–1406. https://doi.org/10.1111/j.1365-2427.2006.01597.x.
- Campos, Carlos J. A., Donald J. Morrisey, and Paul Barter. 2022. "Principles and Technical Application of Mixing Zones for Wastewater Discharges to Freshwater and Marine Environments." *Water* 14 (8): 1201. https://doi.org/10.3390/w14081201.
- Castelar, Sara, Susana Bernal, Miquel Ribot, Stephanie N. Merbt, Marta Tobella, Francesc Sabater, José L. J. Ledesma, et al. 2022. "Wastewater Treatment Plant Effluent Inputs Influence the Temporal Variability of Nutrient Uptake in an Intermittent Stream." *Urban Ecosystems* 25 (4): 1313–26. https://doi.org/10.1007/s11252-022-01228-5.
- Chapra, Steven. 1997. "Surface Water-Quality Modeling" 1 (January).
- Chen, X., W. Dong, G. Ou, Z. Wang, and C. Liu. 2013. "Gaining and Losing Stream Reaches Have Opposite Hydraulic Conductivity Distribution Patterns." *Hydrology and Earth System Sciences* 17 (7): 2569–79. https://doi.org/10.5194/hess-17-2569-2013.
- Clean Water Act Section 316(a). 2007. "Point Sources with Thermal Discharges," January.
- Cleasby, Thomas, and Kent Dodge. 1999. "Effluent Mixing Characteristics below Four Wastewater-Treatment Facilities in Southwestern Montana, 1997." https://doi.org/10.3133/wri994026.
- Cooke, Jim, Kit Rutherford, and Philip Milne. 2010. A Review of Definitions of "Mixing Zones" and "Reasonable Mixing" in Receiving Waters.
- Davis, Theresa. 2022. "Water Authority Project Aims to Excavate, Realign South Valley Wastewater Outfall Site Albuquerque Journal." August 2022. https://www.abqjournal.com/2525297/utility-will-restore-south-valley-wastewater-outfall-site.html.
- Ding, Tengda, Liyan Wei, Zhangming Hou, Juying Li, Chunlong Zhang, and Daohui Lin. 2022. "Microplastics Altered Contaminant Behavior and Toxicity in Natural Waters." *Journal of Hazardous Materials* 425 (March): 127908. https://doi.org/10.1016/j.jhazmat.2021.127908.

- Duró, Gonzalo, Alessandra Crosato, Maarten G. Kleinhans, Timotheus G. Winkels, Hessel A.G. Woolderink, and Wim S.J. Uijttewaal. 2020. "Distinct Patterns of Bank Erosion in a Navigable Regulated River." *Earth Surface Processes and Landforms* 45 (2): 361–74. https://doi.org/10.1002/esp.4736.
- Elçi, Şebnem. 2008. "Effects of Thermal Stratification and Mixing on Reservoir Water Quality." Limnology 9 (2): 135–42. https://doi.org/10.1007/s10201-008-0240-x.
- Environmental Quality Standards. 2008. "Technical Background Document on Identification of Mixing Zones."
- EPA 305(b) report. 2009. "National Water Quality Inventory Report to Congress | Water Data and Tools | US EPA." 2009. https://www.epa.gov/waterdata/national-water-quality-inventory-report-congress.
- Fischer, Hugo. 1979. "Mixing In Inland & Coastal Waters: Hugo Fischer: Hardcover: 9780122581502: Powell's Books." 1979. https://www.powells.com/book/mixing-in-inland-coastal-waters-9780122581502.
- Gholizadeh, Mohammad, Assefa Melesse, and Lakshmi Reddi. 2016. "A Comprehensive Review on Water Quality Parameters Estimation Using Remote Sensing Techniques." *Sensors* 16 (8): 1298. https://doi.org/10.3390/s16081298.
- Gomolka, Zbigniew, Boguslaw Twarog, and Ewa Zeslawska. 2022. "State Analysis of the Water Quality in Rivers in Consideration of Diffusion Phenomenon." *Applied Sciences* 12 (3): 1549. https://doi.org/10.3390/app12031549.
- Hernando, M, M Mezcua, A Fernandezalba, and D Barcelo. 2006. "Environmental Risk Assessment of Pharmaceutical Residues in Wastewater Effluents, Surface Waters and Sediments." *Talanta* 69 (2): 334–42. https://doi.org/10.1016/j.talanta.2005.09.037.
- Hur, Jin, Mark A. Schlautman, Tanju Karanfil, John Smink, Hocheol Song, Stephen J. Klaine, and John C. Hayes. 2007. "Influence of Drought and Municipal Sewage Effluents on the Baseflow Water Chemistry of an Upper Piedmont River." *Environmental Monitoring and Assessment* 132 (1): 171–87. https://doi.org/10.1007/s10661-006-9513-1.
- Isaak, Daniel J., Charles H. Luce, Bruce E. Rieman, David E. Nagel, Erin E. Peterson, Dona L. Horan, Sharon Parkes, and Gwynne L. Chandler. 2010. "Effects of Climate Change and Wildfire on Stream Temperatures and Salmonid Thermal Habitat in a Mountain River Network." *Ecological Applications: A Publication of the Ecological Society of America* 20 (5): 1350–71.
- Issac, Merlin N, and Balasubramanian Kandasubramanian. 2021. "Effect of Microplastics in Water and Aquatic Systems." *Environmental Science and Pollution Research* 28 (16): 19544–62. https://doi.org/10.1007/s11356-021-13184-2.
- Jirka, Gerhard H, Robert L Doneker, and Steven W Hinton. 1996. "USER'S MANUAL FOR CORMIX [1996]."
- Jirka, Gerhard, and Volker Weitbrecht. 2005. "Mixing Models for Water Quality Management in Rivers: Continuous and Instantaneous Pollutant Releases." *Water Quality Hazards and Dispersion of Pollutants*, January, 1–34. https://doi.org/10.1007/0-387-23322-9_1.
- Kamjunke, Norbert, Liza-Marie Beckers, Peter Herzsprung, Wolf von Tümpling, Oliver Lechtenfeld, Jörg Tittel, Ute Risse-Buhl, et al. 2022. "Lagrangian Profiles of Riverine Autotrophy, Organic Matter Transformation, and Micropollutants at Extreme Drought." *Science of The Total Environment* 828 (July): 154243. https://doi.org/10.1016/j.scitotenv.2022.154243.
- Khandelwal, Aashish, R. González-Pinzón, and Tzion Castillo. 2023. "Development of The Navigator: A Lagrangian Sensing System to Characterize Surface Freshwater Ecosystems."
- Kraus, Tamara E. C., Kurt Carpenter, Brian Bergamaschi, Alexander Parker, Elizabeth Stumpner, Bryan D. Downing, Nicole Travis, Frances Wilkerson, Carol Kendall, and Timothy Mussen. 2017. "A River-Scale Lagrangian Experiment Examining Controls on Phytoplankton Dynamics in the Presence and Absence of Treated Wastewater Effluent High in Ammonium." *Limnology and Oceanography*. https://doi.org/10.1002/lno.10497.

- Lalli, Francesco, Antonello Bruschi, Rodolfo Lama, Luca Liberti, Stefania Mandrone, and Valeria Pesarino. 2010. "Coanda Effect in Coastal Flows." *Coastal Engineering* 57 (3): 278–89. https://doi.org/10.1016/j.coastaleng.2009.10.015.
- Lewis, Quinn, Bruce Rhoads, Alexander Sukhodolov, and George Constantinescu. 2020. "Advective Lateral Transport of Streamwise Momentum Governs Mixing at Small River Confluences." *Water Resources Research* 56 (9): e2019WR026817. https://doi.org/10.1029/2019WR026817.
- Martí, Eugènia, Joan Lluís Riera, and Francesc Sabater. 2009. "Effects of Wastewater Treatment Plants on Stream Nutrient Dynamics Under Water Scarcity Conditions." In *Water Scarcity in the Mediterranean*, edited by Sergi Sabater and Damià Barceló, 8:173–95. The Handbook of Environmental Chemistry. Berlin, Heidelberg: Springer Berlin Heidelberg. https://doi.org/10.1007/698 2009 33.
- Meng, Yuchuan, Frank J. Kelly, and Stephanie L. Wright. 2020. "Advances and Challenges of Microplastic Pollution in Freshwater Ecosystems: A UK Perspective." *Environmental Pollution* 256 (January): 113445. https://doi.org/10.1016/j.envpol.2019.113445.
- Mizyed, Numan R. 2013. "Challenges to Treated Wastewater Reuse in Arid and Semi-Arid Areas." *Environmental Science & Policy* 25 (January): 186–95. https://doi.org/10.1016/j.envsci.2012.10.016.
- Mortensen, Jacob G., Ricardo González-Pinzón, Clifford N. Dahm, Jingjing Wang, Lydia H. Zeglin, and David J. Van Horn. 2016. "Advancing the Food-Energy–Water Nexus: Closing Nutrient Loops in Arid River Corridors." *Environmental Science & Technology* 50 (16): 8485–96. https://doi.org/10.1021/acs.est.6b01351.
- Pascual-Benito, M., D. Nadal-Sala, M. Tobella, E. Ballesté, C. García-Aljaro, S. Sabaté, F. Sabater, et al. 2020. "Modelling the Seasonal Impacts of a Wastewater Treatment Plant on Water Quality in a Mediterranean Stream Using Microbial Indicators." *Journal of Environmental Management* 261 (May): 110220. https://doi.org/10.1016/j.jenvman.2020.110220.
- Pebesma, Edzer. 2016. "Handling and Analyzing Spatial, Spatiotemporal and Movement Data." June 27, 2016. https://edzer.github.io/UseR2016/#spatiotemporal-data-movement-data.
- Perkins, Daniel M., Gabriel Yvon-Durocher, Benoît O.L. Demars, Julia Reiss, Doris E. Pichler, Nikolai Friberg, Mark Trimmer, and Guy Woodward. 2012. "Consistent Temperature Dependence of Respiration across Ecosystems Contrasting in Thermal History." *Global Change Biology* 18 (4): 1300–1311. https://doi.org/10.1111/j.1365-2486.2011.02597.x.
- Podder, Aditi, A. H. M. Anwar Sadmani, Debra Reinhart, Ni-Bin Chang, and Ramesh Goel. 2021. "Per and Poly-Fluoroalkyl Substances (PFAS) as a Contaminant of Emerging Concern in Surface Water: A Transboundary Review of Their Occurrences and Toxicity Effects." *Journal of Hazardous Materials* 419 (October): 126361. https://doi.org/10.1016/j.jhazmat.2021.126361.
- Pouchoulin, S., J. Le Coz, E. Mignot, L. Gond, and N. Riviere. 2020. "Predicting Transverse Mixing Efficiency Downstream of a River Confluence." *Water Resources Research* 56 (10). https://doi.org/10.1029/2019WR026367.
- Pratt, Sara. 2022. "Rio Grande Runs Dry, Then Wet." September 2022. https://earthobservatory.nasa.gov/.
- Rice, Jacelyn, Amber Wutich, and Paul Westerhoff. 2013. "Assessment of De Facto Wastewater Reuse across the U.S.: Trends between 1980 and 2008." *Environmental Science & Technology* 47 (19): 11099–105. https://doi.org/10.1021/es402792s.
- Rup. 2006. "Processes of Transferring Pollutants in the Natural Environment." *Scientific and Technical Publishing House, Warsaw*.
- Rutherford. 1994. "River Mixing Rutherford, J. C.: 9780471942825 AbeBooks." 1994. https://www.abebooks.com/9780471942825/River-Mixing-Rutherford-J-C-0471942820/plp.
- Skorbiłowicz, Mirosław, Elżbieta Skorbiłowicz, Paulina Wójtowicz, and Emilia Zamojska. 2017. "DETERMINATION OF MIXING ZONES FOR WASTEWATER WITH RECEIVER WATERS." *Journal of Ecological Engineering* 18 (4): 192–98. https://doi.org/10.12911/22998993/74291.

- Tiwari, Bhagyashree, Balasubramanian Sellamuthu, Yassine Ouarda, Patrick Drogui, Rajeshwar D. Tyagi, and Gerardo Buelna. 2017. "Review on Fate and Mechanism of Removal of Pharmaceutical Pollutants from Wastewater Using Biological Approach." *Bioresource Technology* 224 (January): 1–12. https://doi.org/10.1016/j.biortech.2016.11.042.
- UNESCO. 2020. "United Nations World Water Development Report 2020." 2020. https://unesdoc.unesco.org/ark:/48223/pf0000372985/PDF/372985eng.pdf.multi.
- United Nations Environment Programme. 2021. "The United Nations World Water Development Report 2021: Valuing Water. UNESCO, Paris." 2021. https://unesdoc.unesco.org/ark:/48223/pf0000375724/PDF/375724eng.pdf.multi.
- Wang, Huan, Hao Xi, Linling Xu, Mingkang Jin, Wenlu Zhao, and Huijun Liu. 2021. "Ecotoxicological Effects, Environmental Fate and Risks of Pharmaceutical and Personal Care Products in the Water Environment: A Review." *Science of The Total Environment* 788 (September): 147819. https://doi.org/10.1016/j.scitotenv.2021.147819.
- Ward, Peter R. B. 1973. "Prediction of Mixing Lengths for River Flow Gaging." *Journal of the Hydraulics Division* 99 (7): 1069–81. https://doi.org/10.1061/JYCEAJ.0003677.

Chapter 4

The role of a flood-control lake in attenuating the propagation of wildfire disturbances from the largest fire recorded in New Mexico, USA.

Aashish Sanjay Khandelwal¹ Tzion Castillo², Justin Nichols¹, Asmita Kaphle¹, Paige Tunby¹, ,
Justin Reale³, David J. Van Horn⁴, Ricardo González-Pinzón¹

Department of Civil, Construction and Environmental Engineering, University of New Mexico,
Albuquerque, New Mexico, USA,

²Electrical Engineering, University of New Mexico, Albuquerque, NM USA

4.1 INTRODUCTION

Forested watersheds play a critical role as the world's primary source of freshwater (Pringle 2001; Ice 2004; Sun et al. 2002). However, the frequency and extent of devastating wildfires are increasing (Ball et al. 2021b; Robinne et al. 2021; Gannon, Wei, and Thompson 2020). Increased wildfire activity is closely tied to increasing aridity and variability in precipitation patterns, which are manifestations of global climate change (Macias Fauria, Michaletz, and Johnson 2011). When wildfires occur, the burning of tree canopies, understory vegetation, and soil layers impact the quantity and quality of water resources due to the intensification of overland flow, the release of ash and debris, and the disruption of soil processes (Reale et al. 2015; Mishra, Alnahit, and Campbell 2021; Bladon et al. 2014; Chen, McGuire, and Stewart 2020). The impacts of wildfires extend beyond terrestrial ecosystems, property, and infrastructure, as new evidence reveals that wildfires trigger cascading effects that

³ U.S. Army Corps of Engineers, Albuquerque District, Albuquerque, NM, USA,

⁴Department of Biology, University of New Mexico, Albuquerque, New Mexico, USA

propagate through fluvial networks, affecting hydrologic and environmental processes, as well as ecosystem services (Murphy et al. 2018; McGuire and Youberg 2019; Dahm et al. 2015). In light of these concerns, it is essential to understand the impacts of wildfires on forested watersheds to develop effective management strategies and safeguard the integrity of ecosystems (Hohner et al. 2019; Floyd et al. 2019).

Post-fire precipitation events on burned soil can generate significant changes in runoff patterns (Wibbenmeyer, Sloggy, and Sánchez 2023) and mobilize sediments, ash, and debris through fluvial networks (Murphy et al. 2018). The new influx of sediments can alter the geomorphology and hydrodynamics of river channels and floodplains (Malmon et al. 2007; Barnard et al. 2023), and collapse water intake infrastructure, affecting water supply systems (Robinne et al. 2021). Also, the transport of ash, increased nutrients, and organic matter can change water chemistry and stream metabolism (Sankey et al. 2017).

The impact of wildfire disturbances on fluvial networks is primarily driven by watershedrelated factors associated with fire severity and extent and post-fire dynamics of rainfall-runoff
processes. However, flow and erosion control infrastructure can also play a key role (Floyd et al.
2019). Near burned areas, erosion control structures such as gabions can help mitigate debris and
sediment transport into fluvial networks (Callegary et al. 2021; deWolfe et al. 2008). Farther into
the network, flow-control reservoirs can also play a crucial role in controlling the longitudinal
propagation of disturbances due to their considerable size, the reduction of flow velocities, and
the increase in residence times (Stone et al. 2021; Bonansea and Fernandez 2013). Since low
flow velocities induce particle deposition, including sediments and particulate nutrients, and
organic matter (Bonansea and Fernandez 2013; Goode, Luce, and Buffington 2012), their
settling into reservoir beds and the increased contact times with biomass are potential pathways

for the removal and attenuation of wildfire disturbances. While post-wildfire disturbances have been associated with the deposition of increased amounts of inorganic sediment in reservoirs used for water supply (Emelko et al. 2016), jeopardizing the effectiveness of water treatment for drinking purposes, flow control reservoirs may attenuate the propagation of wildfire disturbance with less immediate impacts for society (Basso et al. 2021).

This study combines datasets from Eulerian monitoring (i.e., at a site) of water quality parameters upstream and downstream of Santa Rosa Lake (Nichols et al.; in review) with Lagrangian monitoring (i.e., following flow paths) along the lake (Khandelwal et al.; in review) to quantify lake-induced changes and determine their role in attenuating the propagation of wildfire disturbances at the fluvial network scale. To achieve this, we established a rapid response team (Tunby et al., in review) dedicated to monitoring water quality dynamics along the Gallinas Creek-Pecos River-Santa Rosa Lake network (190 km) after the Hermit's Peak - Calf Canyon (HPCC) wildfire, the largest recorded fire in New Mexico. We seek to address how far downstream wildfire disturbances from the HPCC wildfire propagated in the fluvial network and the role of Santa Rosa Lake in that propagation.

4.2 METHODS

Study Site

The HPCC wildfire, which started on April 6th, 2022, and was contained on August 21st, 2022, became the largest recorded wildfire in New Mexico after burning 1,382 km². The fire significantly affected the Gallinas Creek watershed, where most of the affected population live (Figure 1). Approximately 87% of its area was burned, with 19% experiencing high-severity, 25% moderate severity, and 43% low severity burns. Gallinas Creek is a perennial stream that relies on snowmelt during spring and monsoonal storms in summer and fall. It originates near

Hermit's Peak and serves as a drinking water source for 7,200 residents in the City of Las Vegas, NM, located approximately 25 km downstream from the headwaters of Gallinas Creek. Further downstream, Gallinas Creek flows through canyons and farmlands before joining the Pecos River, around 128 km from its headwaters. The Pecos River flows into Santa Rosa Lake, located ~40 km downstream of the confluence of Gallinas Creek.

Monitoring Description

Eulerian monitoring: Within two weeks from the beginning of the fire, our rapid response team installed YSI EXO multiparameter water quality sondes at three locations along the Gallinas Creek watershed. These sites include the La Placita fire station in Gallinas, NM (referred to as GFT_{22 km}, because it is located 22 km from the headwaters of Gallinas Creek, our reference point at 0 km), near Montezuma, NM (GMZ_{29 km}), and near Lourdes, NM (GL_{56 km}). Two additional sondes were deployed on the Pecos River (PSR_{170 km} and PBS_{190 km}) in late 2020 as part of a collaborative effort between the US Army Corps of Engineers (USACE) and the University of New Mexico (Figure 1). The EXO sondes recorded water temperature, specific conductivity, dissolved oxygen (DO), turbidity, and pH at 15-minute intervals. Each sonde underwent monthly cleaning and calibration, following the guidelines set by the U.S. Geological Survey (Wagner et al. 2006). In addition to the sondes data, discharge and reservoir data were gathered at 15-min intervals by USGS stream gages 08382650, 08382830, and 08382810, located near the PSR_{170 km}, PBS_{190 km}, and Santa Rosa Lake, respectively (U.S. Geological Survey, 2022). Figure S1 presents the Eulerian data.

Lagrangian monitoring: Between July 15, 2022, and October 12, 2022, we carried four repetitions of Lagrangian monitoring following ~30 km along the transition between the Pecos River (a lotic system) and Santa Rosa Lake (a lentic system) to determine the impacts of wildfire

disturbances on water quality parameters (Figure 1). These Lagrangian monitoring campaigns lasted 2-3 hours to minimize the influence of diurnal variations on the water quality datasets and featured a sampling frequency of one recording every two minutes. After the first campaign, we avoided a reach consisting of rapids and a waterfall due to safety concerns between the 178-179 km section. At the time of sampling, discharges in the Pecos River above Santa Rosa Lake (USGS gage 08382650) were above median historical values from 1977-2022 (Table 1). These higher discharge values were due to post-wildfire runoffs and the historically high monsoon precipitation falling in 2022. Similar trends were observed at GL_{56km} (USGS gage 08382500).

Our Lagrangian monitoring was completed with The Navigator (Khandelwal et al. 2023, under review), an autonomous surface vehicle made of fiberglass, instrumented with a GPS tracker to monitor space-time positioning, a thrust and rudder system to follow a preplanned GPS waypoint, and a Raspberry Pi microcontroller coupled to multiparameter sondes to monitor temperature (temp), optical dissolved oxygen (DO), turbidity (turb), pH and conductivity (Sp Cond). The Navigator features real-time data transmission through cellular service, enabling real-time tracking and easy retrieval when the survey is completed. To avoid data losses from any potential misfunctioning of The Navigator, we also used a kayak carrying a multiparameter YSI EXO2 sonde and a GPS (Figure S2).

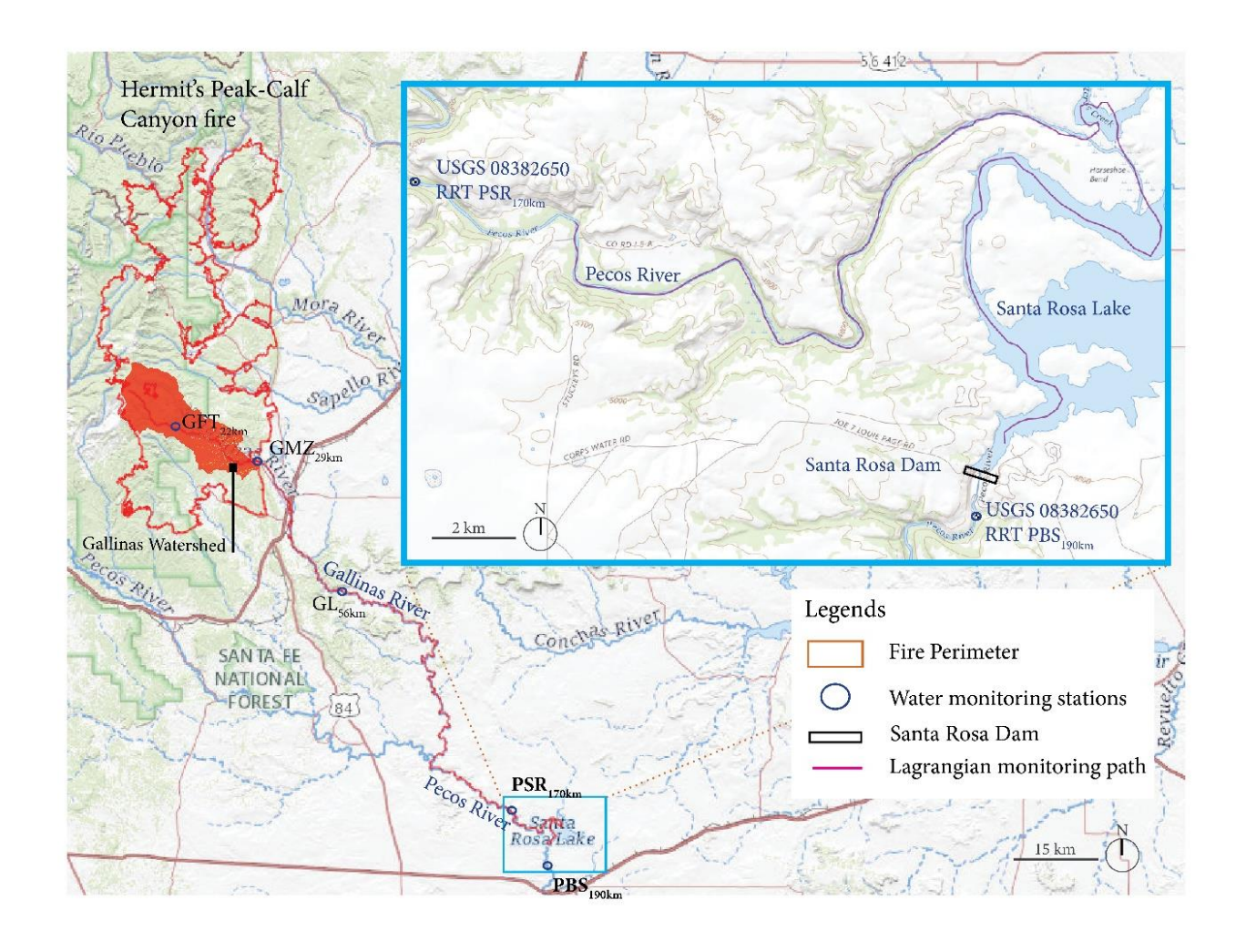


Figure 4.1: Eulerian and Lagrangian monitoring of the Hermit's Peak-Calf Canyon wildfire. The red line represents the burn perimeter. The red area represents the burn scar boundary of the Gallinas Creek watershed. GFT $_{22\,km}$, Gallinas Creek near La Placita fire station, 22 km downstream from the headwaters of Gallinas Creek; GMZ $_{29\,km}$, Gallinas Creek near Montezuma; GL $_{56\,km}$, Gallinas Creek near Lourdes; PSR $_{170\,km}$, Pecos River upstream of Santa Rosa Lake; PBS $_{190\,km}$, Pecos River downstream of Santa Rosa Lake.

Table 4.1: Lake conditions during the Lagrangian monitoring with The Navigator. Discharge values are contextualized with records.

Date	Transect length	Lake elevation	Pecos River discharge 08382650	Comparable median Pecos River discharge (1977-2022)	Gallinas Creek discharge 08382500	Comparable median Gallinas Creek discharge (1951-2022)		
Unit	km	m	m^3/s	m^3/s	m^3/s	m^3/s		
7/15/2022	11.60	1433.68	5.10	0.82	0.85	0.05		
7/29/2022	3.36	1434.77	8.69	1.93	1.56	0.23		
8/19/2022	7.89	1432.51	13.08	0.99	4.13	0.20		
10/12/2022	7.62	1435.83	4.59	0.57	0.08	0.00		

We established three distinct analysis periods based on flow time-series analyses (Nichols et al. 2023 under review), we established three distinct analysis periods. The premonsoon period spanned from the start of our monitoring on April 25th, 2022, to June 26th, 2022. The monsoon period, characterized by high precipitation-runoff, lasted from June 26th, 2022, to September 13th, 2022. The post-monsoon period extended from September 13th, 2022, to December 1st, 2022.

Estimation of changes in sediment transport

The magnitude of turbidity in streams, lakes, and estuaries is often proportional to total suspended solids (TSS) and can be quantified through linear regression analysis (Rasmussen et al. 2011). The turbidity-TSS relation is more reliable than sediment transport curves using streamflow (Lee, Rasmussen, and Ziegler 2008) and computational methods (Porterfield 1972). The USGS collected samples between June 2022 and October 2022 near GMZ_{29km} to estimate TSS as part of their mission to identify and mitigate chronic stresses on water resources post-fire (USGS n.d.):

$$TSS = 2.028 (Turb) + 26.03$$
 (1),

where *Turb* is the turbidity in FNU measured in the field using sonde (Figure S3).

We determined bulk or suspension densities following the approach proposed by Mccullough (1999). Bulk density (ρ , kg/m³) was determined as:

$$\rho_{river\ or\ lake} = TSS + \rho_{rw}(1 - TSS)/\rho_s \tag{2},$$

where ρ_{rw} is the density of water at a given temperature (kg/m³) and ρ_s is the density of the sediments, assumed as 2.5 kg/m³ based on the USGS samples.

We used the approach that Bates (1953) introduced to classify deltas and their deposits based on the differences in bulk density between a flowing river and a lake. When the river's bulk density is higher than the lake's, hyperpycnal or stratified jet flows occur. In such scenarios, the river flow plunges beneath the lake's water surface and continues its course along the lakebed. After wildfires, river bulk densities increase primarily due to increased loads of fine-grained sediments and ash (Kim 2002; Turner and Huppert 1992). Kim (2002) introduced a non-dimensional density parameter, R, expressed as:

$$R = \rho_{lake} - \rho_{river}/\rho_{lake} - \rho_{rw} \tag{3}.$$

R considers the buoyancy effect of the incoming freshwater into the lake. A critical value R_c = -2 was proposed by Kim (2002) to separate weak plunging jets (R_c < R_c <0) from strong plunging jets (R_c <0). In weak plunging jets, the flow originally plunges, but the density difference between the incoming flow and the lake water is not enough to produce a substantial shear and further propagation of the river flow along the lakebed.

Data quality control and assurance:

Raw and converted data were processed for outliers and sensor drift with Aquarius Timeseries 21.1. Erroneous outliers were eliminated using a moving average filter targeting points deviating more than 20% from a two-hour moving window. We corrected sensor drift and biofouling by comparing pre- and post-cleaning and calibration values and applied a linear correction from the date of the previous maintenance (Wagner et al. 2006). Lastly, we performed a final visual inspection of data quality before statistical analyses.

4.3 RESULTS

Flow Dynamics

During the pre-monsoon period, there were no significant high-flow events. Discharges upstream of Santa Rosa Lake, at PSR_{170 km}, reached their lowest values during this period, with average values ranging from 0.02 to 0.17 m³/s. In mid-June, a block release from Santa Rosa Lake caused the average discharge at PBS_{190 km} to increase to 2.81 m³/s for approximately eight days (Figure 3). This event resulted in the lake level dropping from 1436.3 m to 1429.8 m, the lowest level in 2022.

In the monsoon period, 243 mm of precipitation occurred on the burn scar, with the majority falling between July 26th-30th (70 mm) and August 17th -18th (42 mm). During this period, there was one high flow event at $PSR_{170 \text{ km}}$ with a discharge of 68.0 m³/s, i.e., 11x greater than the mean flow for the past 47 years (USGS n.d.), matching similar trends observed across the sites along Gallinas Creek (i.e., $GFT_{22 \text{ km}}$, $GMZ_{29 \text{ km}}$, and $GL_{56 \text{ km}}$) (Nichols et al. 2023 under review). The high flow observed at $PSR_{170 \text{ km}}$ resulted in a surface level of 1438.5 m on August

11th, the highest in 2022. The level fell again to 1431.3 m due to another block release from Santa Rosa Lake, which lasted for approximately ten days (Figure 2)

In the post-monsoon period, 110 mm of precipitation was recorded within the burn scar. The majority of this precipitation occurred between October 3rd-8th and October 16th, with 57 mm and 34 mm of rainfall, respectively. The peak discharge value during this period was 15.1 m^3/s at $PSR_{170 \text{ km}}$ (Figure 2) and the lake level gradually increased from 1435.2 m to 1436.8 m.

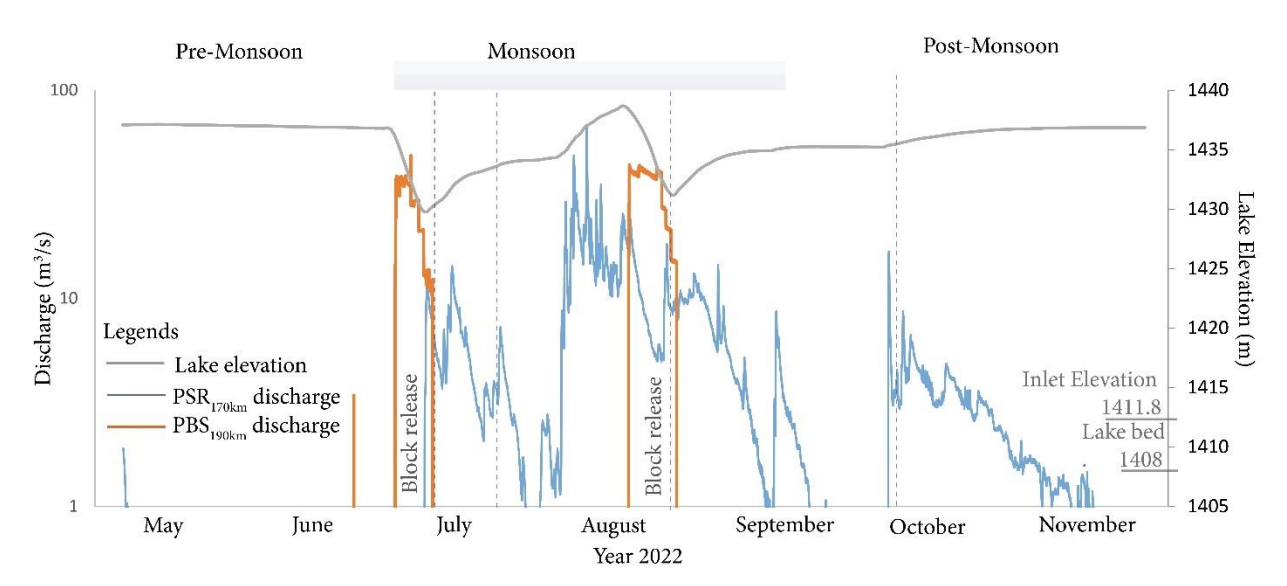


Figure 4.2: Discharges observed near $PSR_{170 \text{ km}}$ Pecos River upstream of Santa Rosa Lake and $PBS_{190 \text{ km}}$, Pecos River downstream of Santa Rosa Lake. Lake levels for Santa Rosa Lake during the study period in 2022.

Water quality dynamics from Eulerian monitoring

During the pre-monsoon period, there was an increase in specific conductivity from the headwaters to the lower sites, with a 1,870 uS/cm difference between GFT_{22 km} and PBS_{190 km} (Figure S2). Turbidity values were at their lowest during the fire year at all sites upstream of Santa Rosa Lake, with average values ranging from 5.9 to 62.7 FNU (Figure S2). On the contrary, PBS_{190 km} had the highest turbidity values of the fire year, with an average of 26.3

FNU. All other water quality parameters were similar between the $PSR_{170 \text{ km}}$ and $PBS_{190 \text{ km}}$ (Figures 3-4).

With respect to the pre-monsoon, most water quality parameters significantly changed at the stations upstream of Santa Rosa Lake (i.e., GFT_{22 km}, GMZ_{29 km}, GL_{56 km}, and PSR_{170 km}) during the monsoon period, and only a few changed downstream of the lake at PBS_{190 km} (Figures 3 and S1). Turbidity experienced a significant increase at the monitoring sites, including PSR_{170 km} upstream of Santa Rosa Lake (Figures 3 and S1), with period averages ranging from 149 to 574 FNU. However, unlike observed values at locations upstream of the lake, PBS_{190 km} experienced minimal reductions in turbidity, with a period average of 16 FNU (Figures 3 and S1). Specific conductivity significantly decreased at monitoring sites upstream of Santa Rosa Lake, with average ranges of 172 to 442 uS/cm, while it remained relatively high at PBS_{190 km}, averaging 2087 uS/cm (Figures 3 and S1).

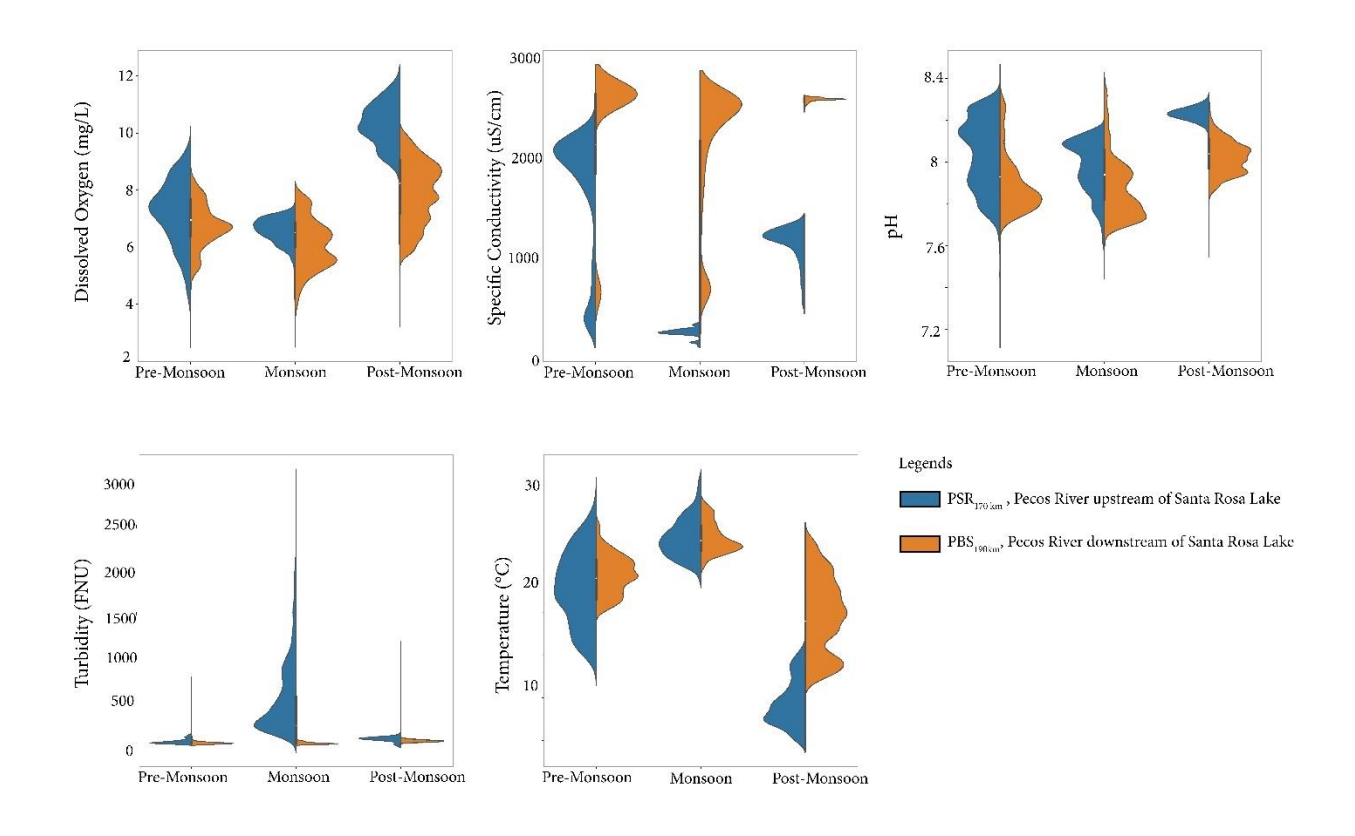


Figure 4.3: Split violin plots showing the variations in water quality at $PSR_{170 \text{ km}}$, Pecos River upstream of Santa Rosa Lake, and $PBS_{190 \text{ km}}$, Pecos River downstream of Santa Rosa Lake, grouped by analysis period.

Water quality changes from Lagrangian monitoring

At the time of sampling, discharges in the Pecos River above Santa Rosa Lake (USGS gage 08382650) were above median historical values from 1977-2022 (Table 1). The Lagrangian data showed a noticeable transition in water quality parameters between the lotic and lentic systems. Moreover, the data showed that the location and timing of such transition regions were dynamic (Figure 4.4 & 4.5). Between 7/29/2022 and 10/12/2022, we observed a shift of the delta positioning of ~ 1.2 km as the lake's elevation rose by 3.3 m.

In July, we observed higher turbidity levels in the Pecos River, ranging from 368.5 to 881.9 FNU, compared to the surface of Santa Rosa Lake, which ranged from 6.24 to 52.9 FNU.

The river's temperature was colder, ranging from 23.5 to 26 °C, while the lake recorded temperatures of 25.8 to 27.11 °C (Figures 4-5). Additionally, the river's specific conductivity was lower than at the lake's surface. These findings suggest that the incoming flow into the river had a higher bulk density than the water near the lake's surface. As there was no water released from the dam during this month, there was a steady increase in the lake's level. No significant differences were observed in the levels of dissolved oxygen and pH during this month. Due to logistical challenges, we do not have any data for the delta region during this period.

Similar turbidity, specific conductivity, and temperature trends were observed for both the river and lake surface water in August (Figures 4-5), with a significant change occurring in the delta region. The delta region experienced dissolved oxygen levels reaching anoxic conditions (~0 mg/L) on 8/19/2022 (Figure 4). This suggests that drops in dissolved oxygen were triggered by runoff draining from the Gallinas Creek watershed, which accounted for approximately 31% of the total discharge near the lake, and the Pecos watershed, which contributed ~ 69% of the total discharge (refer Table 1). During this period, we observed floating debris and foamy water in the delta sections following monsoon precipitation events on the burn scar (see Figure S3). There was a block release during this month between August 11th-21st, which resulted in a drop in the lake's elevation from 1438.5 m to 1431.3 m.

For the October run, we no longer recorded the presence of an anoxic zone in the delta region, as the runoff draining from the Gallinas Creek watershed decreased (~14% of the total discharge near the lake) compared to the Pecos watershed (~ 86% of the total discharge). All other parameters followed a similar trend observed during the monsoon, with significant changes occurring in the delta regions (Figures 4-5). No water was released from the dam this month, resulting in no current due to intake and a steady increase in the lake level.

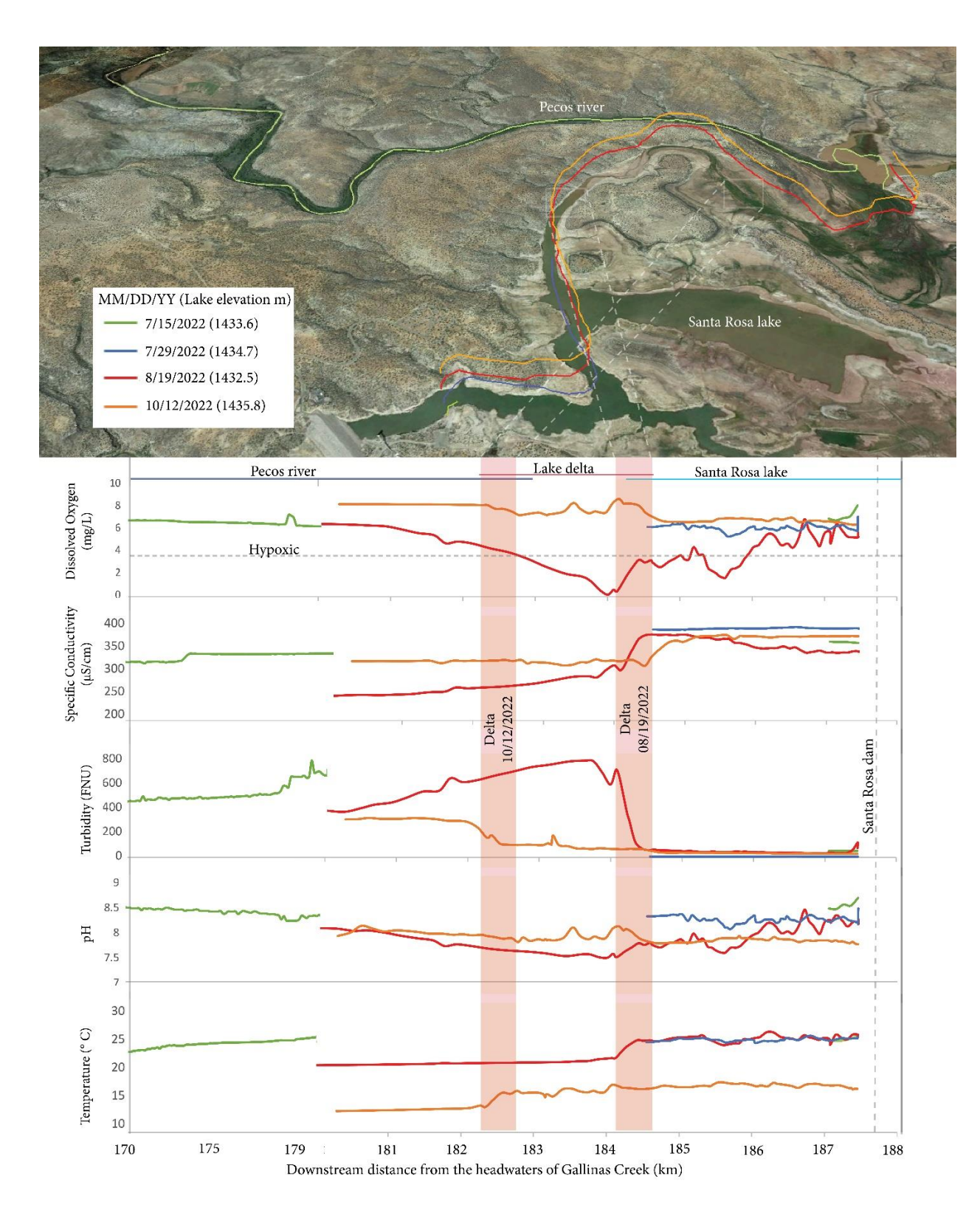


Figure 4.4: Lagrangian data of dissolved oxygen, specific conductivity, turbidity, pH, and water temperature collected with The Navigator. Data were collected during the monsoon (green, blue, and red) and post-monsoon (orange) periods. The red zone indicates the location of the delta, which shifted as the lake level rose from 1432.5 m to 1435.8 m.

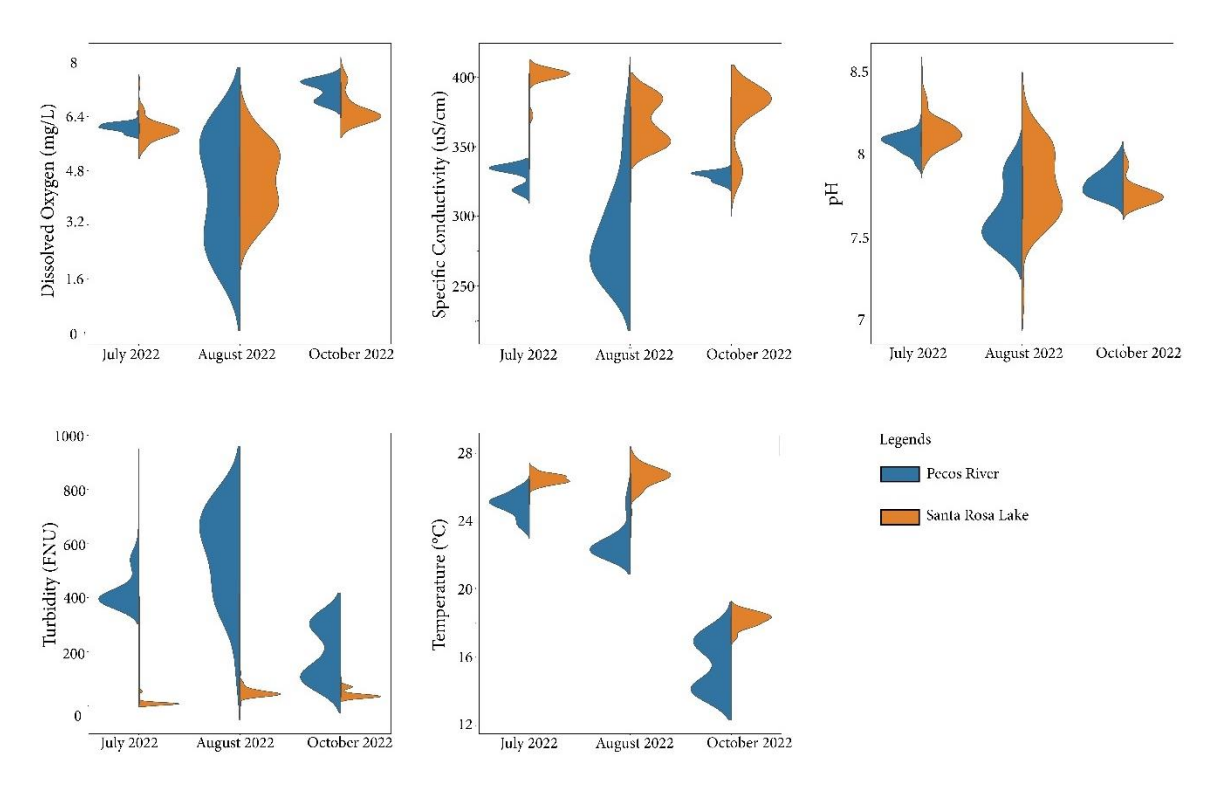


Figure 4.5: Split violin plots showing the variations in water quality from the incoming Pecos River upstream of Santa Rosa Lake and along Santa Rosa Lake.

Changes in sediment transport along the transition between the Pecos River and Santa Rosa Lake

The non-dimensional R parameter (Kim 2002) quantifies buoyancy effects due to density differences when an incoming river merges with a lake. We compared R values with the critical $R_c = -2$. This critical R_c separates weak plunging jets ($R_c < R < 0$) from strong plunging jets ($R < R_c < 0$) (Zavala 2020). We observed R values dropping below R_c (Figure 6) during the monsoon, suggesting strong plunging induced by high incoming sediment loads that develop hyperpycnal subaqueous deltas (Zavala et al. 2021). These high-density hyperpycnal discharges typically consist of suspended sediment loads and may include a bedload component due to its high erosive nature (Lamb et al. 2010). Before and after those strong plunging jets, there were

weaker ones under which the river flow plunges, but the density differences were not enough to produce a substantial shear and erosion at the lake bottom (Lai and Capart 2009). Those weak plunges are referred to as hyperpycnal littoral deltas and are associated with river flows that remain stratified and suspended (Zavala et al. 2021). If they grow enough, hyperpycnal littoral deltas can eventually transport sediments deep into the lakebed.

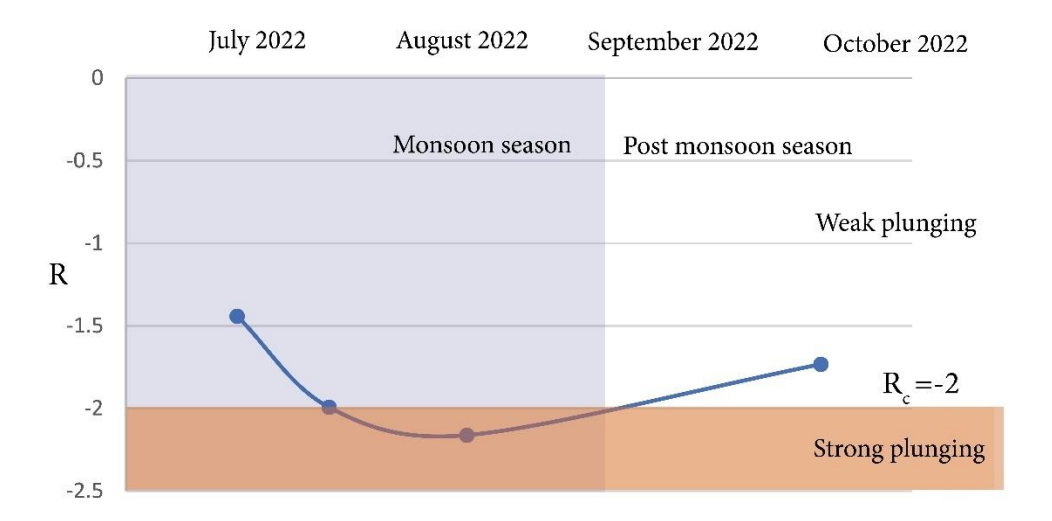


Figure 4.6: To gain insights into hyperpycnal delta dynamics, we examined the seasonal regimes of the non-dimensional density parameter R.

Table 4.2: Average turbidity, temperature, total suspended sediments (TSS), and density of river water and lake water for different Lagrangian monitoring days and the corresponding non-dimensional density parameter R.

		F	River		Lake					
Date	Turbidity (FNU)	Temperature (°C)	TSS (kg/m³)	ρ _{river} (kg/m³)	$ ho_{rw}$ (kg/m³)	Turbidity (FNU)	Temperature (°C)	TSS (kg/m³)	ρ _{lake} (kg/m³)	R (-)
7/15/2022	390	24.8	0.81	997.1	997.9	53	26.5	0.13	996.7	-1.4
7/29/2022	870	22.5	1.85	997.7	999.4	7	26.4	0.04	996.7	-2.0
8/19/2022	470	22.1	0.98	997.8	998.7	42	26.7	0.11	996.6	-2.2
10/12/2022	307	13.99	0.65	999.3	999.9	40	18.34	0.11	998.5	-1.7

4.4 DISCUSSION

Wildfire disturbance propagation: Eulerian monitoring

The most significant changes to water quality parameters observed in our study occurred during the monsoon period. We observed high-flow events coupled with a rapid increase in turbidity from GFT_{22 km} to PSR_{170 km}. Due to the low probability nature of these flows with respect to historical records (Nichols et al. 2023 under review), they are likely associated with altered hydrologic processes within the burn scar. Turbidity concentrations increased by 25x, 3x, 11x, and 20x at GFT_{22 km}, GMZ_{29 km}, GL_{56 km}, and PSR_{170 km}, respectively, with respect to the premonsoon period. Despite all these consistent turbidity changes upstream of Santa Rosa Lake, there were no changes in turbidity downstream of the lake at PBS_{190 km}. With respect to the premonsoon period, all sites except PBS_{190 km} showed changes in stream metabolism during the monsoon season, indicating that Santa Rosa Lake buffered wildfire disturbances originating from the HPCC wildfire burn scar (Nichols et al. 2023 under review).

Transition zones along Santa Rosa Lake's delta: Lagrangian monitoring

While Eulerian monitoring provided important insights into the generation and propagation of disturbances from the HPCC fire along 190 km, including the role of the lake in buffering those disturbances, this latter understanding comes from a black-box analysis between input signals from PSR_{170km} and output signals from PBS_{190km}. Thus, gaining a mechanistic understanding linking what happened along the lake and why remains elusive with Eulerian data.

Our Lagrangian data from The Navigator provided insights into the processes affecting the propagation of water disturbances from burned areas into the Pecos River and Santa Rosa Lake. These insights cannot be fully resolved with Eulerian monitoring or coarse synoptic

profiling. We observed the formation of hyperpycnal flows when high turbidity and lower temperature flow propagating along the river forced denser waters to plunge below the lake's surface. As a result, on 8/19/2022, for example, we observed a significant drop in turbidity values from around 700 FNU (22°C) to approximately 60 FNU (26°C) along the lake's delta, within merely 250 m (Figure 5). These turbidity changes were also accompanied by increases in dissolved oxygen from ~0 mg/L to ~4 mg/L. Similarly, on 10/12/2022, within 300 m, the turbidity along the delta changed from approximately 300 FNU (14°C) to ~100 FNU (18°C); in this event, however, there was a slight drop in oxygen from ~8 mg/L to ~6 mg/L.

Our Lagrangian monitoring with The Navigator indicated drastic changes in water quality parameters over short distances along the lake in response to post-wildfire rainfall-runoff events occurring hundreds of kilometers upstream. The dissolved oxygen sag and recovery patterns observed were inversely proportional to turbidity, suggesting that oxygen removal from respiration and chemical demands and additions from photosynthesis were out of balance and most likely controlled by sediment fluxes from the wildfire. While reaeration could have played a more significant role in incorporating oxygen into the river, oxygen removal pathways dominated until the delta induced hyperpycnal flows which sank the sediments. pH values were lower in zones with low dissolved oxygen, which could be associated with increased aerobic microbial metabolism and CO₂ releases from increased respiration due to the mobilization of sediments with increased carbon and nutrients (Chapra, 2008). Together, our results bring into focus the importance of Lagrangian monitoring to move beyond black-box analyses and improve mechanistic understanding of hydro biogeochemical processes (Figure 7).

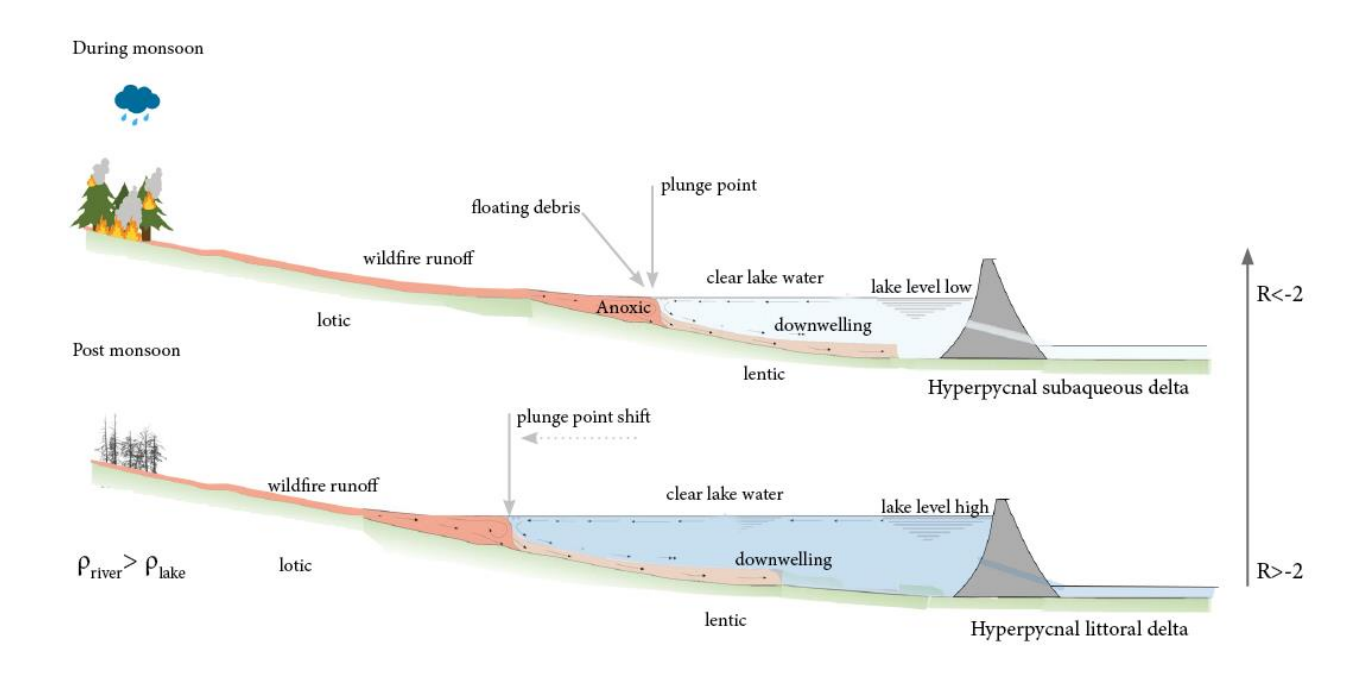


Figure 4.7: Conceptual diagram comparing monsoon and post-monsoon hyperpycnal flows based on Lagrangian monitoring data.

4.5 CONCLUSIONS

The HPCC wildfire was the largest recorded in New Mexico, leaving a burn scar of 1,382 km². Eulerian monitoring with five instrumented sites along the 190 km Gallinas Creek-Pecos River-Santa Rosa Lake fluvial network revealed high flow and turbidity events during the monsoon period. While sites located upstream of Santa Rosa Lake had turbidity increases of 25x, 3x, 11x, and 20x at $GFT_{22 \, km}$, $GMZ_{29 \, km}$, $GL_{56 \, km}$, and $PSR_{170 \, km}$ during the monsoon with respect to the pre-monsoon period, the $PBS_{190 \, km}$ site showed no changes, indicating that Santa Rosa Lake buffered wildfire disturbances originating from the HPCC wildfire burn scar.

We combined Eulerian data from PSR_{170 km} and PBS_{190 km} with Lagrangian data from The Navigator to move beyond black-box analyses and pinpoint where the buffering effects happened and why. From this, we identified the existence of hyperpycnal flows that plunged high turbidity

and colder water from the river into the lakebed, creating contrasting ecotones in short distances (~300 m) along the lake's delta. The simultaneous measurement of spatial and temporal dynamics reduced the need for interpolating data between Eulerian stations to estimate within-lake and highly dynamic processes. Therefore, the availability of The Navigator, an easy-to-deploy, autonomous, and affordable technology to conduct Lagrangian monitoring, was key to providing high-resolution data to resolve mechanistic processes that would be otherwise unobservable.

4.6 CHAPTER REFERENCES

- Ball, Grady, Peter Regier, Ricardo González-Pinzón, Justin Reale, and David Van Horn. 2021. "Wildfires Increasingly Impact Western US Fluvial Networks." *Nature Communications* 12 (1): 2484. https://doi.org/10.1038/s41467-021-22747-3.
- Barnard, David M., Timothy R. Green, Kyle R. Mankin, Kendall C. DeJonge, Charles C. Rhoades, Stephanie K. Kampf, Jeremy Giovando, et al. 2023. "Wildfire and Climate Change Amplify Knowledge Gaps Linking Mountain Source-Water Systems and Agricultural Water Supply in the Western United States."

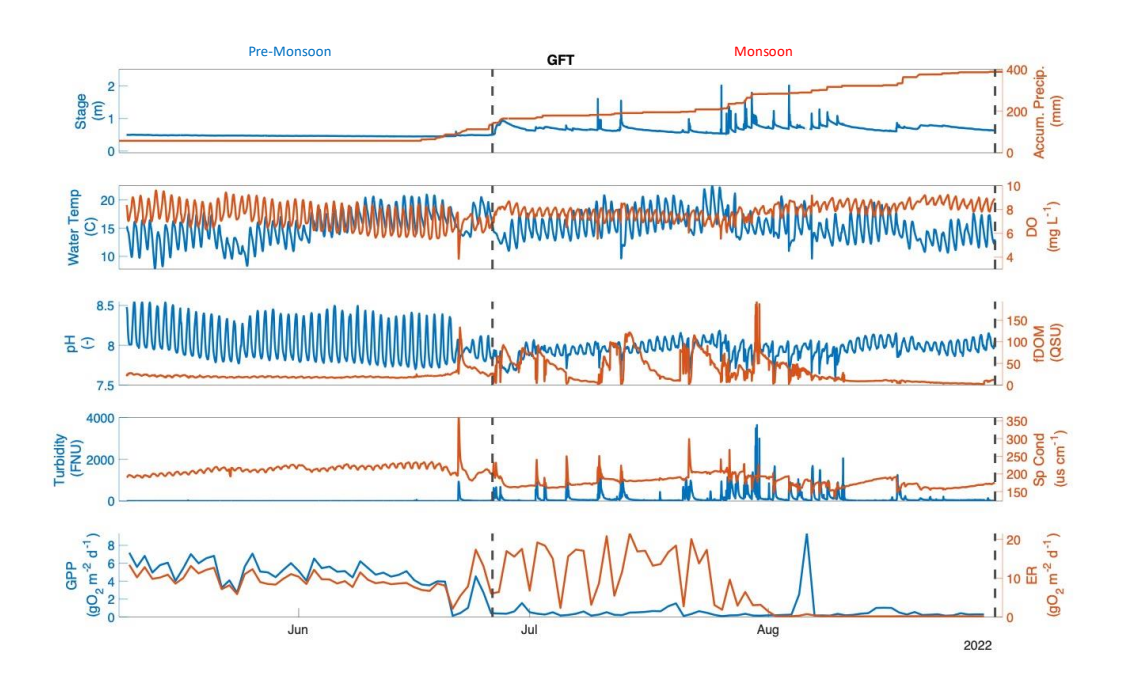
 **Agricultural Water Management 286 (August): 108377. https://doi.org/10.1016/j.agwat.2023.108377.
- Basso, Marta, Marcos Mateus, Tiago B. Ramos, and Diana C. S. Vieira. 2021. "Potential Post-Fire Impacts on a Water Supply Reservoir: An Integrated Watershed-Reservoir Approach." *Frontiers in Environmental Science* 9 (June). https://doi.org/10.3389/fenvs.2021.684703.
- Bates, Charles C. 1953. "RATIONAL THEORY OF DELTA FORMATION1." *AAPG Bulletin* 37 (9): 2119–62. https://doi.org/10.1306/5CEADD76-16BB-11D7-8645000102C1865D.
- Bladon, Kevin D., Monica B. Emelko, Uldis Silins, and Micheal Stone. 2014. "Wildfire and the Future of Water Supply." *Environmental Science & Technology* 48 (16): 8936–43. https://doi.org/10.1021/es500130g.
- Bonansea, M., and R. L. Fernandez. 2013. "Remote Sensing of Suspended Solids Concentration in a Reservoir with Frequent Wildland Fires on Its Watershed." *Water Science and Technology* 67 (1): 217–23. https://doi.org/10.2166/wst.2012.560.
- Callegary, James B, Laura M Norman, Christopher J Eastoe, Joel B Sankey, and Ann Youberg. 2021. "Preliminary Assessment of Carbon and Nitrogen Sequestration Potential of Wildfire-Derived Sediments Stored by Erosion Control Structures in Forest Ecosystems, Southwest USA." *Air, Soil and Water Research* 14 (January): 11786221211001768. https://doi.org/10.1177/11786221211001768.
- Chen, Jingjing, Kevin J. McGuire, and Ryan D. Stewart. 2020. "Effect of Soil Water-Repellent Layer Depth on Post-Wildfire Hydrological Processes." *Hydrological Processes* 34 (2): 270–83. https://doi.org/10.1002/hyp.13583.
- Dahm, Clifford N., Roxanne I. Candelaria-Ley, Chelsea S. Reale, Justin K. Reale, and David J. Van Horn. 2015. "Extreme Water Quality Degradation Following a Catastrophic Forest Fire." *Freshwater Biology* 60 (12): 2584–99. https://doi.org/10.1111/fwb.12548.
- deWolfe, Victor G., Paul M. Santi, J. Ey, and Joseph E. Gartner. 2008. "Effective Mitigation of Debris Flows at Lemon Dam, La Plata County, Colorado." *Geomorphology*, Debris flows initiated by runoff, erosion, and sediment entrainment in western North America, 96 (3): 366–77. https://doi.org/10.1016/j.geomorph.2007.04.008.
- Emelko, Monica B., Micheal Stone, Uldis Silins, Don Allin, Adrian L. Collins, Chris H. S. Williams, Amanda M. Martens, and Kevin D. Bladon. 2016. "Sediment-Phosphorus Dynamics Can Shift Aquatic Ecology and Cause Downstream Legacy Effects after Wildfire in Large River Systems." *Global Change Biology* 22 (3): 1168–84. https://doi.org/10.1111/gcb.13073.

- Floyd, Ian, Marielys Ramos-Villanueva, Ronald Heath, and Stephen Brown. 2019. "Evaluating Post-Wildfire Impacts to Flood Risk Management (FRM): Las Conchas Wildfire New Mexico." Engineer Research and Development Center (U.S.). https://doi.org/10.21079/11681/32910.
- Gannon, Benjamin M., Yu Wei, and Matthew P. Thompson. 2020. "Mitigating Source Water Risks with Improved Wildfire Containment." *Fire* 3 (3): 45. https://doi.org/10.3390/fire3030045.
- Goode, Jaime R., Charles H. Luce, and John M. Buffington. 2012. "Enhanced Sediment Delivery in a Changing Climate in Semi-Arid Mountain Basins: Implications for Water Resource Management and Aquatic Habitat in the Northern Rocky Mountains." *Geomorphology* 139–140 (February): 1–15. https://doi.org/10.1016/j.geomorph.2011.06.021.
- Hohner, Amanda K., Charles C. Rhoades, Paul Wilkerson, and Fernando L. Rosario-Ortiz. 2019. "Wildfires Alter Forest Watersheds and Threaten Drinking Water Quality." *Accounts of Chemical Research* 52 (5): 1234–44. https://doi.org/10.1021/acs.accounts.8b00670.
- Ice, George. 2004. "History of Innovative Best Management Practice Development and Its Role in Addressing Water Quality Limited Waterbodies." *Journal of Environmental Engineering* 130 (6): 684–89. https://doi.org/10.1061/(ASCE)0733-9372(2004)130:6(684).
- Kim, Sunkyoung Annie. 2002. "Discharge of Buoyant Fluid Jets and Particle-Laden Jets into Stratified Ambient Fluid." University of British Columbia. https://doi.org/10.14288/1.0063493.
- Kraus. 2017. "Ecohydrological Interfaces as Hot Spots of Ecosystem Processes Krause 2017 Water Resources Research Wiley Online Library." 2017. https://agupubs.onlinelibrary.wiley.com/doi/10.1002/2016WR019516.
- Lai, Steven Y. J., and H. Capart. 2009. "Reservoir Infill by Hyperpycnal Deltas over Bedrock." *Geophysical Research Letters* 36 (8). https://doi.org/10.1029/2008GL037139.
- Lamb, M. P., B. McElroy, B. Kopriva, J. Shaw, and D. Mohrig. 2010. "Linking River-Flood Dynamics to Hyperpycnal-Plume Deposits: Experiments, Theory, and Geological Implications." *Geological Society of America Bulletin* 122 (9–10): 1389–1400. https://doi.org/10.1130/B30125.1.
- Lee, Rasmussen, and Ziegler. 2008. "Characterization of Suspended Sediment Loading to and from John Redmond Reservoir, East-Central Kansas, 2007–2008." https://pubs.usgs.gov/sir/2008/5123/pdf/sir2008_5123.pdf.
- Macias Fauria, Marc, Sean T. Michaletz, and Edward A. Johnson. 2011. "Predicting Climate Change Effects on Wildfires Requires Linking Processes across Scales." *WIREs Climate Change* 2 (1): 99–112. https://doi.org/10.1002/wcc.92.
- Malmon, Daniel V., Steven L. Reneau, Danny Katzman, Alexis Lavine, and Jared Lyman. 2007. "Suspended Sediment Transport in an Ephemeral Stream Following Wildfire." *Journal of Geophysical Research: Earth Surface* 112 (F2). https://doi.org/10.1029/2005JF000459.
- Mccullough, Greg. 1999. "Chapter 2 (Annex) Transport of Linthipe River Suspended Sediments in Lake Malawi/Nyasa."
- McGuire, Luke A., and Ann M. Youberg. 2019. "Impacts of Successive Wildfire on Soil Hydraulic Properties: Implications for Debris Flow Hazards and System Resilience." *Earth Surface Processes and Landforms* 44 (11): 2236–50. https://doi.org/10.1002/esp.4632.
- Mishra, Ashok, Ali Alnahit, and Barbara Campbell. 2021. "Impact of Land Uses, Drought, Flood, Wildfire, and Cascading Events on Water Quality and Microbial Communities: A Review and Analysis." *Journal of Hydrology* 596 (May): 125707. https://doi.org/10.1016/j.jhydrol.2020.125707.
- Murphy, Sheila F., R. Blaine McCleskey, Deborah A. Martin, Jeffrey H. Writer, and Brian A. Ebel. 2018. "Fire, Flood, and Drought: Extreme Climate Events Alter Flow Paths and Stream Chemistry." *Journal of Geophysical Research: Biogeosciences* 123 (8): 2513–26. https://doi.org/10.1029/2017JG004349.
- Nichols, Kaphle, Tunby, Khandelwal, Reale, Van Horn, and González-Pinzón. 2023. "Longitudinal Propagation of Aquatic Disturbances from the Largest Wildfire Recorded in New Mexico, USA."
- Porterfield, George. 1972. "Computation of Fluvial-Sediment Discharge." USGS Numbered Series 03-C3. *Computation of Fluvial-Sediment Discharge*. Vol. 03-C3. Techniques of Water-Resources Investigations. U.S. Govt. Print. Off.: for sale by the Branch of Distribution, U.S. Geological Survey,. https://doi.org/10.3133/twri03C3.
- Pringle, Catherine M. 2001. "Hydrologic Connectivity and the Management of Biological Reserves: A Global Perspective." *Ecological Applications* 11 (4): 981–98. https://doi.org/10.1890/1051-0761(2001)011[0981:HCATMO]2.0.CO;2.
- Rasmussen, Gray, Glysson, and Ziegler. 2011. "Guidelines and Procedures for Computing Time-Series Suspended-Sediment Concentrations and Loads from In-Stream Turbidity-Sensor and Streamflow Data." Techniques and Methods. Techniques and Methods.

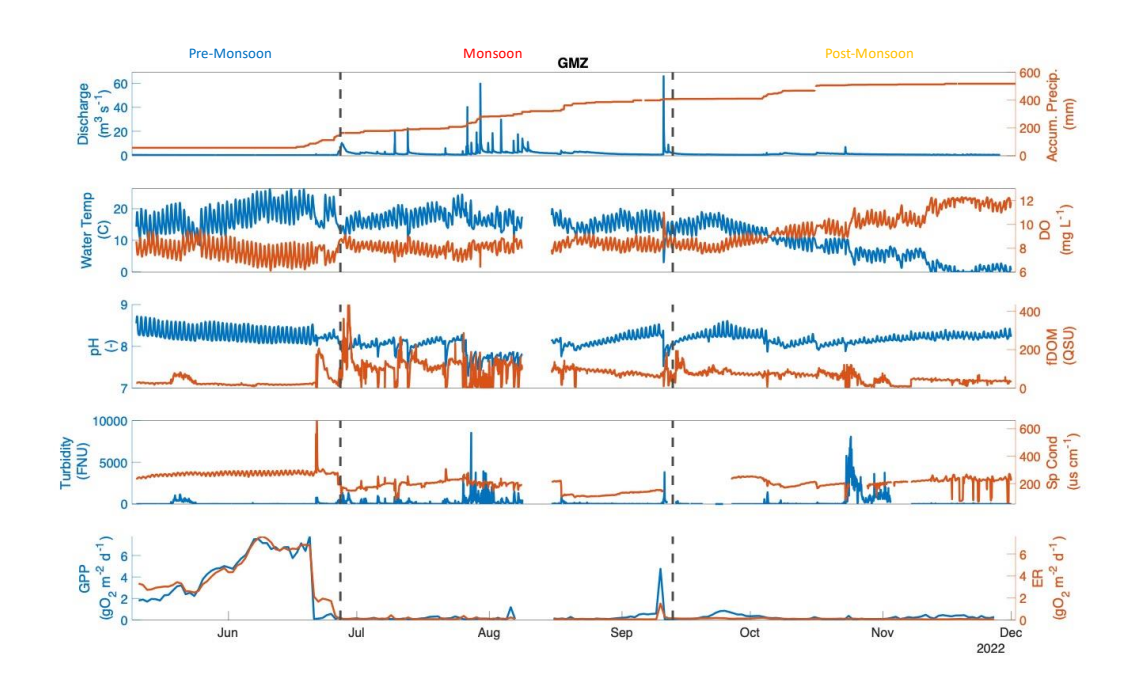
- Reale, Justin K., David J. Van Horn, Katherine E. Condon, and Clifford N. Dahm. 2015. "The Effects of Catastrophic Wildfire on Water Quality along a River Continuum." *Freshwater Science* 34 (4): 1426–42. https://doi.org/10.1086/684001.
- Robinne, François-Nicolas, Dennis W. Hallema, Kevin D. Bladon, Mike D. Flannigan, Gabrielle Boisramé, Christian M. Bréthaut, Stefan H. Doerr, et al. 2021. "Scientists' Warning on Extreme Wildfire Risks to Water Supply." *Hydrological Processes* 35 (5): e14086. https://doi.org/10.1002/hyp.14086.
- Sankey, Joel B., Jason Kreitler, Todd J. Hawbaker, Jason L. McVay, Mary Ellen Miller, Erich R. Mueller, Nicole M. Vaillant, Scott E. Lowe, and Temuulen T. Sankey. 2017. "Climate, Wildfire, and Erosion Ensemble Foretells More Sediment in Western USA Watersheds." *Geophysical Research Letters* 44 (17): 8884–92. https://doi.org/10.1002/2017GL073979.
- Stone, Micheal, Bommanna G. Krishnappan, Uldis Silins, Monica B. Emelko, Chris H. S. Williams, Adrian L. Collins, and Sheena A. Spencer. 2021. "A New Framework for Modelling Fine Sediment Transport in Rivers Includes Flocculation to Inform Reservoir Management in Wildfire Impacted Watersheds." *Water* 13 (17): 2319. https://doi.org/10.3390/w13172319.
- Sun, G., S. G. McNulty, D. M. Amatya, R. W. Skaggs, L. W. Swift, J. P. Shepard, and H. Riekerk. 2002. "A Comparison of the Watershed Hydrology of Coastal Forested Wetlands and the Mountainous Uplands in the Southern US." *Journal of Hydrology* 263 (1): 92–104. https://doi.org/10.1016/S0022-1694(02)00064-1.
- Turner, and Huppert. 1992. "Sedimentation and Mixing at the Top of a Suspended Particles."
- USGS. 2022. "Pecos River Above Santa Rosa Lake, NM." 2022. https://waterdata.usgs.gov/monitoring-location/08382650/.
- Wagner, Richard J., Robert W. Boulger Jr., Carolyn J. Oblinger, and Brett A. Smith. 2006. "Guidelines and Standard Procedures for Continuous Water-Quality Monitors: Station Operation, Record Computation, and Data Reporting." Report 1-D3. Version 1.0. Techniques and Methods. USGS Publications Warehouse. https://doi.org/10.3133/tm1D3.
- Wibbenmeyer, Matthew, Matthew R Sloggy, and José J Sánchez. 2023. "Economic Analysis of Wildfire Impacts to Water Quality: A Review." *Journal of Forestry*, April, fvad012. https://doi.org/10.1093/jofore/fvad012.
- Zavala, Carlos. 2020. "Hyperpycnal (over Density) Flows and Deposits." *Journal of Palaeogeography* 9 (1): 17. https://doi.org/10.1186/s42501-020-00065-x.
- Zavala, Carlos, Mariano Arcuri, Mariano Di Meglio, Agustin Zorzano, Germán Otharán, Ainara Irastorza, and Antonela Torresi. 2021. "Deltas: A New Classification Expanding Bates's Concepts." *Journal of Palaeogeography* 10 (1): 23. https://doi.org/10.1186/s42501-021-00098-w.

4.7 SUPPLEMENTAL INFORMATION

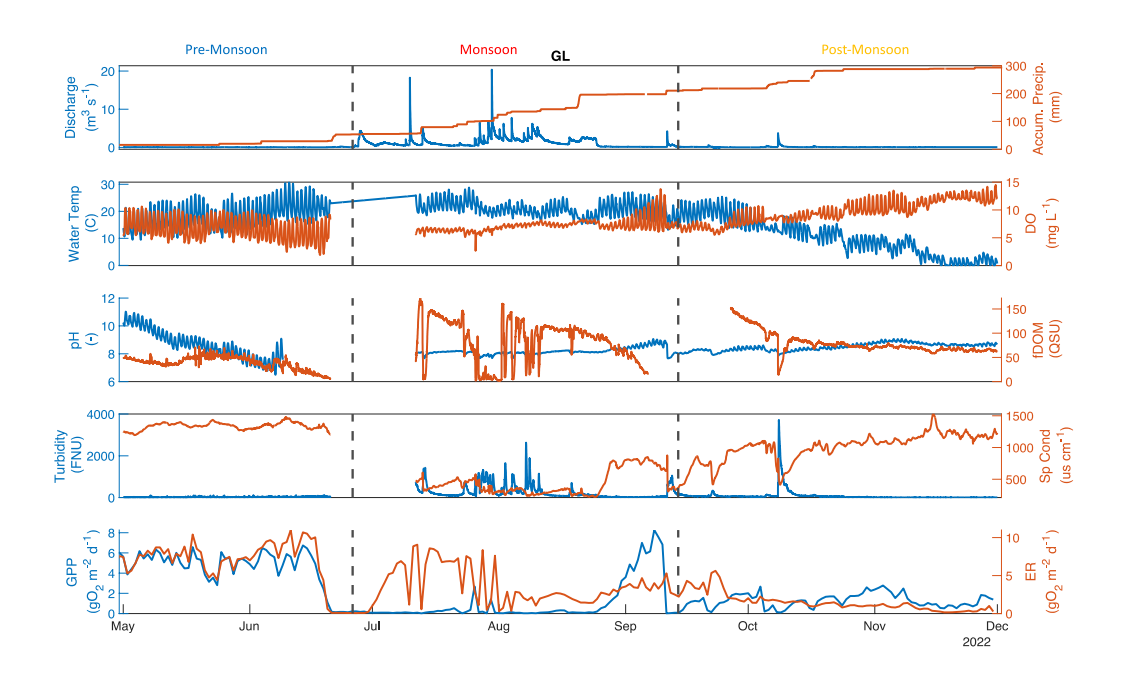
1 GFT monitoring site: upstream of Santa Rosa Lake



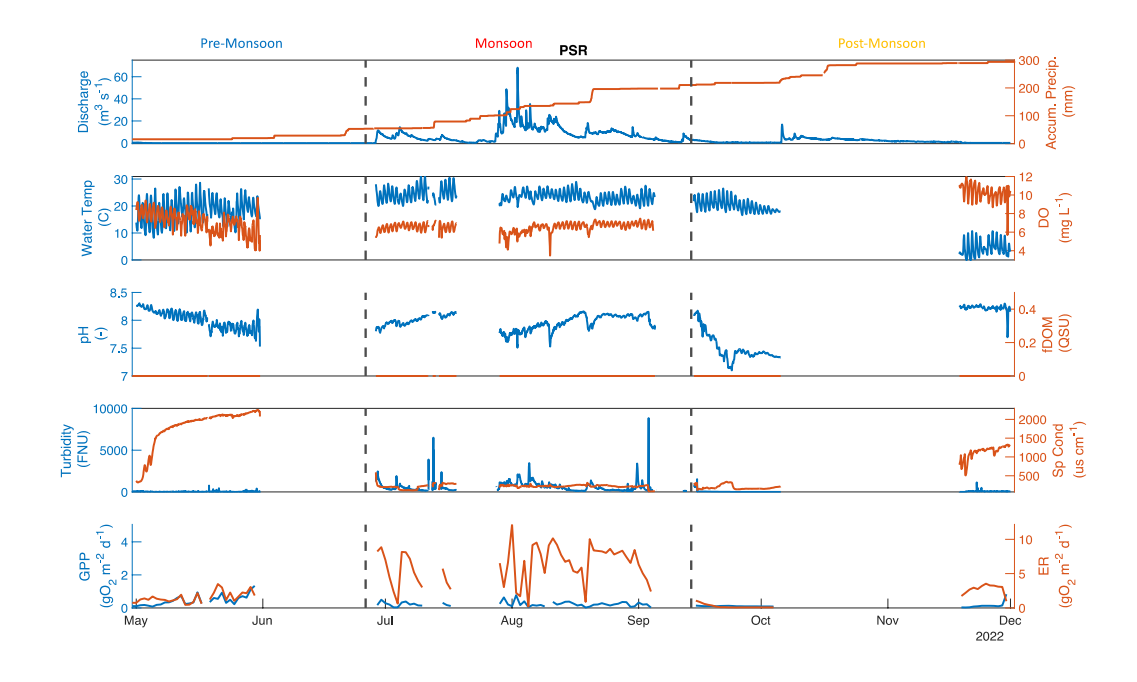
2 GMZ monitoring site: upstream of Santa Rosa Lake



3 GL monitoring site: upstream of Santa Rosa Lake



4 PSR monitoring site: upstream of Santa Rosa Lake



5 PBS monitoring site: downstream of Santa Rosa Lake

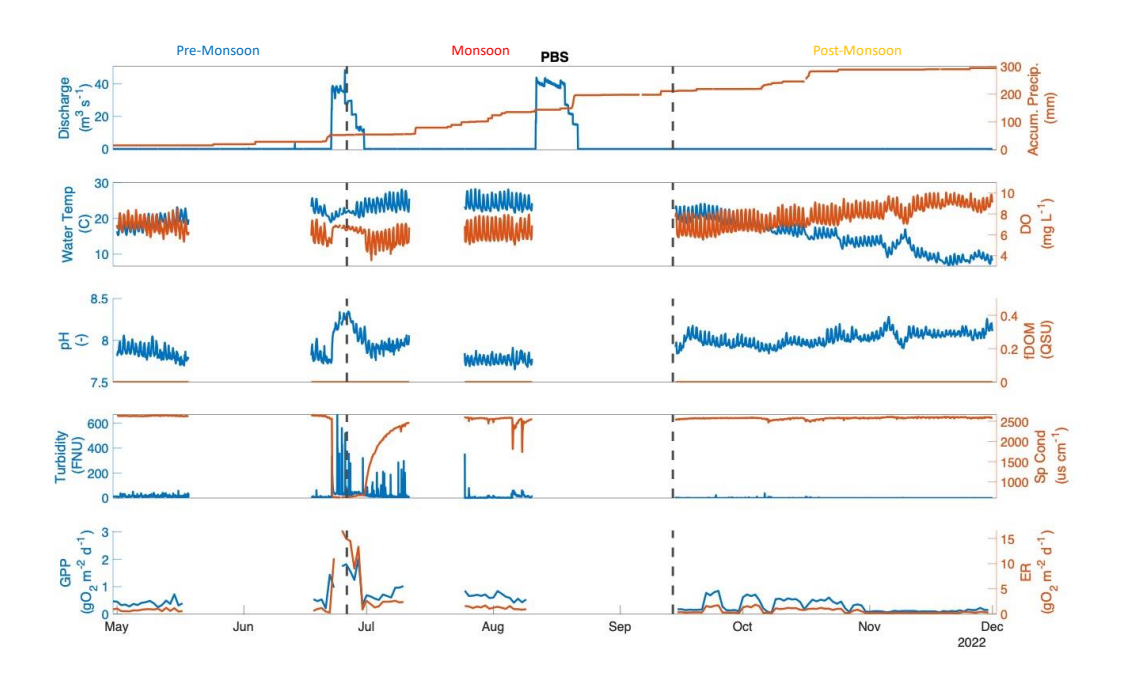


Figure 4.S1) Sonde time series of QA/QC data from monitoring sites



Figure 4.S2: The Navigator monitoring water quality in Santa Rosa Lake (left), and the kayak with the multiparameter sonde monitoring the Pecos River (right).

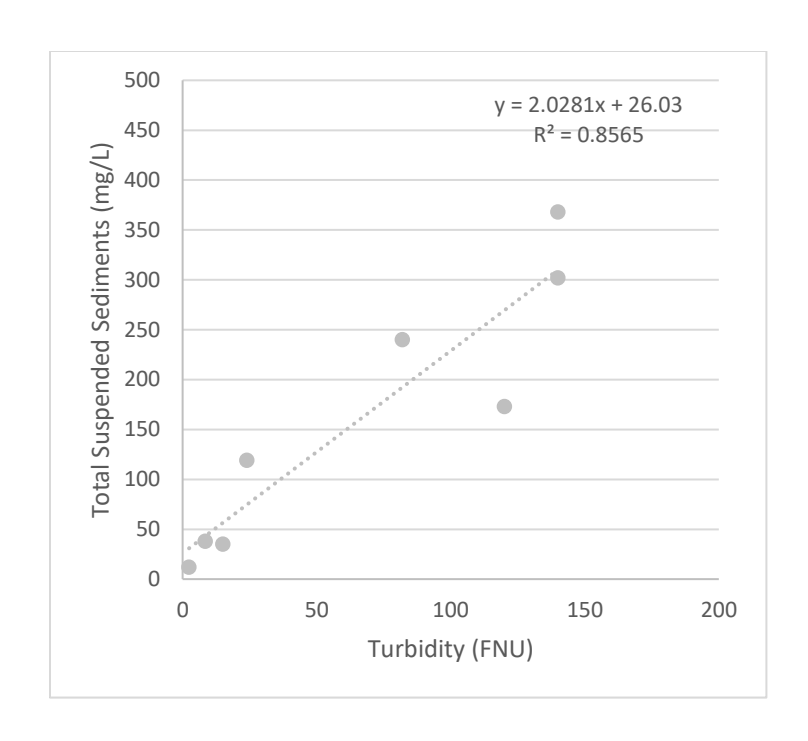


Figure 4.S3: Simple linear regression analysis turbidity and suspended-sediment concentration data for U.S. Geological Survey stream samples on Gallinas River near Montezuma, NM, June 2022- Oct 2022.



Figure 4.S4: Anoxic zone on Pecos river-Santa Rosa Lake delta on Aug 19, 2022.

Chapter 5: Summary

This dissertation focused on the design and development of a Lagrangian (i.e., along a flow path) monitoring system that offers cost-effective solutions for in-situ and real-time data collection. The Navigator was then applied to understand water quality changes associated with lateral effluents and wildfire disturbances.

5.1 CHAPTER SUMMARIES

Chapter 2 of this dissertation focuses on the design, development, and field validation of The Navigator, an autonomous surface vehicle (ASV) for Lagrangian monitoring in freshwater ecosystems. The Navigator offers cost-effective solutions for in-situ, real-time data collection by incorporating various technologies such as GPS, LTE connectivity, water quality sensors, depth sonar, a camera, and a webpage dashboard for data visualization. Multiple field tests were conducted in freshwater bodies in New Mexico, including the Rio Grande, Santa Rosa Lake, and a recreational fishing pond in Albuquerque. The successful tests confirmed the affordability and effectiveness of The Navigator in monitoring water quality parameters at high spatial-temporal resolution, enabling the identification of water quality changes associated with land use changes, the assessment of the fate of wildfire disturbances, and the monitoring of recreational fishing ponds.

Chapter 3 describes the application of The Navigator for the Lagrangian-based quantification of mixing lengths downstream of a wastewater treatment plant discharging into the Rio Grande. We tested and evaluated the accuracy of long-standing empirical equations used to predict mixing lengths in the field. Despite advances in wastewater treatment plant efficiencies, multiple contaminants of concern, such as microplastics, pharmaceuticals, and per- and

polyfluoroalkyl substances (PFAS) remain largely untreated near discharge points and can be highly concentrated before they are fully mixed within the receiving river. Environmental agencies enforce mixing zone permits for the temporary exceedance of water quality parameters beyond targeted control levels under the assumption that contaminants are well-mixed and diluted downstream of mixing lengths, which are typically quantified using empirical equations derived from one-dimensional transport models. Most of these equations were developed in the 1970s and have been assumed to be standard practice since then. However, their development and validation lacked the technological advances required to test them in the field and under changing flow conditions. While new monitoring techniques such as remote sensing and infrared imaging have been employed to visualize mixing lengths and test the validity of empirical equations, those methods cannot be easily repeated due to high costs or flight restrictions. Our data spans river to WWTP discharges ranging between 1-33x, thus providing a unique dataset to test long-standing empirical equations in the field. Our results consistently show empirical equations could not describe our experimental mixing lengths. Specifically, while our experimental data revealed "bell-shaped" mixing lengths as a function of increasing river discharges, all empirical equations predicted monotonically increasing mixing lengths. Those mismatches between experimental and empirical mixing lengths are likely due to the existence of threshold processes defining mixing at different flow regimes, i.e., jet diffusion at low flows, the Coanda effect at intermediate flows, and turbulent mixing at higher flows, which are unaccounted for by the one-dimensional empirical formulas.

In Chapter 4, we used The Navigator to investigate the role of Santa Rosa Lake in attenuating the propagation of wildfire disturbances from the Hermit's Peak-Calf Canyon wildfire, which had propagated 170 km along the Gallinas Creek-Pecos River-Santa Rosa Lake

fluvial network. Eulerian monitoring through a network of sensors identified discharge and turbidity increases during high-precipitation monsoon periods. In the lake, Lagrangian monitoring revealed sudden changes to turbidity and dissolved oxygen levels along the delta. Our data suggest that the formation of hyperpycnal flows sink highly turbid and colder waters from the river into the lakebed, inducing fast sedimentation of wildfire disturbances. The study concludes that hyperpycnal flow formation acts as the primary mechanism responsible for the buffering capacity that halted the propagation of disturbances from the wildfire.

5.2 PATENT

We submitted the work behind The Navigator to get a US provisional patent on November 17th, 2022, titled "Lagrangian Smart Sensing System for Characterizing Aquatic Resources," through UNM Rainforest Innovations (UNM Rainforest Innovations Portfolio 2022). This patent introduces significant advancements over the previous technologies, including:

- Integrated Hardware and Software System: The Navigator incorporates a seamlessly integrated
 hardware and software system that combines water quality sensors with autopilot systems. This
 integration enhances the overall functionality and performance of the device.
- 2. Active and Passive Navigation: The Navigator is designed to autonomously switch between active navigation, which relies on the propulsion system, and passive navigation, which utilizes the natural currents of the aquatic resource. This dynamic navigation approach enhances the vehicle's adaptability and efficiency in different environmental conditions.
- 3. Real-time Data Transmission: The Navigator is equipped with a radio frequency transmitter and a cellular modem that are connected to the electronic controller. This configuration enables the device to transmit data in real-time. By leveraging these communication technologies, data collected by the Navigator can be instantly shared and accessed remotely.

4. Camera-Assisted Obstacle Avoidance: The Navigator includes a camera that is connected to the electronic controller. The electronic controller is specifically programmed to analyze camera data, identify obstacles, and maneuver around them using the propulsion system. This feature ensures improved safety and navigation capabilities.

These advancements enable the solar-powered autonomous surface vehicle to combine current-driven and on-demand maneuvering with water sensors and a camera system. This integration empowers The Navigator to perform autonomous, long-range data collection missions in rugged environments. Furthermore, these improvements facilitate the quantification of water quantity and quality through a web-integrated platform. Users can access real-time visualization of the collected data and remotely control monitoring flow paths and routines via a user-friendly interface.

5.3 COMMERCIALIZATION EXPLORATION

We conducted a comprehensive market analysis through UNM's Rainforest Accelerator Program in Fall 2021 and MIT Water Innovation in Spring 2022 to identify target industries and sectors that can benefit from the Lagrangian Smart Sensing System. Our analysis revealed potential customers, including environmental monitoring agencies, research institutions, water resource management organizations, and industries reliant on accurate water quality data through 150+ industry interviews. The Navigator offers a wide range of critical applications primarily in the water technology sector, as well as the energy and food sectors.

The smart sensors and AI analytics of the Navigator enable timely and spatially informed water management practices. It can be utilized by water and wastewater utilities for quantifying point and nonpoint sources and watershed preservation, sedimentation, seawater intrusion, algae bloom, wildfire impacts and wet carbon monitoring to understand aquatic ecosystems sources and sinks. Researchers, practitioners, and third-party contractors can leverage The Navigator for quantifying mass and energy balances and assessing spatial and temporal trends in variability.

Moreover, the spatiotemporal water quality data generated by the Navigator proves valuable for governmental agencies and NGOs in quantifying and addressing pollution dynamics, enforcing regulations, and evaluating restoration and post-disturbance solutions. Various industries, including governmental agencies, city water authorities, mines, power plants, carbon markets, aquaculture, and manufacturing plants, have shown interest in utilizing The Navigator to address similar issues. Its affordability compared to existing alternatives opens market opportunities in multiple countries worldwide. In 2021 and 2022, I won two pitch contests describing The Navigator and its potential applications for Lagrangian monitoring in freshwater systems.

The Total Available Market (TAM) for Water Quality Monitoring Devices was estimated at US \$3.4 billion in 2022 and is projected to reach US \$4.3 billion by 2027, with a compound annual growth rate of 5%. The US market alone was \$728.4 million in 2021, leading to a serviceable and attainable market size of \$728 million in 2022 (Sushant C 2018). While brand recognition poses a barrier to entry for The Navigator, we are actively addressing this challenge through our current investor. Our focus extends beyond competition to improving water equity, resilience, and mitigating the impact of water shortage and quality issues. Through potential customer outreach, we are refining our pricing strategy and product offerings, ensuring alignment with customer needs and pain points. The primary revenue streams for the Navigator will be licensing and subscriptions across three product segments: the Autonomous Surface Vehicle (ASV), the Real-time Intelligent Analytics platform, and the Dataset.

5.4 CHAPTER REFRENCES:

Sushant C. 2018. "Water Quality Monitoring Systems Market by Component (PH Sensors, DO Sensors, Temperature Sensors, Turbidity Sensors, and Others) and Application (Utilities, Industrial, Commercial, and Residential): Global Opportunity Analysis and Industry Forecast, 2018 - 2025."

Market Overview.

UNM Rainforest Innovations Portfolio. 2022. "2023-005 - The Navigator: A Lagrangian Smart Sensing System to Characterize Aquatic Ecosystems." November 2022. https://innovations.unm.edu/technologies/technology-portfolio/.

Appendix A: Participation in peer-reviewed manuscripts

During my Ph.D. training, I participated in the following peer-reviewed manuscripts:

Nichols, Justin., Khandelwal, Aashish Sanjay., Regier, Peter., Summers, Betsy., Van Horn, David J. and González-Pinzón., Ricardo 2022. "The Understudied Winter: Evidence of How Precipitation Differences Affect Stream Metabolism in a Headwater." *Frontiers in Water* https://doi.org/10.3389/frwa.2022.1003159.

Abstract

Climate change is causing pronounced shifts during winter in the US, including shortening the snow season, reducing snowpack, and altering the timing and volume of snowmelt-related runoff. These changes in winter precipitation patterns affect in-stream freeze-thaw cycles, including ice and snow cover, and can trigger direct and indirect effects on in-stream physical, chemical, and biological processes in ~60% of river basins in the Northern Hemisphere. We used high-resolution, multi-parameter data collected in a headwater stream and its local environment (climate and soil) to determine interannual variability in physical, chemical, and biological signals in a montane stream during the winter of an El Niño and a La Niña year. We observed ~77% greater snow accumulation during the El Niño year, which caused the formation of an ice dam that shifted the system from a primarily lotic to a lentic environment. Water chemistry and stream metabolism parameters varied widely between years. They featured anoxic conditions lasting over a month, with no observable gross primary production (GPP) occurring under the ice and snow cover in the El Niño year. In contrast, dissolved oxygen and GPP remained relatively high during the winter months of the La Niña year. These redox and metabolic changes driven by changes in winter precipitation have significant implications for water chemistry and biological

functioning beyond the winter. Our study suggests that as snow accumulation and hydrologic conditions shift during the winter due to climate change, hot-spots and hot-moments for biogeochemical processing may be reduced, with implications for the downstream movement of nutrients and transported materials.

Regier, Peter J., González-Pinzón, Ricardo., Van Horn, David J., Reale, Justin K., Nichols, Justin and Khandewal, Aashish. 2020. "Water Quality Impacts of Urban and Non-Urban Arid-Land Runoff on the Rio Grande." Science of The Total Environment 729 (August): 138443. https://doi.org/10.1016/j.scitotenv.2020.138443.

Abstract

Urban surface runoff from storms impacts the water quality dynamics of downstream ecosystems. While these effects are well-documented in mesic regions, they are not well constrained for arid watersheds, which sustain longer dry periods, receive intense but short-lived storms, and where stormwater drainage networks are generally isolated from sewage systems. We used a network of high-frequency in situ water quality sensors located along the Middle Rio Grande to determine surface runoff origins during storms and track rapid changes in physical, chemical, and biological components of water quality. Specific conductivity (SpCond) patterns were a reliable indicator of source, distinguishing between runoff events originating primarily in urban (SpCond sags) or non-urban (SpCond spikes) catchments. Urban events were characterized by high fluorescent dissolved organic matter (fDOM), low dissolved oxygen (including short-lived hypoxia <2 mg/L), smaller increases in turbidity and varied pH response. In contrast, non-urban events showed large turbidity spikes, smaller dissolved oxygen sags, and consistent pH sags. Principal component analysis distinguished urban and non-urban events by

dividing physical and biogeochemical water quality parameters, and modeling of DO along the same reach demonstrated consistently higher oxygen demand for an urban event compared to a non-urban event. Based on our analysis, urban runoff poses more potential ecological harm, while non-urban runoff poses a larger problem for drinking water treatment. The comparison of our results to other reports of urban stormwater quality suggests that water quality responses to storm events in urban landscapes are consistent across a range of regional climates.